Multi-Actuated Vehicle Control and Path Planning/Tracking at Handling Limits

by

Reza Hajiloo

A thesis
presented to the University of Waterloo
in fulfillment of the
thesis requirement for the degree of
Doctor of Philosophy
in
Mechanical and Mechatronics Engineering

Waterloo, Ontario, Canada, 2021

Examining Committee Membership

The following served on the Examining Committee for this thesis. The decision of the Examining Committee is by majority vote.

External Examiner:	Name: Farrokh Janabi-Sharifi Title: Professor Department: Mechanical and Industrial Engineering University: Ryerson University
Supervisors:	Name: Amir Khajepour Title: Professor Name: Alireza Kasaiezadeh Title: Adjunct Assistant Professor Department: Mechanical and Mechatronics Engineering
Internal Member:	Name: Baris Fidan Title: Professor Department: Mechanical and Mechatronics Engineering
Internal Member:	Name: Soo Jeon Title: Associate Professor Department: Mechanical and Mechatronics Engineering
Internal-External Member:	Name: Mohammad Javad Shafiee Title: Research Assistant Professor Department: Systems Design Engineering

Author's Declaration

I hereby declare that I am the sole author of this thesis. This is a true copy of the thesis, including any required final revisions, as accepted by my examiners.

I understand that my thesis may be made electronically available to the public.

Abstract

The increasing requirements for vehicle safety along with the impressive progress in vehicle actuation technologies have motivated manufacturers to equip vehicles with multiple control actuations that enhance handling and stability. Moreover, multiple control objectives arise in vehicle dynamics control problems, such as yaw rate control and rollover prevention, therefore, vehicle control problems can be defined as multi-actuation multi-objective vehicle control problems.

Recently, the importance of integrating vehicle control systems has been highlighted in the literature. This integration allows us to prevent the potential conflicting control commands that could be generated by individual controllers. Existing studies on multi-actuated vehicle control offer a coordinated control design that shares the required control effort between the actuations. However, they mostly lack an appropriate strategy for considering the differences among vehicle actuations in their energy usage, capabilities, and effectiveness in any given vehicle states. Therefore, it is very important to develop a cost-performance strategy for optimally controlling multi-actuated vehicles.

In this thesis, a prioritization model predictive control design is proposed for multi-actuated vehicles with multiple control objectives. The designed controller prioritizes the control actuations and control objectives based on, respectively, their advantages and their importance, and then combines the priorities such that a low priority actuation will not kick in unless a high priority objective demands it. The proposed controller is employed for several actuations, including electronic limited slip differential (ELSD), front/rear torque shifting, and differential braking. In this design, differential braking is engaged only when it is necessary, thus limiting or avoiding its disadvantages such as speed reduction and maintenance.

In addition, the proposed control design includes a detailed analysis of the above-mentioned actuations in terms of modelling, control, and constraints. A new vehicle prediction model is designed for integrated lateral and roll dynamics that considers the force coupling effect and allows for the optimal control of front/rear torque distribution. The existing methods for ELSD control may result in chattering or unwanted oversteering yaw moments. To resolve this problem, a dynamic model is first designed for the ELSD clutch to properly estimate the clutch torque. This ELSD model is then used to design an intelligent ELSD controller that resolves the issues mentioned above.

Experimental tests with two different vehicles are also carried out to evaluate the performance of the prioritization MPC controller in real-time. The results verify the capability of the controller in properly activating the control actuations with the designed priorities to improve vehicle handling and stability in different driving maneuvers. In addition, the test results confirm the performance of the designed ELSD model in ELSD clutch torque estimation and in enabling the controller to prevent unwanted oversteering yaw moments.

The designed stability controller is extended to use for emergency collision avoidance in autonomous vehicles. This extension in fact addresses a local path planning/tracking problem with control objectives prioritized as: 1) collision avoidance, 2) vehicle stability, and 3) tracking the desired path. The controller combines a conservative form of torque/brake vectoring with front steering to improve the lateral agility and responsiveness of the vehicle in emergency collision avoidance scenarios. In addition, a contingency MPC controller is designed with two parallel prediction horizons - a nominal horizon and a contingency horizon - to maintain avoidance in identified road condition uncertainties.

The performance of the model predictive controllers is evaluated in software simulations with high fidelity CarSim models, in which different sets of actuation configurations in various driving and road conditions are assessed. In addition, the effectiveness of the local path planning/tracking controller is evaluated in several emergency and contingency collision avoidance scenarios.

Acknowledgements

Foremost, I would like to express my sincere gratitude to my supervisors, Prof. Amir Khajepour and Prof. Alireza Kasaiezadeh, for their exceptional support, guidance, and encouragement throughout my PhD research and education. I am very grateful to have had the critical opportunity to work with them, and it is to them I owe my present academic skills, vision of the profession, and insights into engineering ethics.

I gratefully acknowledge the financial support of the Ontario Research Fund (ORF), the Natural Sciences and Engineering Research Council of Canada (NSERC), and the technical and financial support of General Motors. Special thanks to Dr. Bakhtiar Litkouhi, Dr. Alireza Kasaiezadeh, Dr. Shih-ken Chen, and Dr. Yubiao Zhang of the GM Research and Development Center in Warren, Michigan, USA, and Dr. Asal Nahidi of the GM Technical Center in Markham, Canada for the technical support and valuable inputs that have improved my research, especially during my work in GM as a visiting researcher.

Thanks are also due to the technicians of Waterloo's Mechatronics Vehicle Systems laboratory, namely Jeff Graansma, Adrian Neill, and Aaron Sherratt, for making the experimental tests possible. Additionally, I am grateful to Dr. Ehsan Hashemi and Dr. Iman Fadakar for their valuable technical support and advice during my PhD research. My colleagues and friends at Waterloo have been a valuable source of encouragement, assistance, and friendship, so thanks to Amin Habibnejad, Shamim Mashrouteh, Mehdi Abroshan, Ehsan Mohammadbagher, Hassan Askari, Halit Zengin, Chen Tang, and Mansour Ataei and all the others who have been part of my journey.

Most importantly, I would like to thank my family - my parents, my brothers, and my sister - for supporting me spiritually throughout my life and for their encouragement during this endeavor.

Dedication

This dissertation is dedicated to my parents for all their love and support.

Table of Contents

List of Tables xi

List of Figures xii

Nomenclature xviii

1 Introduction 1

1.1 Motivation 1

1.2 Objectives 3

1.3 Thesis Outline 4

2 Literature Review 6

2.1 Direct Yaw Control 6

2.2 Indirect Yaw Control 9

2.3 Multi-Actuated Vehicle Control 11

2.4 Roll Stability 13

2.5 Path Planning/Tracking and Collision Avoidance 15

2.6 Summary 21

3 Prioritization Model Predictive Control Design for Multi-Actuated Vehicles **23**

3.1 Road Angles' Effect on Vehicle Chassis Dynamics 24
3.2 Vehicle Prediction Model 27
3.3 ELSD Model Development 35
3.4 Actuator Constraints 39
3.5 State Constraints 42
3.6 Desired Vehicle Response 45
3.7 Prioritization Model Predictive Controller 46
3.8 Prioritization Control of Vehicle Dynamics 48
3.9 Summary 51

4 Simulation and Experimental Results **52**

4.1 Case Study 1: Differential Braking and Front/Rear Torque Shifting 55
4.1.1 Acceleration in Flick Maneuver on Wet Road - Simulation 56
4.1.2 Acceleration in DLC Maneuver on Wet Road - Simulation 59
4.1.3 Acceleration in Slalom Maneuver on Wet Road - Experiment 60
4.2 Case Study 2: ELSD and Differential Braking 63
4.2.1 ELSD Model Evaluation - Experiment 66
4.2.2 DLC Maneuver on Wet Road - Experiment 68
4.2.3 Acceleration in Slalom Maneuver on Dry Road - Experiment 74
4.2.4 Acceleration in Turn Maneuver on Dry Road - Experiment 75
4.3 Case Study 3: Integrated Lateral and Roll Stability 78
4.3.1 Acceleration in Turn Maneuver on Dry Road - Simulation 78
4.3.2 Acceleration in Flick Maneuver on Sticky Road - Simulation 80
4.3.3 Acceleration in Slalom Maneuver on Wet Banked Road - Simulation 82
4.3.4 Acceleration in Slalom Maneuver on Dry Banked Road - Simulation 84
4.4 Summary 86

5 Integrated Vehicle Stability and Path Planning/Tracking Control Design 89

5.1 System Modelling 90

5.2 System Constraints 94

5.3 Emergency Path Planning/Tracking Controller 98

5.3.1 Longitudinal Controller 98

5.3.2 Lateral Controller 100

5.4 Contingency Path Planning/Tracking Controller 101

5.5 Numerical Study 105

5.5.1 Emergency Scenario 1: Straight Road with a Sudden Obstacle . . . 106

5.5.2 Emergency Scenario 2: Curved Road with Two Sudden Obstacles . 109

5.5.3 Contingency Scenario 1: Mixed Wet and Icy Road with Two Obstacles 112

5.5.4 Contingency Scenario 2: Left Turn on Mixed Snowy and Icy Road . 114

5.5.5 Contingency Scenario 3: Potential Change in Road Bank in a Curved Road 115

5.6 Summary 117

6 Conclusions and Future Work 121

6.1 Conclusions 121

6.2 Future Work 124

References 125

List of Tables

3.1 ELSD Model Parameters. 39

4.1 Specifications of the Test Vehicles. 53

4.2 Controller Parameters. 54

5.1 Path Planning/Tracking Controller Parameters. 106

List of Figures

2.1 Autonomous system architecture. 16

3.1 Successive rotations of vehicle body's coordinate axes, (a) road direction ψ_r, (b) road grade θ_r, (c) road bank ϕ_r, and (d) vehicle's heading deviation $\Delta\psi$. 25

3.2 Vehicle model diagram, (a) top view, (b) back view. 28

3.3 Linearization of the tire model with respect to (a) slip angle α and (b) derating factor ξ. 30

3.4 Variations of (a) $\bar{C}_\alpha$ and (b) $\bar{C}_Q$ versus α for different values of $\xi = 0.2, 0.4, 0.6, 0.8, 1$. 31

3.5 The yaw moment capacity produced by front/rear torque distribution versus driver torque. 32

3.6 (a) Steer angle, (b) axle torque, (c) the vehicle yaw rate, and (d) the ELSD clutch torque in an acceleration in turn maneuver with 60 percent constant clutch pressure. The clutch torque provides both understeering and oversteering yaw moments. 37

3.7 Schematic of ELSD model in the rear axle. 38

3.8 Tire force vector in the friction force limit circle, (a) with no longitudinal force at the corners, and (b) the optimum force vectors for generating understeering yaw moment by differential braking. 41

3.9 (a) The $\beta - r$ phase plane, and (b) the $\phi - \dot{\phi}$ phase plane. They are divided to green, yellow, and red regions. 45

3.10 General form of the prioritization controller. The priority of control actuations and control objectives are combined within λ priority levels. 46

3.11 The prioritization controller is used for three case studies. (a) Case study 1, (b) Case study 2, (c) Case study 3. 50

4.1 Test vehicles used in experimental verifications, (a) the electric all-wheel-drive Chevrolet Equinox vehicle, and (b) the Cadillac CTS vehicle. 53

4.2 The experimental setup of the vehicle and the communication network. . . 54

4.3 Control structure for Case 1. The controller calculates the adjustments of front/rear torque distribution and the yaw moment by differential braking, which is converted into corner brakes. 55

4.4 (a) The steering wheel angle, (b) driver's torque request, and (c) the vehicle longitudinal velocity in an accelerating Flick maneuver on a wet road. . . . 57

4.5 (a) The front/rear torque allocation for Controller A, (b) the yaw moment by differential braking for Controllers A and B, (c) the yaw rate, and (d) the rear tire slip angle, with controller ON (A and B) and OFF in an accelerating Flick maneuver on a wet road. 58

4.6 (a) The steering wheel angle, (b) driver's torque request, and (c) the vehicle longitudinal velocity in an accelerating DLC maneuver on a wet road. . . . 59

4.7 (a) The front/rear torque allocation for Controller A, (b) the yaw moment by differential braking for Controllers A and B, (c) the yaw rate, and (d) the rear tire slip angle, with controller ON (A and B) and OFF in an accelerating DLC maneuver on a wet road. 61

4.8 The steering wheel input, driver's torque request, and the vehicle longitudinal velocity in accelerating slalom maneuver on a wet asphalt patch, with controller OFF (a,c,e) and controller ON (b,d,f). 62

4.9 (a) The front/rear torque allocation, and (b) the yaw moment by differential braking, in the controlled accelerating slalom maneuver on a wet asphalt patch. 63

4.10 The vehicle's yaw rate and the rear tire slip angle in accelerating slalom maneuver on a wet asphalt patch, with controller OFF (a,c) and controller ON (b,d). 64

4.11 Control structure for Case 2. The controller calculates the ELSD clutch pressure and the corner braking forces. 65

4.12 (a) The steering wheel input, (b) driver's torque request, (c) wheel speed difference, and (d) ELSD clutch torque in an slalom maneuver with 40 percent clutch pressure performed on a dry asphalt patch. 67

4.13 (a) The steering wheel input, (b) driver's torque request, (c) wheel speed difference, and (d) ELSD clutch torque in an AIT maneuver with 50 percent clutch pressure performed on a dry asphalt patch. 68

4.14 (a) The steering wheel input, (b) driver's torque request, (c) wheel speed difference, and (d) ELSD clutch torque in the AIT maneuver shown in Fig. 3.6. 69

4.15 (a) The steering wheel input, (b) driver's torque request, (c) wheel speed difference, and (d) ELSD clutch torque in an AIS maneuver with 40 percent clutch pressure on a wet asphalt patch 70

4.16 The driver's steering wheel and torque in a double lane change maneuver on a wet asphalt patch, with controller OFF (a,b), controller ON (c,d), and differential braking (e,f). 71

4.17 The vehicle's yaw rate and longitudinal velocity in a double lane change maneuver on a wet asphalt patch, with controller OFF (a,b), controller ON (c,d), and differential braking (e,f). 72

4.18 (a) Controlled ELSD clutch pressure, (b) controlled ELSD clutch torque. Front and rear differential braking with controller ON (c,d) and differential braking only (e,f) in a double lane change maneuver on a wet asphalt patch. 73

4.19 The driver's steering wheel and torque (a,b), and the vehicle's longitudinal velocity and yaw rate (c,d) in an acceleration in slalom maneuver on a dry asphalt patch with controller in the loop. 75

4.20 (a) ELSD clutch pressure, (b) ELSD clutch torque, (c) front differential braking, and (d) rear differential braking in an acceleration in slalom maneuver on a dry asphalt patch with controller in the loop. 76

4.21 The steering wheel input, driver's torque request, and the vehicle's longitudinal velocity in an acceleration in turn maneuver on a dry asphalt patch, with controller OFF (a,c,e) and controller ON (b,d,f). 77

4.22 (a) The yaw rate of uncontrolled vehicle, (b) the yaw rate of controlled vehicle; (c) ELSD clutch pressure, (d) ELSD clutch torque, (e) front differential braking, and (f) rear differential braking in an acceleration in turn maneuver on a dry asphalt patch. 79

4.23 (a) Steering wheel angle, and (b) driver's torque request in an acceleration in turn maneuver on a dry road. 80

4.24 (a) Front/rear torque allocation, and (b) the yaw moment M_{F_x}, in the controlled AIT maneuver on a dry road. 81

4.25 (a) The yaw rate, (b) the rear tire slip angle, and (c) the roll index, with controller ON and OFF in an acceleration in turn maneuver on a dry road. 81

4.26 (a) The steering wheel angle, and (b) driver's torque request in an acceleration in a flick maneuver on a sticky road. 82

4.27 (a) The front/rear torque allocation, and (b) the yaw moment by differential braking, in the controlled acceleration in flick maneuver on a sticky road. . 83

4.28 (a) The yaw rate, (b) the rear tire slip angle, and (c) the roll index, with controller ON and OFF in an acceleration in flick maneuver on a sticky road. 83

4.29 (a) The steering wheel angle, and (b) driver's torque request in an acceleration in a slalom maneuver on a wet banked road. 84

4.30 (a) The front/rear torque allocation, and (b) the yaw moment by differential braking, in the controlled acceleration in a slalom maneuver on a wet banked road. 85

4.31 (a) The yaw rate, (b) the rear tire slip angle, and (c) the roll index, with controller ON and OFF in an acceleration in a slalom maneuver on a wet banked road. 85

4.32 (a) The steering wheel angle, and (b) driver's torque request in an acceleration in a slalom maneuver on a dry banked road. 86

4.33 (a) The front/rear torque allocation, and (b) the yaw moment by differential braking, in the controlled acceleration in a slalom maneuver on a dry banked road. 87

4.34 (a) The yaw rate, (b) the rear tire slip angle, and (c) the roll index, with controller ON and OFF in an acceleration in a slalom maneuver on a dry banked road. 87

5.1 Bicycle model diagram. 90

5.2 Friction force circle. Applying a limited longitudinal force has minimal effect on the lateral force capacity. 92

5.3 The safe region for position states is represented by defining a constraint on the lateral deviation. 96

5.4 The maximum yaw moment $M_{F_{x,max}}$ and the braking distribution ratio η are adjusted out of the stable region using the scaling variable χ. 98

5.5 Control structure. The designed controller calculates longitudinal and lateral control inputs, based on which drive, brake, and steering commands are obtained. 99

5.6 Contingency MPC prediction horizon. A nominal and contingency trajectory are computed, which have equal control action at the first step. 103

5.7 A contingency event with possible icy patches on a wet road. 105

5.8 (a) The optimized paths and (b) 3D results for Controllers A (blue) and B (green) confronting a pop-up obstacle suddenly introduced (magenta dashed in (a)) in a straight road (scenario 1). The red rectangle in (a) and the crates in (b) indicate the obstacle area to be avoided. 107

5.9 The vehicle trajectory in the phase plane of lateral velocity and yaw rate for Controllers A (blue) and B (green) in scenario 1. 108

5.10 (a) The steer angle and (b) M_{F_x} for Controllers A (blue) and B (green) in scenario 1. 109

5.11 Vehicle response (a) yaw rate, (b) lateral acceleration, (c) speed for Controllers A (blue) and B (green) in scenario 1. 109

5.12 (a) The optimized paths and (b) 3D results for Controllers A (blue) and B (green) confronting two pop-up obstacles suddenly introduced at distances 1 and 2 (magenta dashed in (a)) in a curved road (scenario 2). The red rectangles in (a) and the crates in (b) indicate the obstacle area to be avoided. 110

5.13 The vehicle trajectory in the phase plane of lateral velocity and yaw rate for Controllers A (blue) and B (green) in scenario 2. 111

5.14 (a) The steer angle and (b) M_{F_x} for Controllers A (blue) and B (green) in scenario 2. 112

5.15 Vehicle response (a) lateral deviation, (b) yaw rate, (c) lateral acceleration, and (d) speed for Controllers A (blue) and B (green) in scenario 2. 112

5.16 The first contingency scenario is a straight road with two obstacles. (a) Road A is totally wet, and (b) Road B is wet in the middle and icy near the sides. 113

5.17 The vehicle track paths calculated by the deterministic and contingency path planners on (a) Road A and (b) Road B in the first contingency scenario. 113

5.18 (a) The steer angle, (b) yaw rate, and (c) lateral acceleration for the deterministic and contingency controllers on Road A and Road B in the first contingency scenario. 114

5.19 The second contingency scenario is a 90-degree turn. (a) Road A is totally snowy, and (b) Road B is snowy before the turn and icy after that. 115

5.20 The vehicle paths controlled with the deterministic and contingency path planners on (a) Road A and (b) Road B in the second contingency scenario. 116

5.21 (a) The steer angle, (b) yaw rate, and (c) lateral acceleration for the deterministic and contingency path planners on Road A and Road B in the second contingency scenario. 117

5.22 The third contingency scenario is a curved road with potential change road bank. (a) Road A is totally flat, and (b) Road B is flat in the straight section and banked in the curved section. 118

5.23 The vehicle paths controlled with the deterministic and contingency path planners on (a) Road A and (b) Road B in the third contingency scenario. 118

5.24 (a) The steer angle, (b) yaw rate, and (c) lateral acceleration for the deterministic and contingency path planners on Road A and Road B in the third contingency scenario. 119

Nomenclature

α	Lateral slip angle $[rad]$
$\bar{C}_\alpha$	Sensitivity of the lateral force with respect to slip angle $[N/rad]$
$\bar{C}_\xi$	Sensitivity of the lateral force with respect to derating factor $[N]$
$\bar{C}_Q$	Sensitivity of the lateral force with respect to torque $[1/m]$
β	Vehicle's sideslip angle $[rad]$
δ	Steering angle $[rad]$
κ	Road curvature $[1/m]$
λ_t	ELSD clutch forgetting factor $[1/s]$
μ	Road friction coefficient
ω	Wheel speed $[rad/s]$
ϕ	Roll angle $[rad]$
ϕ_r	Road bank angle $[rad]$
τ	Time constant
θ_r	Road grade angle $[rad]$
ξ	A derating factor representing the remaining lateral force capacity
a_x	Longitudinal acceleration $[m/s^2]$

a_y	Lateral acceleration $[m/s^2]$
c_t	ELSD clutch damper coefficient $[N.m.s/rad]$
C_α	Tire cornering stiffness $[N/rad]$
c_ϕ	Equivalent roll damping
e	Lateral deviation $[m]$
F_x	Longitudinal force $[N]$
F_y	Lateral force $[N]$
F_z	Vertical force $[N]$
g	Gravitational constant $[m/s^2]$
h	Vehicle's height $[m]$
h_s	Distance from the roll center to the CG of the sprung mass $[m]$
I_z	Vehicle's yaw Inertia
$I_{x,s}$	Vehicle's roll inertia about the roll axis
k_t	ELSD clutch spring coefficient $[N.m/rad]$
k_ϕ	Equivalent roll stiffness
k_{us}	Vehicle understeer gradient
l_f	Distance between the front axle and CG $[m]$
l_r	Distance between the rear axle and CG $[m]$
l_s	Track width $[m]$
LTR	Lateral load transfer ratio
m	Total mass of the vehicle $[kg]$
m_s	Sprung mass of the vehicle $[kg]$

M_z Yaw moment $[N.m]$

M_{DBF} Corrective yaw moment by front differential braking $[N.m]$

M_{DBR} Corrective yaw moment by rear differential braking $[N.m]$

M_{DY} Direct corrective yaw moment $[N.m]$

M_{ED} Corrective yaw moment by ELSD $[N.m]$

M_{F_x} Yaw moment by longitudinal forces $[N.m]$

M_{F_y} Yaw moment by lateral forces $[N.m]$

P ELSD clutch pressure

Q Torque $[N.m]$

r Yaw rate $[rad/s]$

R_e Effective radius $[m]$

T_C ELSD clutch torque $[N.m]$

t_s Sampling time $[s]$

u Longitudinal velocity $[m/s]$

v Lateral velocity $[m/s]$

CCW Counterclockwise

CG Center of Gravity of the vehicle

DCI Driver command interpreter

DYC Direct Yaw Control

ELSD Electronic limited slip differential

GPS Global Positioning System

IMU Inertial Measurement Unit

MPC Model Predictive Control

PID Proportional-Integral-Derivative (controller)

SUV Sport Utility Vehicle

Chapter 1

Introduction

1.1 Motivation

Every year, many lives are lost in road accidents when drivers lose control of their vehicles. These accidents mainly happen at high vehicle speeds, on low friction roads, or with sudden changes in road conditions. Driver-assist technologies are aiming at eliminating driver mistakes by introducing active safety systems that assist drivers in unfavorable driving conditions and so improve vehicle stability.

Recent progress in vehicle actuation technologies has facilitated equipping modern vehicles with multiple control actuations to improve vehicle handling and stability. In addition, the vehicle dynamics control problem can include several control objectives such as yaw rate control, sideslip control, and roll control. Therefore, a multi-actuation multi-objective control problem can be defined for vehicle dynamics control. Each vehicle control actuation may be employed for a specific control objective. For instance, active suspensions are mainly used to control a vehicle's vertical movement and improve ride quality [1]. Active anti-roll bar systems are usually used to change the roll stiffness of the vehicle and prevent potential roll-overs [2]. However, some control actuations can be effective for several control objectives. For instance, differential braking and torque distribution can contribute to yaw control, sideslip control, wheel slip control, and roll motion control.

The multi-actuation multi-objective vehicle control problem needs an appropriate control technique. Generally, control techniques can be divided into two groups: model-free

[3] and model-based [4] control methods. Model-free control techniques such as PID control [5, 6], learning-based control [7], and delayed feedback control ones [8] do not need system model equations to obtain the control actions. On the other hand, model-based control techniques such as sliding mode control [9, 10, 11], backstepping control [12], feedback linearization [13, 14], and model predictive control methods [15] require the governing equations of the system. For vehicle dynamics control, despite potential uncertainties in vehicle and tire model, the model predictive control (MPC) method is considered promising due to its undeniable advantages.

The MPC control technique calculates an optimal solution for the control problem. It is also capable of predicting system behavior in the future over a finite horizon. The main reason for the popularity of model predictive control is related to its capability of explicitly considering the actuator and state constraints within the control design and prediction horizon. These capabilities of the MPC control method provide the desired preventive measures such as keeping the yaw rate away from the instability margin or preventing collisions in a path planning/tracking problem. A model predictive control solves an optimization problem at each time step to determine the optimized sequence of inputs that will minimize the objective function and satisfy the constraints over a specified control time horizon. The first optimized input in the sequence is applied to the system and the optimization problem is solved again for the next time step.

A model predictive control design can easily include multiple control actuations and control objectives in its cost function; however, the best cost-performance strategy for optimally controlling multi-actuated vehicles is yet to be determined. A good control strategy should consider the priority of the control objectives at each time based on their importance. The control strategy should also include the priority of the control actuations based on their performance and energy use. Therefore, a high-level control structure is needed to define the priority of the control actuations and control objectives.

Vehicle safety actuations are also used in autonomous vehicles, which have additional control objectives such as avoiding collisions and tracking the desired path and speed. Therefore, autonomous vehicle control can also be considered as a multi-actuation multi-objective control problem. Many different control techniques have been proposed for collision avoidance in autonomous vehicles. Among these, the model predictive control design can properly consider local path planning, path tracking, and collision avoidance objectives. Therefore, the vehicle dynamics control objective can be integrated with the path plan-

ning/tracking control objectives within one model predictive controller. However, these control objectives may need different prediction horizons. For instance, the collision avoidance objective needs a longer prediction horizon because the vehicle needs more reaction time to deviate from its path and prevent a collision.

Road angles can significantly affect vehicle dynamics. A vehicle dynamic controller designed for a flat road may fail to properly respond on a non-flat road. For instance, vehicle rollover is more likely to happen in a banked road. The road angle can also affect the performance of path planning and collision avoidance. A collision avoidance controller plans a path based on vehicle dynamics. Therefore, an incorrect assumption of the future road angle may result in a collision. Thus, the control design should include the effect of road angles on vehicle dynamics.

1.2 Objectives

The first objective of this thesis is to develop an optimal controller for the multi-actuation multi-objective vehicle control problem at handling limits by considering the priority of control actuations and control objectives. In this control design, the engagement of each control actuation is determined based on its priority among the control actuations and the control objectives' demands. A linear time-varying model predictive control technique will be employed to properly include vehicle stability constraints, which are set as the control objectives. This control design is implemented for several case studies with different actuations and objectives.

The second objective is to design appropriate actuator models and vehicle prediction models to use in the model predictive control design. The front/rear torque shifting actuation generates an indirect corrective yaw moment due to the longitudinal and lateral force coupling effect, which necessitates a coupled force vehicle prediction design. The electronic limited slip differential (ELSD) actuation generates a left/right torque differential by decreasing the wheel speed difference. The proper control of ELSD requires accurate knowledge of the ELSD clutch torque direction and its capability. Therefore, a dynamic model will be designed for ELSD to predict the ELSD clutch torque capability.

The third objective is to include the effect of road angles in the controller design because road bank and grade angles can significantly affect the vehicle dynamics and increase the

chance of instability modes. Therefore, the effect of road angles on vehicle dynamics will be considered in the vehicle prediction model and state constraints.

The fourth objective is to extend the designed vehicle dynamics controller to an integrated vehicle dynamics and path planning/tracking controller for autonomous vehicles. To this end, the control objectives are expanded by including the collision avoidance and path tracking objectives. The system modeling and prediction horizon will be designed such that both the collision avoidance and vehicle stability objectives can be properly addressed in the controller. Direct yaw control actuations are incorporated to improve vehicle responsiveness in emergency scenarios. In addition, the deterministic path planner will be extended to a contingency path planner to properly handle uncertain road conditions.

Finally, the designed model predictive controller will be evaluated numerically as well as experimentally. Ultimately, the controller should be able to run in real-time for implementation on the vehicles available in our lab.

1.3 Thesis Outline

The second chapter of this thesis reviews relevant literature on vehicle stability control and autonomous vehicle path planning control. The vehicle control actuations are divided into direct yaw control and indirect yaw control, and their contributions to vehicle handling and stability control are discussed. The literature on multi-actuated vehicle control and multi-objective vehicle control, vehicle roll control, autonomous vehicle collision avoidance is also reviewed.

In the third chapter, a prioritization model predictive control design is developed for multi-actuated vehicles with multiple control objectives. The actuations studied are front/rear torque shifting, ELSD, and differential braking. A coupled force vehicle prediction model is developed that considers the effect of longitudinal forces on lateral forces and allows for optimally distributing the drive torque between the front and rear axles. The vehicle model includes the lateral motion, yaw motion, and roll motion, and it also considers the effect of road angles on vehicle dynamics. Next, an ELSD model is designed to properly estimate the ELSD clutch torque distribution and support the intelligent control of ELSD. Next, the actuator constraints and state constraints are illustrated. The constraints on the vehicle yaw rate, sideslip, and roll index define the control objectives.

Next, a prioritization structure is defined for the control objectives and control actuations, and then implemented for three case studies.

Chapter four presents numerical and experimental results for vehicle performance in the three case studies. Software simulations are performed using the MATLAB/Simulink and CarSim software packages. Real-time validation is achieved by implementing the controller on dSpace Autobox and testing it on two different vehicles. The closed-loop vehicle response is compared with the uncontrolled vehicle response in a variety of driving maneuvers and on different road surfaces. The simulations as well as experiments demonstrate the effectiveness of the proposed control strategy in all driving conditions.

In Chapter five, the controller is extended to deal with the integrated collision avoidance and stabilization of autonomous vehicles. A short prediction horizon for vehicle stability and a long prediction horizon for local path planning/tracking are considered in the model predictive controller. Next, conservative differential braking is integrated with the front steering to improve the vehicle's lateral agility in emergency collision avoidance scenarios. In addition, a contingency MPC controller is designed to maintain avoidance in contingency scenarios. Simulations are performed to evaluate the controllers' performance at handling limits.

Chapter six highlights the conclusions and contributions of this thesis research. In addition, some possible directions for future work are suggested.

Chapter 2

Literature Review

This chapter presents a review on the literature of vehicle control actuations and multi-actuated vehicle control. The vehicle control actuations are divided into two categories: direct yaw control and indirect yaw control methods. This review includes different vehicle control objectives such as lateral stability, yaw stability, and rollover prevention. The literature of path planning/tracking control of autonomous vehicles, with emphasis on emergency collision avoidance control is also studied.

2.1 Direct Yaw Control

The direct yaw moment control (DYC) refers to the corrective yaw moments achieved by torque/brake vectoring. In other words, the DYC method controls the vehicle yaw rate by direct effect of longitudinal forces. Differential braking is one of the DYC methods which has received the most attention from researchers and manufacturers from among all the vehicle stability control actuations. Differential braking generates a corrective yaw moment in the desired direction by applying braking action on the wheels on one side of the vehicle (both axles).

The contribution of differential braking on vehicle control has been investigated in many studies in the literature. For instance, a Linear Parametric Varying (LPV) robust controller was proposed in [16] for vehicle yaw control using differential braking. The controller used gain scheduling and considered the effect of load transfer during braking. In [17], a fuzzy

logic-based control algorithm was designed for vehicle stabilization using a brake-by-wire differential braking system. The control design used a nonlinear vehicle model including both lateral dynamics and wheel dynamics. It was assumed that the yaw rate is always within a reasonable range such that the driver can respond to the yaw rate disturbances quick enough to avoid instability.

In [18], a model predictive controller was designed for stabilizing tractor-trailer vehicles using differential braking. The controller's performance was evaluated comparatively when differential braking is applied only to the tractor and only to the trailer. The corrective yaw moment was constrained by considering the remaining capacity of the tires, which was obtained using the friction circle.

The electrification of the automotive powertrain provides an effective approach to improve the vehicle's handling and stability by controlling the torque distribution of individual wheels in an axle (torque differential) [19]. While differential braking reduces the vehicle speed, torque vectoring does not affect it. Therefore, torque vectoring is more advantageous than differential braking. Active torque distribution systems distribute the torque between the wheels via electric motors and active differentials respectively in electric vehicles and conventional vehicles.

In [20], a generalized integrated control strategy was proposed for vehicle control using an optimal torque vectoring control approach. The controller generated optimal adjustments in tire forces and yaw moment by applying individual wheel torques to keep the vehicle on a target path. The control method was subjected to constraints on the applicable differential torque, resulting in a constrained optimization problem for vehicle control applications.

In [21], a modular optimal control design was proposed for integrated longitudinal and lateral vehicle control by controlling torque at individual wheels. A high-level MPC controller was used to determine the longitudinal force and yaw moment adjustments required for minimizing the tracking error of the vehicle's longitudinal and lateral states. A low-level controller was employed to optimally regulate torque at each wheel based on the control actions calculated in the high-level controller.

In [22], an integrated model predictive control of vehicle stability and wheel traction was developed by controlling wheel torques at individual wheels. The control objective was tracking the desired yaw rate while maintaining tire slip ratios and lateral velocity within predefined safe regions. The controller achieved the lateral stability of the vehicle

indirectly by adjusting the reference yaw rate. This technique reduced the size of the prediction model and consequently computational complexity.

In [23], a combined second-order sliding mode controller with the backstepping method was proposed to improve the maneuverability and stability of a vehicle using torque vectoring. In [24], a real-time nonlinear MPC was proposed for stabilization of an electric vehicle at the limits of handling. Rear axle torque vectoring was used as control actuation and three MPC strategies were designed for vehicle stability, compared against each other.

An alternative for torque distribution by individual electric motors is to use active differentials to control torque transfer and create torque differential when needed. There are two main types of active differentials: the electronic limited-slip differential (ELSD) [25, 26] and the torque vectoring differential (TVD) [27, 28]. Electronic limited slip differentials are much simpler and less expensive than active torque vectoring differentials, but they can control only the magnitude of the torque transfer, not its direction. The limited slip differentials are usually used to improve wheel stability and traction. When one wheel loses traction, a clutch transfers additional torque to the wheel having the most traction so that the vehicle can maintain longitudinal motion [25]. However, this torque bias may cause undesired yaw motion and eventually degrade the lateral dynamics of the vehicle if it is not controlled properly. When the differential is controlled properly, it significantly improves the vehicle yaw stability.

In [29], a stability-enhanced traction control system was proposed to improve vehicle stability in slippery conditions. A PI controller was used to calculate the ELSD clutch torque required for yaw damping. A simple ON-OFF switch, triggered by the vehicle's yaw rate, was used to lock the ELSD clutch whenever there is too much yaw rate overshoot to transfer torque from the outer wheel to the inner wheel and produce an understeering yaw moment.

In [30], two torque biasing components were used to improve vehicle stability and handling performance in a four-wheel drive vehicle. The vehicle driveline included an electronically controlled center coupler that allows for torque transfer from the front wheels to the rear wheels and a rear electronically limited slip differential. An upper controller was used to determine the required yaw moment, and a lower controller provided the torque biasing level. A proportional controller was used to transfer torque from front to rear wheels when the vehicle is understeering, and another proportional controller was used to bias torque at the rear ELSD when the vehicle was oversteering. In [31], a model

predictive controller was designed for yaw stability control using an electronic limited slip differential on the rear axle. The controller generated the differential torque command using a Coulomb friction model. The control objective was defined as tracking the desired yaw rate and sideslip angle, calculated based on steady-state cornering.

Lateral torque-vectoring differentials consist of two slip clutches, one for torque vectoring from right to left and the other one for torque vectoring from left to right, differential gears, and some planetary gears which generate the differential speeds of the slip clutches. In [28], the maximum acceptable differential speed ratio was introduced as a design parameter to analyze the lateral torque-vectoring differentials. The differential speed ratio caused by vehicle cornering was shown to be proportional to the inverse of the cornering radius.

2.2 Indirect Yaw Control

The indirect yaw moment control refers to the corrective yaw moments achieved by control of lateral forces. Active steering control is an indirect yaw moment control method, and it can enhance lateral vehicle dynamics and steerability by directly adjusting tire slip angles and thus the lateral tire forces. Active steering can be used both in the front axle (active front steering) and in the rear axle (active rear steering). Active front steering is used to provide an additive steering angle that is added to the driver's steering input at the front wheels to achieve the desired performance. Active rear steering is used to turn the rear wheels of a vehicle to improve high-speed stability and low-speed agility. The authority of active steering is limited by tire saturation. When the lateral tire force saturates, further increase in the wheel slip angle does not generate additional lateral force. In addition, steering systems are usually constrained to a few amounts of adjustability [32].

In [33], a pulse active steering system was developed for improving vehicle yaw stability. The pulse signals were sent to the steerable rear wheels whenever the yaw rate tracking error was more than a predefined threshold. In [34], a feedforward and feedback H-infinite controller was developed for vehicle handling improvement. The controller used a linear vehicle model including the yaw motion and disturbance input with speed and road adhesion variations. The applied control action was an additional steering angle based on the feedback of the yaw rate and the driver input.

In [35], a vehicle stability controller was proposed using active front steering system by applying the stable handling envelope in a model predictive control design. The proposed control method penalized exits from the safe envelope, deviation from the desired trajectory, and disruptive interventions. Although envelope control is a simple control method for vehicle stability, it requires the knowledge of friction coefficient, making a challenge for actual applications.

In [36], a Lyapunov based control allocation algorithm was proposed for vehicle yaw stabilization using active steering and adaptive braking systems. The control structure included three levels: high level, intermediate level, and low level. The high-level module generated the yaw rate reference for the vehicle motion control objective and tracking. The intermediate-level module was responsible for generating the longitudinal slip reference and commanding the front wheel steering angle corrections. Finally, the braking control for each wheel including the longitudinal slip control and maximal tire-road friction estimation was handled in the low-level module.

Another technique for indirect yaw moment control is torque shifting between the front and rear axles. Although left/right torque vectoring is an effective approach to improve the handling and stability of a vehicle, manufacturers may not use this actuation to decrease the cost, weight, and complexity for mass production. For instance, in all-wheel-drive electric vehicles, they may decide to equip the vehicle with an electric motor and an open differential per axle. In an open differential, torque is distributed equally between the left and right wheels, and therefore there is no torque vectoring. However, a significant yaw moment can be produced by controlling torque distribution between the front and rear axles, because of the indirect effect of the longitudinal forces on the lateral forces. This indirect effect arises from the longitudinal and lateral tire force coupling. Although the corrective yaw moment produced by the front/rear torque distribution is less than that of torque vectoring, it can considerably enhance the vehicle's handling response and stability.

While torque vectoring and differential braking have been studied extensively in the literature, fewer studies have investigated the contribution of the torque distribution between the front and rear axles in vehicle handling performance. The front/rear torque distribution has been investigated in both feedforward and feedback control schemes. In [37], a feedforward strategy was presented for front/rear torque distribution to improve the vehicle's lateral grip at handling limits. A quasi steady-state vehicle dynamic was used to saturate the front and rear axles at the same time by properly adjusting the torque distri-

bution. The study used the dynamic square method for evaluating the effect of front/rear torque distribution on the lateral grip margin. In [38] and [39], a yaw moment analysis was performed to identify the contributions of the longitudinal and lateral forces on the vehicle's handling characteristics for front-wheel-drive, rear-wheel-drive, and all-wheel-drive architectures. It was shown that the handling characteristics vary with the vehicle speed and front-to-rear wheel torque distribution. In [40], the capability of front/rear torque shifting in producing the vehicle body yaw moment was investigated. The effectiveness and the capacity of the yaw moment produced for different values of longitudinal acceleration were also examined in the study.

In [30], a simple strategy was used to overcome the vehicle's understeer behavior by transferring torque to the rear axle to provide indirect oversteering yaw moment. A similar strategy was used in [41] and [42] to improve yaw rate tracking using a simple PI controller. The controller shifted the torque to the front axle whenever the yaw rate response indicated oversteer behavior, thus inducing understeering and vice versa. In this method, the drive torques of the front and rear axles are adjusted to change the vehicle yaw rate before ESP intervention, while the driver torque demand remained unchanged. In [43], a feedback controller was designed for an all-wheel-drive vehicle with independent control of the drive torque on each wheel. A PI control strategy was implemented to adjust the front/rear torque distribution by applying yaw rate feedback and change the left/right distribution by using the lateral acceleration feedback. In [44, 45], a central differential was used with a small electric motor to distribute the driver's torque request between the front and rear axles. The study proposed a control allocation algorithm for following a desired yaw rate using the lateral stiffness of the tires. In this method, since the torque requests are calculated indirectly by using the stiffness of the tires, it is hard to consider the physical limits of actuators and tires.

2.3 Multi-Actuated Vehicle Control

The increasing requirements for safety along with the increasing level of vehicle actuation technologies encourage manufacturers to equip vehicles with multiple control actuations to improve vehicle handling and stability. However, despite such improvements in vehicle actuation capabilities, the best cost-performance strategy for optimally controlling multi-actuated vehicles is yet to be determined. Many studies in the literature propose a

combined use of control actuations for improving vehicle control performance. However, none of them propose a control structure for coordination or prioritization of the control actuations based on their advantages and disadvantages.

One of the common actuator combinations is combined use of active steering and differential braking. In [46], a model predictive controller was designed for vehicle lateral stability using coordinated active front steering and differential braking. The vehicle prediction model calculated the vehicle yaw rate, lateral velocity, and tire slip angles over the prediction horizon. The vehicle sideslip was enforced within a safe region using soft constraints on the lateral velocity to ensure that the optimization problem has always a feasible solution.

A feedback linearization method was used in [47] to design integrated vehicle stability control with active steering and braking systems. The designed controller mainly used the steering correction to achieve the control objective and employed braking correction only when it was necessary. Some other studies also investigated the integration of active steering with differential braking to improve vehicle handling performance and stability such as [48, 49, 50].

In [51], a coordinated control strategy was proposed to improve handling stability, safety, and ride comfort using a coordination among active steering, differential braking, and active suspension systems. Active front steering and differential braking were used to reduce respectively the yaw rate error and the sideslip error using sliding model control method. Active suspension was controlled using backstepping control method to decrease the effect of irregularities of the road and to improve the roll dynamics and ride comfort. A nonlinear tire model was used for vehicle modelling, and the actuator model was included in the control design.

In [52], a modular hierarchical controller was proposed for vehicle motion control using coordinated active steering and individual wheel torque control. A high-level sliding mode controller was designed to calculate the generalized forces/moments for satisfying the vehicle control objectives. Then, a control allocation method was used to efficiently distribute the control effort to the slip and slip angle of each wheel.

In [53], an integrated control of torque vectoring and differential braking was used to enhance vehicle directional stability and steerability. The corrective yaw moment was calculated using a constrained nonlinear controller with input and state constraints. The controller improved steerability by tracking the desired yaw rate and constrained the sideslip

within a safe region. Based on the designed integration policy, the controller initially uses active torque vectoring in the rear wheels to generate the required yaw moment. If active torque vectoring cannot generate all the required yaw moment, differential braking is activated in the front axle to compensate the limitation of active torque vectoring.

In [54], an adaptive feedback linearization control method was designed for vehicle handling control using the combination of active front steering with rear torque vectoring. The performance of the controller showed its robustness to parameter variations and external disturbances. In [55], an integrated control of active front steering and active roll moment systems was proposed to enhance the vehicle controllability in emergency situations. A robust sliding mode controller was designed for the active front steering system to improve yaw tracking performance. The active roll moment control system was used to resist the roll motion and also to improve the yaw rate performance by changing the difference between the normal forces of the front and rear axles.

In [56], a model predictive control design was proposed for improving vehicle yaw dynamics using a coordination of active front steering and differential braking. A piecewise affine approximation of the tire forces was used in the prediction model of a hybrid MPC control strategy. In [57], a control allocation algorithm was proposed for coordinating multiple vehicle subsystems including in-wheel electric motors, friction brake system, and wheel steer actuators to control vehicle motion. A high-level second-order sliding mode controller was designed to calculate the generalized demands of longitudinal forces, lateral forces, and yaw moment. A mid-level optimization-based control allocation was designed with restriction weights into the cost function to determine the priorities of the vehicle subsystems. Then, the calculated control actions were applied to the actuators using a low-level controller.

2.4 Roll Stability

Vehicle rollover is a serious safety problem for light vehicles. Rollover accidents are one of the most dangerous and fatal accidents [58]. There are two steps in rollover prevention of a vehicle. The first step is a proper detection of a rollover risk, and the second step is the development of a rollover mitigation technique. To determine an accurate measure about the rollover risk, different rollover indices have been proposed in the literature. In [59], some of the well-known rollover indices are compared under different rollover situations.

After choosing an appropriate rollover index, a rollover prevention controller should be designed. The rollover prevention techniques can directly or indirectly influence the roll motion and rollover behavior [60]. Active suspensions and active anti-roll bars directly influence the roll motion. The indirect effect on roll motion is achieved by actuation systems that control the planar motion such as differential braking and torque vectoring. Active suspension can directly affect the rollover behavior by controlling the lateral load transfer [61, 62]. Differential braking and active front steering can be employed for indirect control of rollover by reducing the lateral acceleration [63, 64]. This technique, however, may result in the loss of maneuverability [60, 61]. Lateral acceleration is the most dominant factor for rollovers on flat roads. Therefore, the most common technique for rollover mitigation is to decrease the lateral acceleration by controlling the vehicle's yaw rate.

Uneven roads are also another reason for rollover. The road bank angle directly affects rollover risk. Road disturbances such as road bumps and curbs may also result in vehicle rollover. In this regard, vehicle rollovers are categorized into two main types: un-tripped rollovers and tripped rollovers [65]. A rollover caused by fast maneuvering on smooth roads is named an un-tripped rollover. On the other hand, a tripped rollover refers to a rollover caused by sudden impacts that may apply lateral or vertical forces to the vehicle, e.g., hitting curbs or bumps.

In [66], a reconfigurable integrated control design was proposed for integrated control of lateral stability, rollover prevention, and the longitudinal slip. The designed control structure was reconfigurable for different types and combinations of actuators including torque vectoring, differential braking, and active steering for three-wheeled as well as four-wheeled vehicles without reformulating the problem. In [67], a model predictive controller was designed for rollover prevention using active front steering. A new rollover index was presented by vehicle parameters and state variables to be capable of being incorporated into the MPC cost function. The effects of lateral load transfer and the road bank were considered in vehicle modelling to provide an appropriate control action when it is necessary.

In [68], an integrated vehicle lateral and roll stability control was designed for narrow tilting vehicles. A high-level controller was designed to manage vehicle stability and control energy consumption. The calculated forces were then distributed to available actuators using a reconfigurable control allocation. In [69], an MPC controller was designed for integrated control of longitudinal slip, lateral stability, handling improvement, and rollover

prevention using torque vectoring. The interactions of different stability objectives were considered in the controller, and an optimal solution was calculated by including all objectives, simultaneously. Barrier functions were used to confine the vehicle states within their safety limits.

In [70], un-tripped vehicle rollover was controlled using a model predictive control design via torque vectoring. The vehicle roll angle was estimated in real-time using an observer on a combined model of vehicle kinematics and roll dynamics. The controller used a soft constraint to enforce the roll index within the predefined safe region and prevent rollover. In [71], a new rollover index was developed to predict the risk of vehicle rollover under both un-tripped and special tripped situations. An H-infinity controller with electro-hydraulic brake system was used to improve the rollover prevention performance of the vehicle. The robustness and stability of the active rollover prevention control system were analyzed using CarSim simulations.

In [72], a multivariable adaptive sliding mode control design was proposed for the purpose of lane keeping control and rollover prevention in the presence of disturbances with unknown bound. To ensure the vehicle roll stability, the load transfer ratio (LTR) was restricted within a safe region using a barrier function. Moreover, the transient response of the closed-loop system was improved by adaptively modifying the damping ratio of the system.

Because of the delay of active braking actuators, a vehicle with a traditional stability control system may be in danger of sideslip or rollover. In [73], the adverse effect of time delay on vehicle stability control was mitigated using a three-dimensional dynamic stability controller designed for control of yaw stability, yaw-roll stability, and rollover prevention. A model predictive control design was used for calculating the tire forces of four wheels, and then a hydraulic pressure controller was designed to apply the tire forces.

2.5 Path Planning/Tracking and Collision Avoidance

The introduction of new sensing technologies like cameras and radar along with the actuation technologies such as active steering and active braking are making self-driving cars possible. The reliability and safety of autonomous vehicles are still a big research topic for academia and industry to ensure their acceptance by customers and regulatory bodies.

A complete autonomous vehicle system comprises perception, global planning, local path planning, vehicle model, and estimation as depicted in Fig. 2.1. The available sensors in the vehicle such as camera, GPS, and IMU prepare the required data for the perception module [74]. The perception module provides the necessary environmental information like obstacles for the local path planning controller [75]. This environmental information with the vehicle states and tire forces calculated by the estimation module [76, 77] enables the local path planning controller to plan a path that best follows a desired path generated by the global planning module. In this thesis, the environmental information such as obstacle locations and road boundaries and curvature from the perception module, the vehicle states and tire forces from the estimation module [78, 79], and the desired path from the global planning module are supposed to be known and given to the local path planning module.

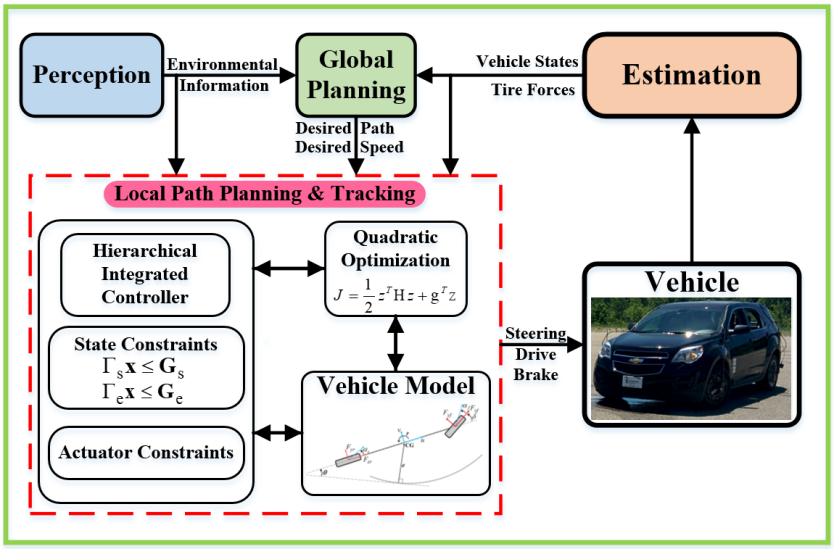

Figure 2.1: Autonomous system architecture.

In an autonomous vehicle, the controller usually is composed of a path planner and a path tracker. The path planner generates a desired path using the given information by perception systems, and the path tracker calculates the required control action for tracking the desired path. If the vehicle cannot follow the planned path perfectly, environmental information about where it is safe to deviate from the desired path should be given.

One of the most challenging missions for an autonomous vehicle is to plan an appropriate collision-avoidance path in emergency scenarios when an obstacle such as a deer suddenly appears in the middle of the road [80]. In such conditions, an autonomous vehicle is expected to be capable of making the best decision and optimally using available control actuations and tire forces to properly swerve and avoid any collision. This problem, however, can become more difficult when the planned path for swerving requires friction forces near the tires' saturation limits.

Many researchers utilize a path planner to generate a collision-free trajectory and a tracking controller to guide the vehicle along the planned path [81, 82, 83]. They have proposed different methods for path planning, such as the smooth curve planner [84], neural-network-based [85] and fuzzy-based control [86], artificial potential field [87, 88], and optimal control methods [89, 90]. Smooth curve planning methods implement different techniques for path smoothing and curve generation, such as spline curves [91] and Bezier curves [92]. The curve planning methods generate smooth and obstacle-avoiding paths by considering feasibility, comfort, and other safety parameters.

Fuzzy and neural-network-based methods are very useful in representing human knowledge in designing collision avoidance or collision warning algorithms [93]. For instance, in [94], a fuzzy control approach was proposed to avoid rear-end collisions in congested traffic situations. In [95], a fuzzy-control-based automatic lane-change system was designed for overtaking maneuvers when a slower vehicle appears in front of an autonomous vehicle. The lateral motion of an autonomous vehicle was controlled using adaptive-neural-network-based robust steering controller in [96].

In [97], a parallel motion planning approach was proposed to handle emergency situations. A deep planning model including a convolutional neural network combined with the Long Short-Term Memory module was designed to make the planning decisions. In addition, a parallel deep reinforcement learning technique was also employed to decrease the planning error and enhance its robustness.

The artificial potential field method is also used for path planning and obstacle avoidance in autonomous vehicles. This method considers the obstacle as a repulsive potential field added to the optimization cost function [98, 99, 100, 101]. In [101], a motion planning method was proposed to prevent collision with vulnerable obstacles like pedestrians when avoiding all obstacles is infeasible. A model predictive controller was used in this method by applying lexicographic optimization. A similar approach was employed in [102], and

ethical decision-making during inevitable crashes was included in the design by using rational ethics. Another approach for avoiding obstacles is constraining the vehicle position states in an obstacle-free region [103, 104, 105]. These methods require a nonlinear optimization solver because the cost function is nonlinear and nonconvex. The nonlinearity and non-convexity of this method make it unsuitable in terms of computational complexity and run time.

In [106], the artificial potential field method was employed for assigning different potential functions to different obstacles. The obstacle-free area was meshed and assigned resistance values in each edge based on the potential functions, and then a collision-free path was obtained using a local current comparison technique. Similar approach was used in [107], where different driver styles were also included such as conservative, moderate, and aggressive.

In emergency situations when a vehicle cannot safely track the planned path, built-in stability control systems may be relied on [108, 109]. However, this approach cannot ensure collision avoidance objectives because the stability controller modifies the control actions requested by the path tracking controller with no knowledge of an obstacle's position. This problem can be addressed by incorporating the stability controller and collision avoidance objective into the path tracking controller.

In [110], a model predictive control approach was used to integrate the local path planning, path tracking, and vehicle stability objectives. The controller used a long-enough prediction horizon that provides sufficient time to respond to dangerous situations that may arise. The planned trajectory was forced to remain inside two safe envelopes, while following the desired path. The first envelope used in the control design was the stability envelope, and the second one was related to environmental constraints. The controller addressed both environmental constraints and stability constraints; however, the preference was given to collision avoidance objective if stabilization actions were in conflict with the required actions for collision avoidance. A simple longitudinal controller was also used to calculate the required longitudinal forces for following a desired speed profile. This research was extended in [111] by using a variable time step prediction that included a correction time step between short time steps and long time steps to ensure that the stationary obstacles would not appear to move from the controller's perspective. Another extension was conducted in [112] by improving the accuracy of the model linearization.

In [113], a feedback-feedforward steering controller was proposed for vehicle stability

and path tracking at the limits of handling. The desirable path tracking behavior was achieved by aligning the steady-state vehicle sideslip with the desired path heading through the feedforward controller. The feedforward approach had no conflict with the robust stability properties of the feedback controller.

In [114], a shared steering controller was designed for vehicle stability and obstacle avoidance. The stability envelope and the environmental envelope were used for enforcing vehicle stability and obstacle avoidance, respectively. The controller was designed so as to intervene only when the vehicle trajectory exits the two safe envelopes. This approach made the shared controller minimally invasive with the driver while avoiding a collision and spinning out. Similar approaches were practiced in [115, 116].

In [117], a new path tracking controller was designed for autonomous vehicles at handling limits. It was discussed in the study that a slip angle-based steering controller is significantly less sensitive to the accuracy of friction estimation. This approach was inspired from the data collected from a race car driver to understand vehicle through slip angle control. In [118], a convex optimization method was presented for optimally allocating tire forces in an over-actuated vehicle. The approach was built based on the idea of equally using the total tire force capacity over all tires. This technique allowed to saturate all the tires at the same time, providing the vehicle with the full lateral grip. The optimal tire force allocation algorithm was combined with a trajectory tracking controller near the limits of handling to follow the desired longitudinal and lateral motions.

Most research done in autonomous vehicle path tracking employs front steering as the main actuation for controlling a vehicle's lateral dynamics. However, incorporating other actuators into the control system may improve the performance of autonomous vehicles, especially in emergency situations. In [119], a collision avoidance control system was designed using autonomous steering and differential braking. A feedforward controller was used to calculate the steering angle needed to guide a vehicle to the adjacent lane, and then an MPC controller was designed to track the centerline of this adjacent lane. A separate subsystem was used for differential braking to improve vehicle stability.

In [120], a model predictive controller was designed for autonomous vehicles by using combined braking and steering. The controller's objective was to track a reference path generated by a high-level controller. The stability constraint was considered in the control design, but the effect of deviations from the reference path forced by stability constraint, which may result in a collision, was not. This work was extended in [121] by adding active

differentials to front steering and braking to allow for controlling traction and braking forces at each corner independently. The extension enabled the controller to achieve better tracking performance without reducing the vehicle speed excessively.

In [122], a nonlinear model predictive controller was presented for a path tracking and obstacle avoidance problem using front steering and braking at the four wheels. To reduce the computational complexity of the optimization problem, an algorithm was designed for iterative linearization of vehicle dynamics and convexification of constraints. The experimental results conducted at high speeds on snow showed the controller's ability in avoiding a collision in emergency scenarios involving multiple obstacles.

In [123], two control methods were presented for tracking a given trajectory while maintaining collision avoidance in an autonomous vehicle using active front steering and differential braking. The first method was designed based on a single nonlinear MPC controller with a long prediction horizon. In the second method, a high-level controller was used to plan a trajectory that avoids the obstacle using a simple point-mass vehicle model. Then, at low-level, a model predictive controller was used to optimize the vehicle inputs based on a nonlinear vehicle model to best track the planned trajectory. It was shown that the two-level method performs better than the one-level approach at high speeds in terms of computation time.

In an emergency collision avoidance scenario, it is important to know how to properly and wisely use the available control inputs to prevent a collision as well as instability. If the collision avoidance constraint is in conflict with the stability constraint, the controller should carefully use the vehicle's actuators to guide it. For instance, differential braking can assist in improving yaw rate responsiveness but at the expense of a drop in the lateral force capacity. This indirect effect of longitudinal forces, known as force coupling effect, can exacerbate the problem if it is not considered. The force coupling effect can result in understeer or oversteer behavior by reducing the lateral forces of the front or rear axles, respectively, thereby affecting both the vehicle's stability and its capability to operate near the limits of handling. Therefore, integrating other actuators into autonomous vehicles should be done conservatively and wisely to improve vehicle performance. Doing so can provide an additional yaw moment necessary for preventing collisions.

2.6 Summary

In this chapter, the literature of vehicle stability control and vehicle path planning/tracking control was studied, with special attention to the multi-actuated vehicle control problem. The vehicle control actuations were divided into direct and indirect yaw control methods. The literature of direct yaw control actuations such as differential braking and left/right torque distribution were investigated in Section 2.1. Different methods of generating left/right torque distribution including individual electric motors, electronic limited slip differentials, and torque vectoring differentials were discussed.

The literature of the indirect yaw control actuations including active front steering, active rear steering, and front/rear torque shifting was investigated in Section 2.2. It was discussed that the indirect yaw control is the corrective yaw moment generated by control of lateral forces. The control of front/rear torque shifting generates a significant yaw moment due to the effect of longitudinal forces on the lateral forces. The front/rear torque distribution is one of the main control actuations studied in this thesis, which can make a considerable improvement in vehicle's handling response and stability.

In Section 2.3, the literature of combining vehicle actuations for improving vehicle stability was investigated. The existing research mostly offers an actuator coordination by sharing the required control effort between the actuators, and none of them propose a priority structure between the actuations. In addition, the vehicle control problem can have different control objectives which can be prioritized based on their importance. Therefore, this thesis studies the multi-actuation multi-objective vehicle control problem and aims to develop a prioritization control structure for this problem. Model predictive control method is adopted in this thesis due to its undeniable advantages and its capability to properly consider several actuations and several objectives within the control design.

In Section 2.4, the importance of including the rollover prevention objective into the control design was discussed, and the related literature was investigated. In addition, the effect of road angles on vehicle stability was illustrated. In this thesis, the roll dynamics and the effect of road angles on vehicle dynamics are included in the controller design.

In Section 2.5, the literature of vehicle path planning/tracking and collision avoidance controller design was investigated. In the literature, different methods have been employed for path planning/tracking control design. In this thesis, LTV MPC control method is employed for local path planning/tracking because of its capability to properly integrate

vehicle stability and path planning/tracking control objectives. The existing research does not provide an appropriate method for collision avoidance in multi-actuated autonomous vehicles. Therefore, this thesis focuses on an integrated control design to incorporate torque/brake vectoring for improving the lateral agility of autonomous vehicles in emergency collision avoidance scenarios.

Chapter 3

Prioritization Model Predictive Control Design for Multi-Actuated Vehicles

In this chapter, a prioritization model predictive control design is proposed for a multi-actuation multi-objective vehicle control problem capable of working up to handling limits. The proposed design first prioritizes the control actuations and the control objectives, and then combines the actuator priorities and the objective priorities such that the low priority actuation is activated only when the high priority objective demands it. This prioritization control scheme considers the actuator and state constraints within the prediction horizon. The control actuations studied in this chapter are front/rear torque distribution, ELSD, and differential braking.

This chapter is structured as follows. First, the effect of road angles on vehicle chassis dynamics is fully modeled using successive rotations of coordinate axes. Next, a coupled force vehicle prediction model is developed including the lateral motion, yaw motion, and roll motion. Then, an ELSD model is designed to properly predict ELSD clutch torque distribution. Next, a prioritization model predictive controller is developed for a multi-actuation multi-objective control problem. Then, this prioritization control scheme is illustrated for three different case studies. Finally, actuator constraints, state constraints, and the desired vehicle response are illustrated.

3.1 Road Angles' Effect on Vehicle Chassis Dynamics

Road angles can significantly affect vehicle dynamics. In this section, the effect of road angles on vehicle chassis dynamics is fully modeled using successive rotations of vehicle body's coordinate axes. To do so, four rotations are defined with the sequence of 1) road direction ψ_r, 2) road grade θ_r, 3) road bank ϕ_r, and 4) vehicle's heading deviation $\Delta\psi$, as shown in Fig. 3.1. In fact, the first three coordinate rotations are associated with the rotation of the road surface, and the last one is related to the rotation of the vehicle body on the road surface. These successive rotations can be represented as below:

$$\left(\hat{I}, \hat{J}, \hat{K}\right) \rightarrow \left(\hat{i}_1, \hat{j}_1, \hat{k}_1\right), \; R_Z(\psi_r) = \begin{bmatrix} \cos\psi_r & -\sin\psi_r & 0 \\ \sin\psi_r & \cos\psi_r & 0 \\ 0 & 0 & 1 \end{bmatrix}, \tag{3.1}$$

$$\left(\hat{i}_1, \hat{j}_1, \hat{k}_1\right) \rightarrow \left(\hat{i}_2, \hat{j}_2, \hat{k}_2\right), \; R_{y_1}(\theta_r) = \begin{bmatrix} \cos\theta_r & 0 & \sin\theta_r \\ 0 & 1 & 0 \\ -\sin\theta_r & 0 & \cos\theta_r \end{bmatrix}, \tag{3.2}$$

$$\left(\hat{i}_2, \hat{j}_2, \hat{k}_2\right) \rightarrow \left(\hat{i}_3, \hat{j}_3, \hat{k}_3\right), \; R_{x_2}(\phi_r) = \begin{bmatrix} 1 & 0 & 0 \\ 0 & \cos\phi_r & -\sin\phi_r \\ 0 & \sin\phi_r & \cos\phi_r \end{bmatrix}, \tag{3.3}$$

$$\left(\hat{i}_3, \hat{j}_3, \hat{k}_3\right) \rightarrow \left(\hat{i}, \hat{j}, \hat{k}\right), \; R_{z_3}(\Delta\psi) = \begin{bmatrix} \cos\Delta\psi & -\sin\Delta\psi & 0 \\ \sin\Delta\psi & \cos\Delta\psi & 0 \\ 0 & 0 & 1 \end{bmatrix}. \tag{3.4}$$

The total rotational velocity of the vehicle, $\vec{\omega}$, can be obtained by summing the four rotations as:

$$\vec{\omega} = \left(\kappa\,\hat{k}_1 + \lambda_\theta\,\hat{j}_2 + \lambda_\phi\,\hat{i}_3\right) u + \Delta\dot{\psi}\,\hat{k}, \tag{3.5}$$

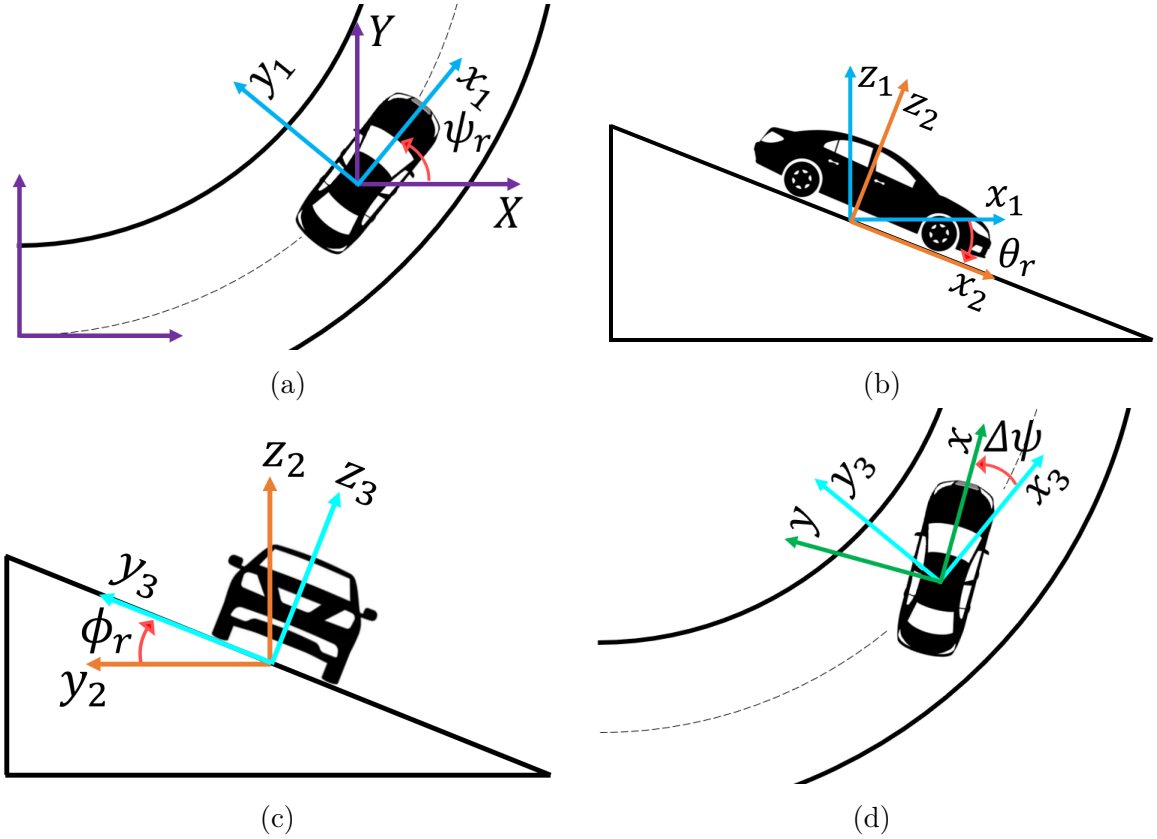

(a) (b) (c) (d)

Figure 3.1: Successive rotations of vehicle body's coordinate axes, (a) road direction ψ_r, (b) road grade θ_r, (c) road bank ϕ_r, and (d) vehicle's heading deviation $\Delta\psi$.

where u is the vehicle's longitudinal velocity; and κ, λ_θ, and λ_ϕ are respectively the variations of the road direction, grade, and bank angles with respect to the arc length s, which are calculated as:

$$\kappa = \frac{\partial \psi_r}{\partial s}, \tag{3.6}$$

$$\lambda_\theta = \frac{\partial \theta_r}{\partial s}, \tag{3.7}$$

$$\lambda_\phi = \frac{\partial \phi}{\partial s}. \tag{3.8}$$

Although the effect of road grade derivative, λ_θ, and road bank derivative, λ_ϕ, may be considerable for race car driving, their magnitudes are mostly negligible compared to the other terms. Therefore, the vehicle's rotational velocity can be simplified to:

$$\vec{\omega} = \kappa u \, \hat{k}_1 + \Delta\dot{\psi} \, \hat{k}. \tag{3.9}$$

The rotation transformation matrix R that relates the global coordinate system with the vehicle body coordinate system can be obtained as:

$$R = R_Z(\psi_r) \, R_{y_1}(\theta_r) \, R_{x_2}(\phi_r) \, R_{z_3}(\Delta\psi). \tag{3.10}$$

Using Eq. (3.10) to substitute for $\hat{k}_1$ in Eq. (3.9) and making small angle assumption for the vehicle's heading deviation give the vehicle's rotational velocity in the vehicle body coordinate system as:

$$\begin{aligned}\vec{\omega} = {} & (\kappa u \sin\theta_r - \kappa u \cos\theta_r \sin\phi_r \Delta\psi) \, \hat{i} - (\kappa u \sin\theta_r \Delta\psi + \kappa u \cos\theta_r \sin\phi_r) \, \hat{j} \\ & + \left(\kappa u \cos\theta_r \cos\phi_r + \Delta\dot{\psi}\right) \hat{k}.\end{aligned} \tag{3.11}$$

The vehicle's linear velocity in the vehicle body coordinate system can be written as:

$$\vec{\nu} = u \, \hat{i} + v \, \hat{j}. \tag{3.12}$$

Then, the vehicle's linear acceleration can be obtained by taking the derivative of the linear velocity, $\vec{\nu}$, as:

$$\vec{a} = \dot{\vec{\nu}} = \dot{u} \, \hat{i} + \dot{v} \, \hat{j} + u \, \dot{\hat{i}} + v \, \dot{\hat{j}}, \tag{3.13}$$

where $\dot{\hat{i}} = \vec{\omega} \times \hat{i}$ and $\dot{\hat{j}} = \vec{\omega} \times \hat{j}$. Using Eq. (3.11), the components of the vehicle's linear acceleration can be calculated as:

$$a_x = \dot{u} - v \left(\kappa u \cos\theta_r \cos\phi_r + \Delta\dot{\psi}\right), \tag{3.14}$$

$$a_y = \dot{v} + u \left(\kappa u \cos\theta_r \cos\phi_r + \Delta\dot{\psi}\right), \tag{3.15}$$

$$a_z = -\kappa u^2 \left(\cos\theta_r \sin\phi_r + \sin\theta_r \Delta\psi\right) - \kappa u v \left(\sin\theta_r - \cos\theta_r \sin\phi_r \Delta\psi\right). \tag{3.16}$$

Knowing that the vehicle's yaw rate is $r = \omega_z = \kappa u \cos\theta_r \cos\phi_r + \Delta\dot{\psi}$, the longitudinal and lateral accelerations can be simplified to $a_x = \dot{u} - vr$ and $a_y = \dot{v} + ur$. Moreover, considering that $v/u \ll 1$, and assuming that $\Delta\psi \approx 0$ results in $a_z = -\kappa u^2 \cos\theta_r \sin\phi_r$. The above equations are used in the rest of this thesis.

3.2 Vehicle Prediction Model

The variations of the road friction coefficient can excite and affect the vehicle's lateral dynamics and roll dynamics in a different way. In a low friction surface, the chance of vehicle lateral instability is more than vehicle roll-over. However, the chance of vehicle roll-over compared to lateral instability increases by increasing the road friction, especially for SUVs as they have a higher CG location. The integration of vehicle lateral and roll stability objectives enables the controller to ensure that both the control objectives are addressed in any condition. The other control objective in vehicle control problem is wheel stability. In this thesis, however, it is assumed that the wheel stability control is performed by a separate controller to prevent wheel spinout or locking which is not the focus of this study.

The model predictive control design needs a prediction model. The vehicle prediction model is created using a double track vehicle model (Fig. 3.2) and includes the lateral motion, yaw motion, and roll motion. Longitudinal velocity, u, is considered constant over the prediction horizon of the MPC controller. The dynamic equations of the vehicle's sideslip, β, yaw rate, r, and roll angle, ϕ, are expressed as:

$$\dot{\beta} = \frac{m_s h_s}{mu}\left(\frac{m_s g h_s \cos\phi_r \cos\theta_r - k_\phi}{I_c}\phi - \frac{c_\phi}{I_c}\dot{\phi}\right) - r + \frac{1}{mu}\left(1 + \frac{m_s^2 h_s^2}{m I_c}\right) F_Y - \frac{g}{u}\sin\phi_r \cos\theta_r, \tag{3.17}$$

$$\dot{r} = \frac{1}{I_z}\left(l_f F_{yf}\cos(\delta) - l_r F_{yr} + l_f F_{xf}\sin(\delta) + M_{DY}\right), \tag{3.18}$$

$$\ddot{\phi} = \frac{m_s g h_s \cos\phi_r \cos\theta_r - k_\phi}{I_c}\phi - \frac{c_\phi}{I_c}\dot{\phi} + \frac{m_s h_s}{m I_c} F_Y, \tag{3.19}$$

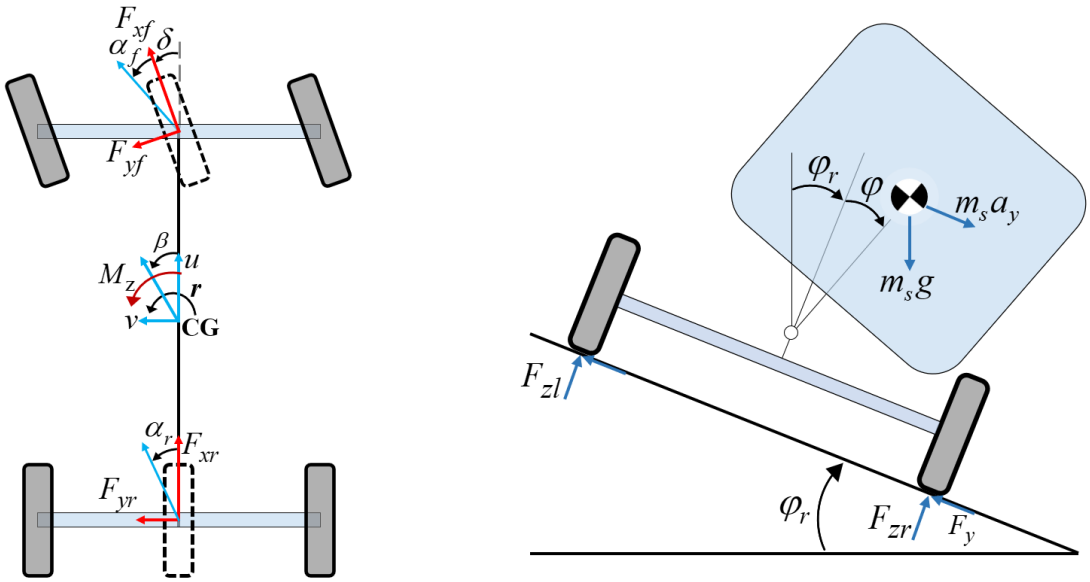

(a) (b)

Figure 3.2: Vehicle model diagram, (a) top view, (b) back view.

with $F_Y = F_{yf}\cos(\delta) + F_{xf}\sin(\delta) + F_{yr}$, and $I_c = I_{x,s} - m_s^2 h_s^2/m$, where m_s and m are the sprung and total mass of the vehicle; l_f and l_r are respectively the distances between the vehicle's CG and the front and rear axles; I_z is the vehicle's inertia about the yaw axis; $I_{x,s}$ is the vehicle's roll inertia about the roll axis; k_ϕ and c_ϕ are the equivalent roll stiffness and roll damping of the vehicle; ϕ_r and θ_r are respectively the road bank and grade angles; h_s is the distance from the roll center to the CG of the sprung mass; g is the gravitational acceleration; and M_{DY} is the direct corrective yaw moment.

One of the control actuations used in this thesis is front/rear torque shifting. This actuation makes an indirect control of the lateral forces achieved by adjusting the applied longitudinal forces to the front and rear axles. This indirect effect of longitudinal forces on lateral forces is due to the force coupling effect [124] and the tires' combined slip effect [125]. Developing a combined-slip prediction model requires a tire model that considers this effect. However, combined slip tire models have a lot of parameters that need to be estimated [126]. In addition, they need an accurate estimation of slip ratio, which may not be available. Therefore, to avoid these challenges and complexities, the force coupling effect is modeled using a brush tire model that captures the effect of the longitudinal force

on the lateral force [127]:

$$F_y = \begin{cases} -C_\alpha \tan\alpha + \frac{C_\alpha^2}{3\xi\mu F_z}|\tan\alpha|\tan\alpha - \frac{C_\alpha^3}{27\xi^2\mu^2 F_z^2}\tan^3\alpha & |\alpha| < \alpha_{sl}, \\ -\xi\mu F_z \operatorname{sign}\alpha & |\alpha| \geq \alpha_{sl}, \end{cases} \tag{3.20}$$
$$\alpha_{sl} = \arctan\frac{3\xi\mu F_z}{C_\alpha},$$

where C_α is the tire cornering stiffness; F_z is the tire normal load; α is slip angle; and ξ is a derating factor representing the remaining lateral force capacity based on the friction limit circle:

$$\xi = \sqrt{1 - \left(\frac{F_x}{\mu F_z}\right)^2}. \tag{3.21}$$

The longitudinal forces are assumed to be linearly proportional to the torques exerted on the wheels $F_x = Q/R_e$. The front and rear tires' slip angles are calculated as follows:

$$\alpha_f = \frac{v + l_f r}{u} - \delta, \quad \alpha_r = \frac{v - l_r r}{u}. \tag{3.22}$$

The nonlinear plant dynamics is successively linearized at each time step to allow for the real-time implementation of the MPC controller using a convex quadratic optimization problem. This linear time-varying model is obtained by linearizing the tire's nonlinear behavior around its operating points. To linearize the nonlinear model, the partial derivatives of the lateral force with respect to slip angle and derating factor are calculated. These partial derivatives create an affine expression for F_{yi} as follows:

$$F_{yi} = \bar{F}_{yi} + \bar{C}_{\alpha_i}\left(\alpha_i - \bar{\alpha}_i\right) + \bar{C}_{\xi_i}\left(\xi_i - \bar{\xi}_i\right), \tag{3.23}$$

where $\bar{F}_{yi}$, $\bar{\alpha}_i$, and $\bar{\xi}_i$ are the calculated lateral force, slip angle, and derating factor at the operating time; $\bar{C}_{\alpha_i}$ and $\bar{C}_{\xi_i}$ are sensitivity of the lateral force with respect to slip angle and derating factor, respectively, at the operating time, shown in Fig. 3.3 and calculated as follows:

$$\bar{C}_{\alpha_i} = \frac{\partial F_{yi}}{\partial \alpha_i}|_{\bar{\alpha}_i,\bar{\xi}_i}, \bar{C}_{\xi_i} = \frac{\partial F_{yi}}{\partial \xi_i}|_{\bar{\alpha}_i,\bar{\xi}_i}. \tag{3.24}$$

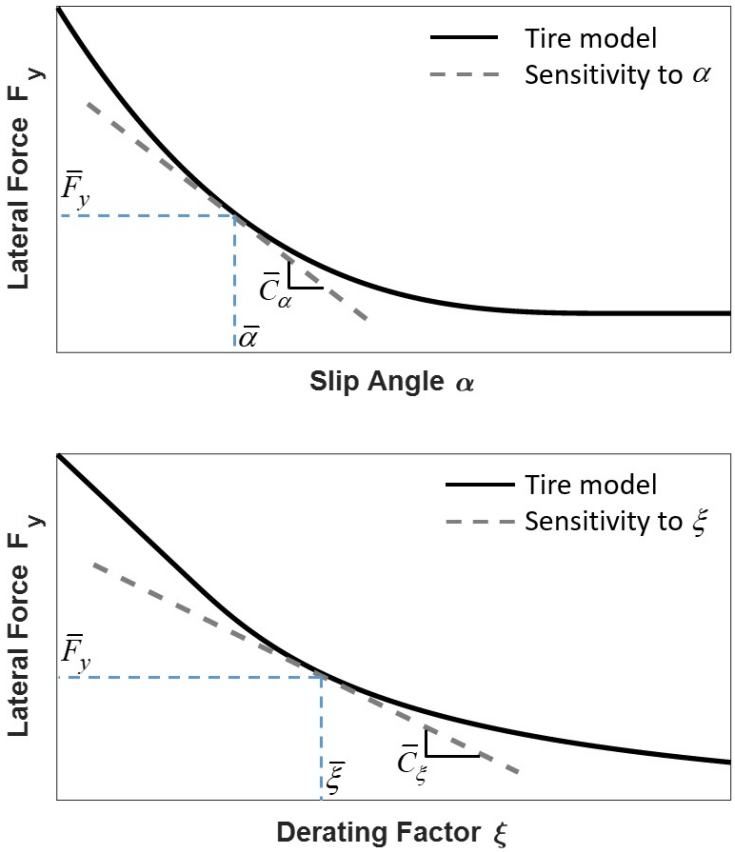

Figure 3.3: Linearization of the tire model with respect to (a) slip angle α and (b) derating factor ξ.

By taking successive partial derivatives, the derived affine equation for lateral force (Eq. (3.23)) can be rewritten in terms of axle torque as:

$$F_{yi} = \bar{F}_{yi} + \bar{C}_{\alpha_i}\left(\alpha_i - \bar{\alpha}_i\right) + \bar{C}_{Q_i}\left(Q_i - \bar{Q}_i\right), \tag{3.25}$$

where $\bar{C}_{Q_i}$ is the sensitivity of the lateral force with respect to the axle's torque at the operating time, defined as:

$$\bar{C}_{Q_i} = \left[\frac{\partial F_{yi}}{\partial \xi_i}\frac{\partial \xi_i}{\partial F_{xi}}\frac{\partial F_{xi}}{\partial Q_i}\right]_{\bar{\alpha}_i,\bar{\xi}_i}. \tag{3.26}$$

The coefficients $\bar{C}_\alpha$ and $\bar{C}_Q$ are updated at each time step. Figure 3.4 shows $\bar{C}_\alpha$ and $\bar{C}_Q$ versus slip angle α for different values of ξ. It can be seen that $\bar{C}_\alpha$ decreases by decreasing the value of ξ. The absolute value of $\bar{C}_Q$ increases from zero to its maximum when α increases from zero to the saturation point. Also, decreasing the value of ξ increases the magnitude of $\bar{C}_Q$, meaning that the sensitivity of the lateral force to the changes in the applied torque increases by decreasing ξ. In other words, the lateral force drop achieved by changing the axle torque from $Q_1 = 0$ to $Q_2 = \delta Q$ is much less than that achieved by changing the axle torque from $Q_1 = \bar{Q}$ to $Q_2 = \bar{Q} + \delta Q$, where δQ is a small variation in torque.

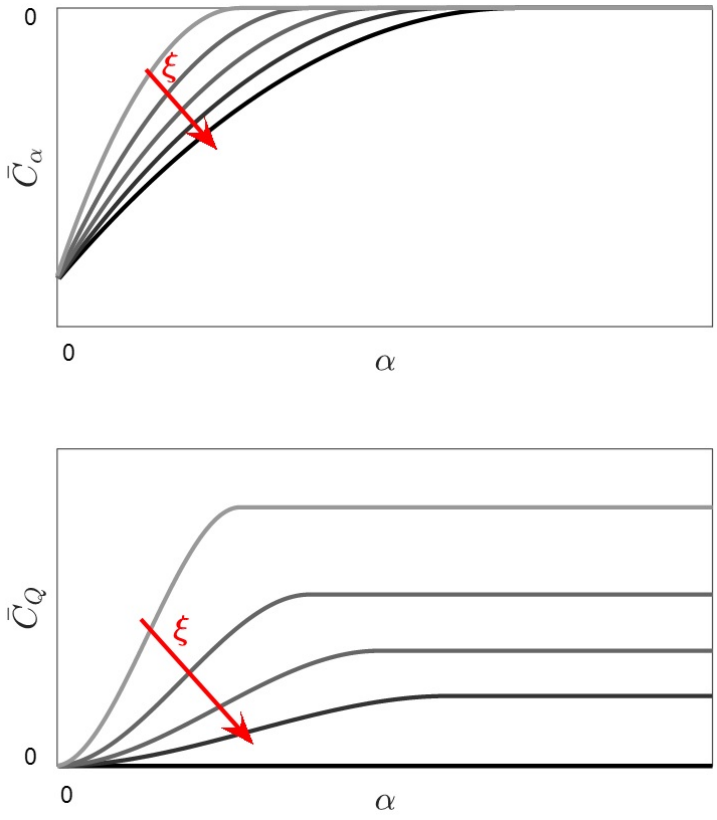

Figure 3.4: Variations of (a) $\bar{C}_\alpha$ and (b) $\bar{C}_Q$ versus α for different values of $\xi = 0.2, 0.4, 0.6, 0.8, 1$.

The capability of front/rear torque distribution in generating corrective yaw moments is highly dependent to the total requested drive torque. Figure 3.5 schematically visualizes

the variations of the yaw moment produced by front/rear torque distribution for different drive torque levels. This figure shows how the available yaw moment capacity, produced by torque distribution between the front and rear axles, changes with an increase in the total drive torque. This yaw moment capacity increases when the drive torque increases up to an optimum point and then starts decreasing. The maximum yaw moment capacity $\Delta M_{z,max}$ is achieved when the total drive torque is able to saturate either the front or the rear axle. For the input torque of Q_d^1, the body yaw moment can decrease from M_z^1 to M_z^2 by transferring torque from one axle to the other. Increasing the driver torque to Q_d^3 can provide more authority on the yaw moment and increase the window of achievable yaw moments.

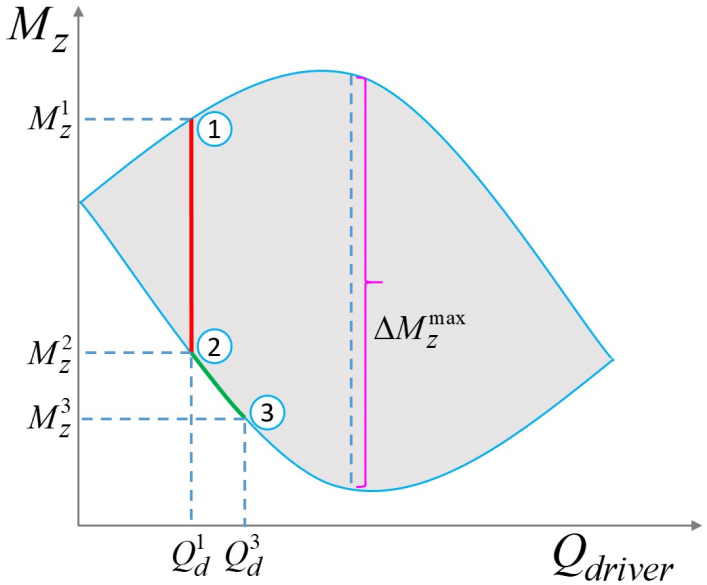

Figure 3.5: The yaw moment capacity produced by front/rear torque distribution versus driver torque.

Substituting Eq. (3.25) into Eqs. (3.17) to (3.19) for the front and rear lateral forces, using Eq. (3.22) for the slip angles, and rewriting the equations in state space form gives:

$$\dot{\mathbf{x}} = \mathbf{A}\mathbf{x} + \mathbf{B}\mathbf{u} + \mathbf{d}, \tag{3.27}$$

with $\mathbf{x} = [\beta, r, \phi, \dot{\phi}]^T$, $\mathbf{u} = [Q_f, M_{DY}]^T$, and

$$\mathbf{A} = \begin{bmatrix} \mathbf{A_{11}} & \mathbf{A_{12}} \\ \mathbf{A_{21}} & \mathbf{A_{22}} \end{bmatrix},$$

$$\mathbf{A_{11}} = \begin{bmatrix} \left(1 + \frac{m_s^2 h_s^2}{m I_c}\right) \frac{\bar{C}_{\alpha_f} \cos\delta + \bar{C}_{\alpha_r}}{mu} & \left(1 + \frac{m_s^2 h_s^2}{m I_c}\right) \frac{l_f \bar{C}_{\alpha_f} \cos\delta - l_r \bar{C}_{\alpha_r}}{mu^2} - 1 \\ \frac{l_f \bar{C}_{\alpha_f} \cos\delta - l_r \bar{C}_{\alpha_r}}{I_z} & \frac{l_f^2 \bar{C}_{\alpha_f} \cos\delta + l_r^2 \bar{C}_{\alpha_r}}{I_z u} \end{bmatrix},$$

$$\mathbf{A_{12}} = \begin{bmatrix} \frac{m_s h_s \left(m_s g h_s \cos\phi_r \cos\theta_r - k_\phi\right)}{mu I_c} & -\frac{m_s h_s c_\phi}{mu I_c} \\ 0 & 0 \end{bmatrix},$$

$$\mathbf{A_{21}} = \begin{bmatrix} 0 & 0 \\ \frac{m_s h_s \left(\bar{C}_{\alpha_f} \cos\delta + \bar{C}_{\alpha_r}\right)}{mu I_c} & \frac{m_s h_s \left(l_f \bar{C}_{\alpha_f} \cos\delta - l_r \bar{C}_{\alpha_r}\right)}{mu I_c} \end{bmatrix},$$

$$\mathbf{A_{22}} = \begin{bmatrix} 1 & 0 \\ \frac{m_s g h_s \cos\phi_r \cos\theta_r - k_\phi}{I_c} & -\frac{c_\phi}{I_c} \end{bmatrix},$$

$$\mathbf{B} = \begin{bmatrix} \frac{\bar{C}_{Q_f} \cos\delta - \bar{C}_{Q_r}}{mu} + \frac{\sin\delta}{muR_e} & 0 \\ \frac{l_f \bar{C}_{Q_f} \cos\delta + l_r \bar{C}_{Q_r}}{I_z} + \frac{l_f \sin\delta}{I_z R_e} & \frac{1}{I_z} \\ 0 & 0 \\ \frac{m_s h_s}{mu I_c}\left(\bar{C}_{Q_f} \cos\delta - \bar{C}_{Q_r} + \frac{\sin\delta}{R_e}\right) & 0 \end{bmatrix},$$

$$\mathbf{d} = \begin{bmatrix} \frac{\bar{F}_{y_f} \cos\delta + \bar{F}_{y_r} - \bar{C}_{\alpha_f} \bar{\alpha}_f \cos\delta - \bar{C}_{\alpha_r} \bar{\alpha}_r - \bar{C}_{Q_f} \bar{Q}_f \cos\delta - \bar{C}_{Q_r} \bar{Q}_r - \bar{C}_{\alpha_f} \delta \cos\delta - mg \sin\phi_r \cos\theta_r}{mu} \\ \frac{l_f \bar{F}_{y_f} \cos\delta - l_r \bar{F}_{y_r} - l_f \bar{C}_{\alpha_f} \bar{\alpha}_f \cos\delta + l_r \bar{C}_{\alpha_r} \bar{\alpha}_r - l_f \bar{C}_{Q_f} \bar{Q}_f \cos\delta + l_r \bar{C}_{Q_r} \bar{Q}_r - l_f \bar{C}_{\alpha_f} \delta \cos\delta}{I_z} \\ 0 \\ \frac{m_s h_s \left(\bar{F}_{y_f} \cos\delta + \bar{F}_{y_r} - \bar{C}_{\alpha_f} \bar{\alpha}_f \cos\delta - \bar{C}_{\alpha_r} \bar{\alpha}_r - \bar{C}_{Q_f} \bar{Q}_f \cos\delta - \bar{C}_{Q_r} \bar{Q}_r - \bar{C}_{\alpha_f} \delta \cos\delta - mg \sin\phi_r \cos\theta_r\right)}{mu I_c} \end{bmatrix}.$$

The corrective direct yaw moment M_{DY} is the summation of the yaw moments generated by ELSD, the front differential braking, and the rear differential braking $M_{DY} = M_{ED} + M_{DBF} + M_{DBR}$, which are studied in this thesis.

Actuator Dynamics:

Vehicle actuation systems have inherent dynamics resulting in a delay from the actuation command to actuation effect. The inherent dynamics of actuation systems can be modeled using first-order models as [128, 129]:

$$u_i = \frac{1}{1 + \tau_i s} \tilde{u}_i, \tag{3.28}$$

where τ_i is the time constant, u_i is the actual control command, and $\tilde{u}_i$ is the requested control command. The actuator dynamics can be written as:

$$\dot{\mathbf{u}} = \mathbf{A}_\tau \mathbf{u} + \mathbf{B}_\tau \tilde{\mathbf{u}}, \tag{3.29}$$

with $\tilde{\mathbf{u}} = \left[\tilde{Q}_f, \tilde{M}_{DY}\right]^T$, $\mathbf{A}_\tau = \begin{bmatrix} -1/\tau_1 & 0 \\ 0 & -1/\tau_2 \end{bmatrix}$, and $\mathbf{B}_\tau = \begin{bmatrix} 1/\tau_1 & 0 \\ 0 & 1/\tau_2 \end{bmatrix}$.

To improve the accuracy and performance of the controller, the actuator dynamics is added to the vehicle dynamics, and an integrated dynamic equation is constructed as:

$$\begin{bmatrix} \dot{\mathbf{x}} \\ \dot{\mathbf{u}} \end{bmatrix} = \begin{bmatrix} \mathbf{A} & \mathbf{B} \\ 0 & \mathbf{A}_\tau \end{bmatrix} \begin{bmatrix} \mathbf{x} \\ \mathbf{u} \end{bmatrix} + \begin{bmatrix} 0 \\ \mathbf{B}_\tau \end{bmatrix} \tilde{\mathbf{u}} + \begin{bmatrix} \mathbf{d} \\ 0 \end{bmatrix}. \tag{3.30}$$

This augmented dynamic model is denoted as:

$$\dot{\mathbf{x}}_a = \mathbf{A}_a \mathbf{x}_a + \mathbf{B}_a \tilde{\mathbf{u}} + \mathbf{d}_a. \tag{3.31}$$

This continuous-time augmented model must be discretized to form a discrete-time model that can be implemented in an MPC controller. The discretization is performed using zero-order hold (ZOH) method and with the sampling time of t_s as:

$$\mathbf{x}_a(k+1) = \mathbf{A}_d \, \mathbf{x}_a(k) + \mathbf{B}_d \, \tilde{\mathbf{u}}(k) + \mathbf{d}_d, \tag{3.32}$$

where $\mathbf{A}_d = e^{\mathbf{A}_a t_s}$, $\mathbf{B}_d = \int_0^{t_s} e^{\mathbf{A}_a \tau} \mathbf{B}_a \, d\tau$, and $\mathbf{d}_d = \int_0^{t_s} e^{\mathbf{A}_a \tau} \mathbf{d}_a \, d\tau$. The vehicle prediction model developed in this section considers the longitudinal and lateral force coupling as well as the actuator dynamics. This coupled force prediction model is used in the MPC control design.

3.3 ELSD Model Development

An electronic limited slip differential has similar components to an open differential except that it can provide an additional path for torque transfer by a clutch. In an open differential, torque is distributed equally between the left and right wheels, and therefore there is no torque vectoring. An electronically controlled limited slip differential, however, can bias the shaft torque to right and left wheels. There are two main types of electronic limited slip differentials: electro-hydraulic limited slip differential [130] and electro-magnetic limited slip differential [131, 132]. The active differential studied in this thesis is an electro-hydraulic limited slip differential.

As discussed in the previous section, when the ELSD differential clutch is activated, it will try to make the speeds of the left and right wheels the same. Most studies assume that the speed of the outside wheel is always larger than the speed of the inner wheel while the vehicle is turning, because the outer wheel experiences a turn with a larger radius of curvature. As a result, if the ELSD differential clutch is activated, it is assumed to reduce the outer wheel speed and acceleration. Consequently, the device only transfers the driving torque from the outside wheel to the inside wheel [133]. Thus, a yaw moment is generated in the opposite direction to the turn, which increases the understeer tendency of the vehicle. This paper criticizes the assumptions made for ELSD functionality. The assumption that the speed of the outside wheel is larger than the inner wheel's speed may be inaccurate in some situations. The outside wheel can be assumed to be faster in off-throttle or low-throttle cases. However, the inner wheel may rotate faster in an on-throttle case, as is illustrated below.

Vehicle lateral acceleration during a turn reduces the normal load of inner wheels and increases the normal load of outside wheels. Therefore, if the axle torque is distributed equally between the inner and outside wheels (open differential), increasing the axle torque will decrease the difference between the outside wheel speed and the inner wheel speed, and it can even make the inner wheel rotate faster. The ELSD clutch torque capacity is

constrained by the maximum ELSD differential capability and the maximum friction force capacity between tires and road. Therefore, increasing the axle torque decreases the torque transfer capacity from the outside wheel to the inner wheel; eventually, it can also change the direction of the differential clutch torque from the inner wheel to the outer wheel when the inner wheel rotates faster. Thus, the ELSD differential clutch can also generate a yaw moment in the direction of the turn and increase a vehicle's oversteer tendency.

To better illustrate the point mentioned above, an open loop test result of an acceleration in turn maneuver is presented in Fig. 3.6. The ELSD differential is activated with 60 percent clutch pressure during the test. Figures 3.6a and 3.6b show the driver inputs, respectively steering angle and torque request to the rear axle. Figure 3.6c compares the vehicle yaw rate with the desired yaw rate; and Fig. 3.6d shows the ELSD clutch torque, which is the torque difference between the rear wheels $T_C = T_{rr} - T_{rl}$. It can be seen that the ELSD differential provides an understeering yaw moment between $t = 1s$ to $t = 3s$ that contributes to vehicle stability, but then the direction of the clutch torque changes between $t = 3s$ to $t = 4s$, generating an oversteering yaw moment, which triggers vehicle instability. Therefore, this test result clearly shows that an ELSD differential has the capability of generating an oversteering yaw moment and making a vehicle unstable, which necessitates developing an appropriate ELSD model that can predict clutch torque and avoid unwanted oversteering yaw moments.

Some studies assume an algebraic model for ELSD clutch torque such that the sign of the wheel speed difference determines whether the ELSD clutch torque is positive or negative, and they suppose that the maximum clutch torque capacity is always available and achievable [31, 134]. These assumptions, however, fail to correctly predict the magnitude and direction of clutch torque. One main problem is that they lead to chattering in the ELSD clutch when the wheel speed difference chatters around zero. In fact, wheel speed difference may chatter around zero without changing the direction of the differential torque, especially when the clutch is fully engaged.

Therefore, using an algebraic ELSD model based on the current wheel speed difference to design an ELSD controller is not logical. To capture the dynamic behavior of the ELSD clutch, it can be modeled as a torsional spring-damper [30], as shown in Fig. 3.7, with the clutch torque, T_C, calculated as follows:

$$T_C = c_t \, \Delta\omega + \int k_t \, \Delta\omega \, dt, \tag{3.33}$$

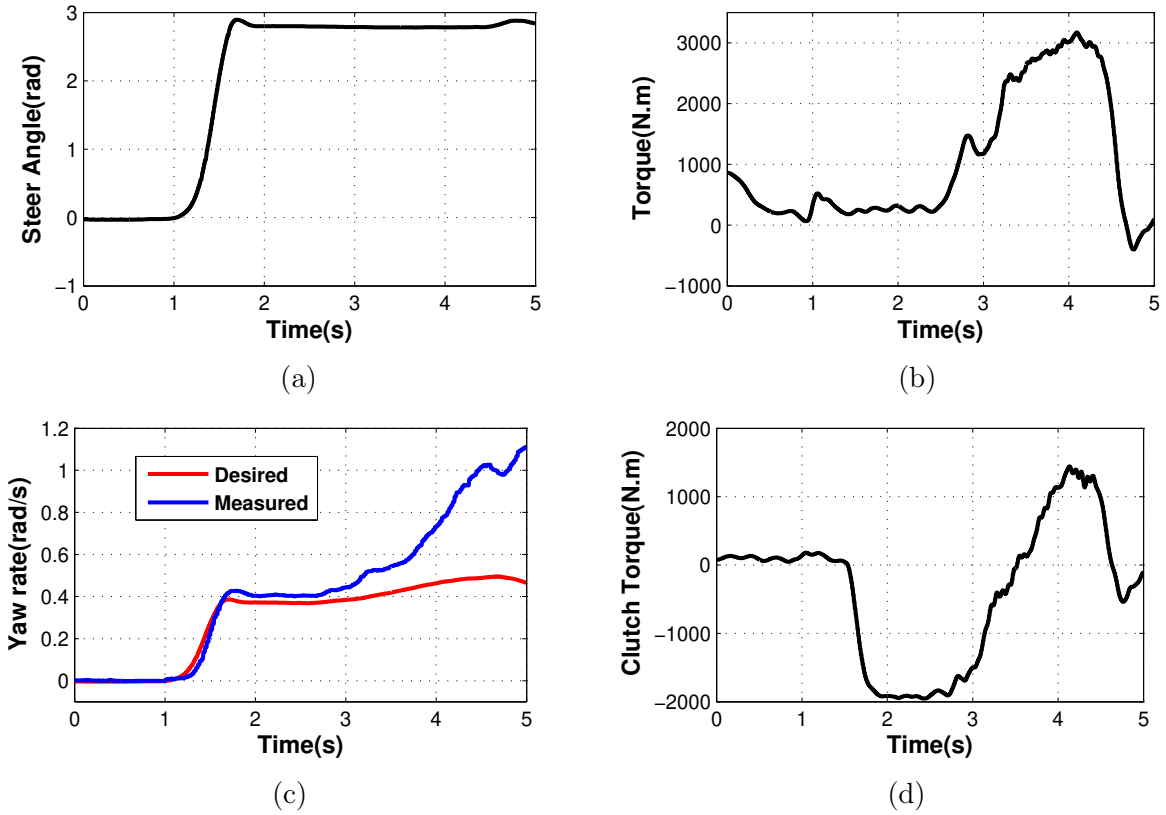

Figure 3.6: (a) Steer angle, (b) axle torque, (c) the vehicle yaw rate, and (d) the ELSD clutch torque in an acceleration in turn maneuver with 60 percent constant clutch pressure. The clutch torque provides both understeering and oversteering yaw moments.

where $\Delta\omega = \omega_{rr} - \omega_{rl}$ is the wheel speed difference, k_t and c_t are the clutch spring and damper coefficients, respectively. The above equation can be written in discrete form as:

$$T_C(t) = T_C(t - \Delta t) + k_t\, \Delta\omega(t)\, \Delta t + c_t\, (\Delta\omega(t) - \Delta\omega(t - \Delta t)), \tag{3.34}$$

In the spring-damper model, the spring element maintains a full history of the previous time steps by integrating the wheel speed difference over time. This integral term may cause an offset in the clutch torque by accumulating the potential errors in the model, especially at low clutch pressures when the clutch plates are not fully locked and are slipping. To remedy this issue, the clutch model presented in Eq. (3.34) can be modified as [135]:

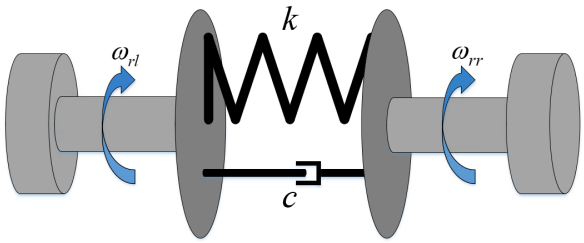

Figure 3.7: Schematic of ELSD model in the rear axle.

$$T_C(t) = (1 - \lambda_t \, \Delta t) T_C(t - \Delta t) + k_t \, \Delta\omega(t) \, \Delta t + c_t \, (\Delta\omega(t) - \Delta\omega(t - \Delta t)), \tag{3.35}$$

where the variable λ_t is introduced as a forgetting factor to allow any accumulated error to gradually fade away. The ELSD clutch torque is limited by the maximum torque capacity that the clutch plates can generate, $T_{C,lim}$, which is a function of the clutch pressure, P. The clutch torque is also constrained by the maximum torque bias, $T_{f,lim}$, that the friction force capacity between tires and road can provide. Thus, the clutch torque limit is expressed as:

$$|T_C| \leq \min(T_{C,lim} \, , \, T_{f,lim}), \tag{3.36}$$

The torque difference between the right and left wheels, $\Delta T_r = T_{rr} - T_{rl}$, can be obtained as follows:

$$\Delta T_r = T_C - (I_{s,rr} \dot{\omega}_{rr} - I_{s,rl} \dot{\omega}_{rl}), \tag{3.37}$$

where $I_{s,rr}$ and $I_{s,rl}$ are the right and left output shafts inertia. Neglecting the shafts inertia, the above equation can be simplified to $\Delta T_r = T_C$.

Variations of the clutch pressure affects the ELSD clutch torque, and consequently the parameters of the ELSD model including the clutch spring coefficient k_t, the damper coefficient c_t, the forgetting factor λ_t, and the clutch saturation limit $T_{C,lim}$. The clutch parameters are obtained by estimation using the data set collected from vehicle tests in different maneuvers with different clutch pressures. The estimated model parameters for different clutch pressures are shown in Table 3.1.

Table 3.1: ELSD Model Parameters.

Clutch Pressure(%)	k_t	c_t	λ_t	$T_{C,lim}[N.m]$
10	8000	400	0.75	330
20	8000	400	0.75	660
40	8700	300	0.5	1350
60	9200	100	0.2	1900
80	11000	50	0.1	2100

It should be noted that although the physical model of the ELSD may be very complicated, this simple model can successfully represent torque biasing dynamics and provide a reasonable prediction of the clutch torque. The performance of the developed ELSD model is evaluated using experimental data in the next chapter.

3.4 Actuator Constraints

The control actuations must be properly constrained in the optimization problem. Generally, there are two main constraints for the actuators in vehicle stability control. The first constraint is related to the maximum physical capability of the actuators. The other constraint is for the maximum friction force capacity between tires and the road.

The ELSD clutch pressure can vary between zero and fully locked. This constraint can be written as:

$$0 \leq P \leq 1. \tag{3.38}$$

The drive torque of the front axle is constrained by the maximum torque capability of the electric motors, $Q_{e,max}$, and the available friction force capacity, $\mu F_{z,f}$. The minimum value for the front drive torque is assumed to be zero. The rear drive torque is not an independent control actuation and is related to the front drive torque with an equality constraint as $Q_f + Q_r = Q_d$. However, the constraints of the rear drive torque must be properly addressed. Considering that $Q_r = Q_d - Q_f$ and $Q_f \leq Q_d$, the rear drive torque

always remains nonnegative, $Q_r \geq 0$. To ensure that the rear drive torque is smaller than its maximum allowable value, $Q_r \leq Q_{r,max}$, the minimum allowable value of the front drive torque is set to $Q_{f,min} = Q_d - Q_{r,max}$. Therefore, the front drive torque is constrained as:

$$Q_{f,min} \leq Q_f \leq Q_{f,max}, \tag{3.39}$$

where $Q_{f,max} = \min\left(Q_{e,max}, \mu F_{z,f}, Q_d\right)$, and $Q_{f,min} = Q_d - \min\left(Q_{e,max}, \mu F_{z,r}, Q_d\right)$.

The available friction force limit forms the basis for constraints on actuation of differential braking. A geometrical analysis of the tire force vector in the force limit circle is performed to obtain the maximum effective corner brake contribution to vehicle stability [136]. Differential braking is used only to improve vehicle stability; therefore, it is activated only in the opposite direction of the turn. Figure 3.8 shows tire force vectors inside the force limit circles at each corner. Figure 3.8a shows tire force vectors when no longitudinal force exists at the corners. Vehicle turns in the positive yaw direction (CCW) lead to braking action in the right corners, generating understeering yaw moment. Figure 3.8b sets out the optimum force vectors at the right corners for generating the maximum understeering yaw moment. If no longitudinal force is present, the front right corner generates oversteering yaw moment. With braking on the front right corner, the force vector direction changes so that the direction of yaw moment generated by this corner changes from oversteering to understeering. In this corner, the optimum force vector occurs when the braking force equals the corner's force limit, $\mu F_{z,fr}$. Therefore, the front differential braking can be constrained as:

$$|M_{DBF}| \leq M_{DBF,max}, \tag{3.40}$$

where $M_{DBF,max} = \frac{l_s}{2}\left(\mu F_{z,fr} + \frac{Q_f}{2R_e}\right)$.

The rear right corner already provides an understeering yaw moment without braking action.The optimum force vector in this corner, which generates the maximum understeering yaw moment, is perpendicular to the line drawn between the vehicle CG and the center of the corner because it has the largest moment arm. This optimum force vector is comprised of a lateral force and a longitudinal braking force. Thus, the optimum braking force can be obtained as:

$$F_{b,rr}^{op} = \mu F_{z,rr} \frac{l_s}{2\sqrt{l_r^2 + \frac{l_s^2}{4}}}. \tag{3.41}$$

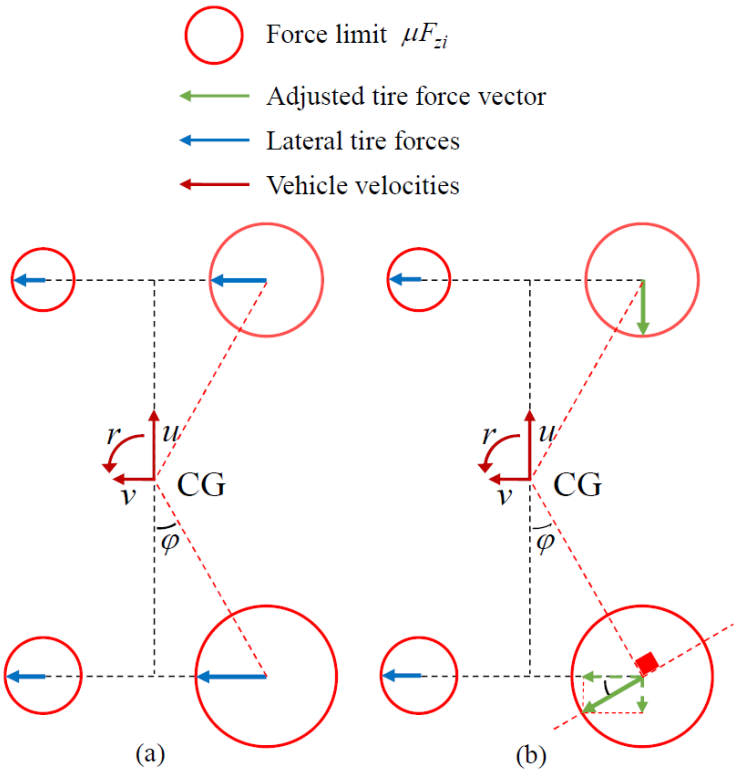

Figure 3.8: Tire force vector in the friction force limit circle, (a) with no longitudinal force at the corners, and (b) the optimum force vectors for generating understeering yaw moment by differential braking.

If there is a longitudinal force in the rear right corner, generated whether by the driver's acceleration pedal or the ELSD, the optimum braking force is added up with $(Q_d + T_C)/2R_e$. Therefore, the maximum rear differential braking is considered to be:

$$M_{DBR,max} = \frac{l_s}{2}\left(\mu F_{z,rr}\frac{l_s}{2\sqrt{l_r^2 + \frac{l_s^2}{4}}} + \frac{Q_r + T_C}{2R_e}\right). \tag{3.42}$$

Then, the control actuation M_{DBR} is constrained as $|M_{DBR}| \leq M_{DBR,max}$. The rear differential braking is activated when the ELSD clutch cannot contribute to vehicle stability, and accordingly the ELSD clutch is disengaged when the rear differential braking is applied.

Therefore, the maximum rear differential braking $M_{DBR,max}$ can be simplified by setting $T_C = 0$ in Eq. (3.42).

3.5 State Constraints

To ensure vehicle stability, safety limits can be defined on the states of the vehicle model. The stable bounds of the vehicle's yaw rate are defined using the steady state assumption ($\dot{v} \approx 0, \ddot{\phi} \approx 0$) in Eqs. (3.17) to (3.19), resulting in:

$$r_{max} = \frac{F_{Y,max} - mg \sin \phi_r \cos \theta_r}{mu}. \tag{3.43}$$

If no longitudinal force is applied to the tires, the maximum lateral force capacity can be assumed to be $F_{Y,max} = \mu N$, where N is the vehicle's total normal force. Applying a longitudinal force on the rear axle decreases the lateral force capacity of the rear axle, thereby increasing the vehicle's oversteer tendency. This reduction in the lateral force capacity of the rear axle is assumed to shrink the stable region of the yaw rate as:

$$r_{max} = \frac{\mu N \xi_r - mg \sin \phi_r \cos \theta_r}{mu}, \tag{3.44}$$

where $\xi_r = \sqrt{(\mu F_{zr})^2 - F_{xr}^2}/(\mu F_{zr})$ is the rear axle's derating factor. The normal load, N, is a function of the road's bank angle, ϕ_r, grade angle, θ_r, and curvature, κ:

$$N = mg \cos \phi_r \cos \theta_r - m\kappa u^2 \sin \phi_r \cos \theta_r. \tag{3.45}$$

Substituting Eq. (3.45) in Eq. (3.44) results in:

$$r_{max} = \frac{\mu \xi_r \left(g \cos \phi_r \cos \theta_r - \kappa u^2 \sin \phi_r \cos \theta_r\right) - g \sin \phi_r \cos \theta_r}{u}. \tag{3.46}$$

The minimum stable yaw rate is similarly obtained as:

$$r_{min} = \frac{-\mu \xi_r \left(g \cos \phi_r \cos \theta_r - \kappa u^2 \sin \phi_r \cos \theta_r\right) - g \sin \phi_r \cos \theta_r}{u}. \tag{3.47}$$

The yaw rate's constraint can be represented by the following linear inequality:

$$\mathbf{H}_r \mathbf{x} \leq \mathbf{G}_r, \tag{3.48}$$

where $\mathbf{H}_r = \begin{bmatrix} 0 & 1 & 0 & 0 & 0 & 0 \\ 0 & -1 & 0 & 0 & 0 & 0 \end{bmatrix}$, and $\mathbf{G}_r = \begin{bmatrix} r_{max} \\ -r_{min} \end{bmatrix}$.

The stable limit of the vehicle's sideslip is determined by constraining the rear slip angle to $|\alpha_r| \leq \alpha_{r,sat}$, resulting in:

$$\frac{l_r r}{u} - \alpha_{r,sat} \leq \beta \leq \frac{l_r r}{u} + \alpha_{r,sat}. \tag{3.49}$$

This inequality constraint can be written in matrix form as:

$$\mathbf{H}_\beta \mathbf{x} \leq \mathbf{G}_\beta, \tag{3.50}$$

where $\mathbf{H}_\beta = \begin{bmatrix} 1 & -l_r/u & 0 & 0 & 0 & 0 \\ -1 & l_r/u & 0 & 0 & 0 & 0 \end{bmatrix}$, and $\mathbf{G}_\beta = \begin{bmatrix} \alpha_{r,sat} \\ \alpha_{r,sat} \end{bmatrix}$.

To ensure the roll stability of the vehicle, the lateral load transfer ratio (LTR) is regarded as a good measure for vehicle rollover tendency. The LTR index is defined based on the difference between the normal forces of the right and left tires as:

$$LTR = \frac{F_{z,r} - F_{z,l}}{F_{z,r} + F_{z,l}}. \tag{3.51}$$

The LTR can be obtained by writing the roll moment equation in the unsprung mass around the midpoint of the right and left contact points as:

$$LTR = \frac{2\left(k_\phi \phi + c_\phi \dot{\phi} + (m h_u + m_s (h_R - h_u))(a_y + g \sin\phi_r \cos\theta_r)\right)}{m l_s (g \cos\phi_r \cos\theta_r - \kappa u^2 \sin\phi_r \cos\theta_r)}. \tag{3.52}$$

The LTR index can be rewritten using the vehicle states to present it as a stability limit in the ϕ - $\dot{\phi}$ phase plane:

$$LTR = \bar{k}_\phi \phi + \bar{c}_\phi \dot{\phi}, \tag{3.53}$$

where $\bar{k}_\phi$ and $\bar{c}_\phi$ depend on vehicle parameters, road angles (bank and grade), and road curvature as:

$$\bar{k}_\phi = \frac{2\left(k_\phi\left(1+\frac{m_s h_R + m_u h_u}{m_s h_s}\right) - (m_s h_R + m_u h_u)\, g \cos\phi_r \cos\theta_r\right)}{m l_s \left(g\cos\phi_r\cos\theta_r - \kappa u^2 \sin\phi_r \cos\theta_r\right)}, \tag{3.54}$$

$$\bar{c}_\phi = \frac{2\, c_\phi\left(1+\frac{m_s h_R + m_u h_u}{m_s h_s}\right)}{m l_s \left(g\cos\phi_r\cos\theta_r - \kappa u^2 \sin\phi_r \cos\theta_r\right)}. \tag{3.55}$$

The stable region in the $\phi - \dot{\phi}$ phase plane is obtained by limiting the LTR within a safe threshold [137]. This constraint can be written as:

$$\mathbf{H}_\phi \mathbf{x} \leq \mathbf{G}_\phi, \tag{3.56}$$

where $\mathbf{H}_\phi = \begin{bmatrix} 0 & 0 & \bar{k}_\phi & \bar{c}_\phi & 0 & 0 \\ 0 & 0 & -\bar{k}_\phi & -\bar{c}_\phi & 0 & 0 \end{bmatrix}$, and $\mathbf{G}_\phi = \begin{bmatrix} LTR_{max} \\ LTR_{max} \end{bmatrix}$.

The defined limits on the vehicle's yaw rate, sideslip, roll angle, and roll rate in the $\beta - r$ and $\phi - \dot{\phi}$ phase planes are shown in Fig. 3.9. In the $\beta - r$ phase plane, the stability limits create a parallelogram, inside of which is shown in green as it satisfies the stability constraints of the yaw rate and sideslip. The region outside the yaw rate's stable limit and within the sideslip's stable bounds is shown in yellow, and the region where the sideslip limit is violated is considered as unstable region (red region). The violation of the stability parallelogram in the $\beta - r$ phase plane mostly starts through the channel of yaw rate. The vehicle trajectory may return from the yellow region to the green region without touching the red region's boundary. Therefore, the violation of the yaw rate limit can be regarded as a warning (low-level unsafe behavior), and the violation of the sideslip limit as a high-level unsafe behavior. In the $\phi - \dot{\phi}$ phase plane, the region outside the safe LTR threshold is regarded as unstable region (red region) because the vehicle tends to roll-over. This classification of the safety constraints is used to design a prioritization controller.

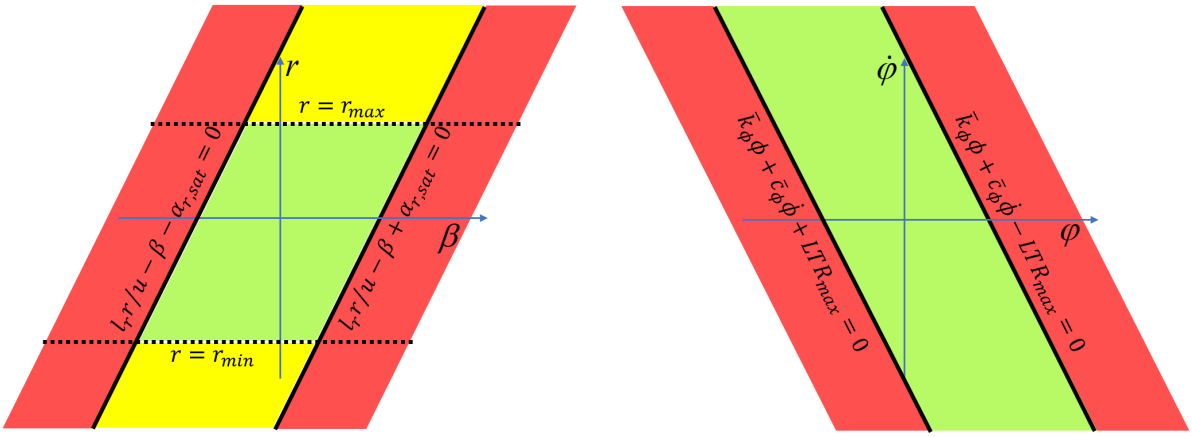

(a) (b)

Figure 3.9: (a) The $\beta - r$ phase plane, and (b) the $\phi - \dot{\phi}$ phase plane. They are divided to green, yellow, and red regions.

3.6 Desired Vehicle Response

The MPC controller is intended to track a desired yaw rate and sideslip for handling improvement. To ensure that the vehicle's sideslip remains small and safe, the desired sideslip is assumed to be $\beta_{des} = 0$. The desired yaw rate is obtained based on the vehicle's linear response to the steering input in the linear range of vehicle operation, which can be expressed as:

$$\bar{r}_{des} = \frac{u}{l + k_{us} u^2} \delta, \tag{3.57}$$

where l is the vehicle's wheelbase, and k_{us} denotes the vehicle understeer coefficient. The understeer coefficient shows the vehicle's sensitivity to the steering input and is an important criterion in the assessment of vehicles' handling characteristics. If sufficient road friction is not available, the desired yaw rate defined in Eq. (3.57) should be adjusted to limit the yaw rate that the vehicle can assume. For this purpose, the maximum safe yaw rate defined in Eq. (3.46) is used to define the modified desired yaw rate as:

$$r_{des} = \min\left(|\bar{r}_{des}|, r_{max}\right) \operatorname{sign} \bar{r}_{des}. \tag{3.58}$$

3.7 Prioritization Model Predictive Controller

A prioritization model predictive control design for a multi-actuation multi-objective system is proposed in this chapter. Figure 3.10 schematically shows the prioritization structure for N control actuations and M control objectives. It is assumed that the control actuations can be prioritized in real-time into λ priority levels based on their advantages and disadvantages in performance, energy usage, constraints, and capabilities. The control objectives are also prioritized in real-time based on their importance. This structure combines the actuation priorities and the objective priorities so as to activate the actuations of the priority level $l_i\,(1 \leq i \leq \lambda)$ when objectives with the same priority level or higher necessitate doing so. As a result, a low priority actuation is activated only for the high priority objectives and will not kick in for a low priority objective [138].

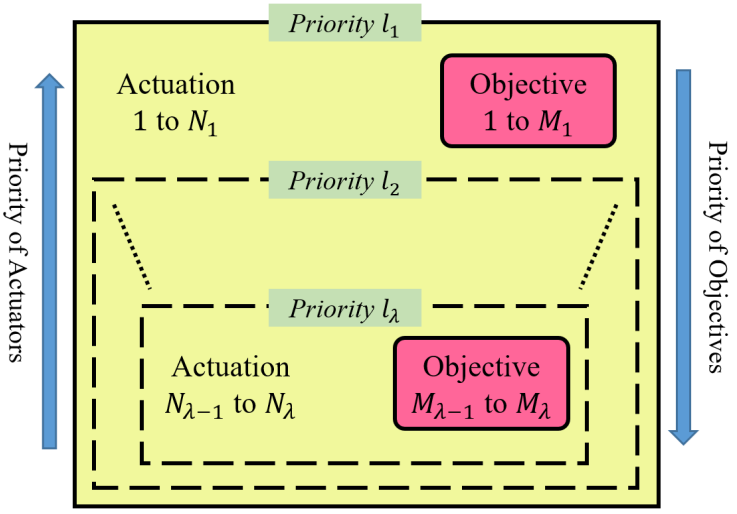

Figure 3.10: General form of the prioritization controller. The priority of control actuations and control objectives are combined within λ priority levels.

The objective of the prioritization model predictive control is to optimize the control actuations within the defined priority structure for control actuations and control objectives. The control objectives are all formulated as soft constraints on the states of the system using slack variables except for one tracking objective. The controller also uses priority variables in actuation constraints, which are introduced to allow for prioritization of the control actuations. The objective function consists of quadratic weights of tracking error

of system states, control effort, and the proximity of the control actuations. It also assigns linear weights for violations of systems constraints by penalizing the slack variables used in the soft constraints. Moreover, the controller penalizes priority variables with linear weights. The cost function is expressed as:

$$\begin{aligned} J = \sum_{k=1}^{N_p} \left(\mathbf{x}(k) - \mathbf{x}_{des}(k)\right)^T \mathbf{Q} \left(\mathbf{x}(k) - \mathbf{x}_{des}(k)\right) + \mathbf{u}^T(k)\, \mathbf{R}_m\, \mathbf{u}(k) \\ + \boldsymbol{\Delta}\mathbf{u}^T(k)\, \mathbf{R}_p\, \boldsymbol{\Delta}\mathbf{u}(k) + \mathbf{W}_s\, \mathbf{s}(k) + \mathbf{W}_\rho\, \rho(k), \end{aligned} \tag{3.59}$$

subject to the vehicle prediction model (Eq. (3.32)) and:

$$\mathbf{H}\mathbf{x}(k) \leq \mathbf{G} + \mathbf{s}(k), \tag{3.60}$$

$$\mathbf{P}\mathbf{u}_{min}(k) \leq \mathbf{u}(k) \leq \mathbf{P}\mathbf{u}_{max}(k), \tag{3.61}$$

$$\mathbf{s}(k) \geq 0, \tag{3.62}$$

$$0 \leq \rho(k) \leq 1, \tag{3.63}$$

where N_p is the number of points in the prediction horizon, $\mathbf{x}_{des}$ denotes the desired states, and $\mathbf{s}$ is the vector of non-negative slack variables that are used to change the hard constraints of the system states to soft constraints to ensure that the optimization problem always has a feasible solution. These slack variables are penalized in the cost function to enforce the system's stability. The vector ρ denotes the priority variables, which are constrained between $[0, 1]$ and are penalized in the cost function to ensure that the low priority actuation is not used unless the high priority objective necessitates its activation. The matrix $\mathbf{P}$ is a diagonal matrix in which the first N_1 diagonal entries, which are associated with the priority level l_1, are equal to one, and the rest are the priority variables.

The relative size of the optimization weights of the slack variables and the priority variables are set as $\mathbf{W}_{s,l_\lambda} \gg \mathbf{W}_{\rho,l_\lambda} \gg \mathbf{W}_{s,l_{\lambda-1}} \gg \cdots \gg \mathbf{W}_{\rho,l_2} \gg \mathbf{W}_{s,l_1} \gg \mathbf{Q}$, where $\mathbf{W}_{s,l_i}$ and $\mathbf{W}_{\rho,l_i}$ denote respectively the weights of the slack variables and the priority variables of the priority level l_i. This control design allows for a combined prioritization of the objectives and the actuators through the prediction horizon.

The proposed prioritization model predictive controller is used for vehicle dynamics control problem. The vehicle control objectives are tracking the desired states and maintaining the vehicle states within the defined safety limits. Therefore, the state constraints of the MPC controller, Eq. (3.60), includes the constraints defined in Eqs. (3.48), (3.50), and (3.56). In addition, the actuator constraints of the controller, Eq. (3.61), is composed of the constraints defined in Eq. (3.38) to (3.40) and (3.42).

The stability of the proposed controller can be shown using the techniques used for stability analysis of the constrained model predictive controllers [139, 140, 141], which is not the focus of our study. The proposed MPC controller is in fact a convex optimization with a quadratic cost function and linear constraints. This quadratic optimization problem is solved using qpOASES solver [142] in the numerical and experimental studies. The solution of this optimization problem is an optimal sequence of control inputs for the entire horizon at each execution of the controller. The first set of control inputs in this sequence is selected and applied to the vehicle and the rest are discarded. The optimization problem is re-solved at the next time step over a shifted horizon with new measurements.

3.8 Prioritization Control of Vehicle Dynamics

The vehicle control problem can have different control actuations and control objectives. There are different vehicle safety actuations such as differential braking, active torque distribution, active steering, and active differentials. The vehicle control objectives include: rollover prevention, maintaining sideslip and yaw rate within their stable limits, wheel stability, and yaw rate tracking.

The prioritization controller is employed for three different vehicles considered as three cases. In Case 1, the vehicle is an electric all-wheel-drive vehicle equipped with actuations of front/rear torque shifting and differential braking. Between front/rear torque shifting and differential braking, using the former first is preferred because of the drawbacks of differential braking such as energy waste, speed reduction, and noise. Therefore, the priorities of actuators are (1) front/rear torque shifting, (2) differential braking. The control objectives and their priorities are (1) enforcing the sideslip constraint, (2) enforcing the yaw rate constraint, and (3) tracking the desired states.

In Case 2, the vehicle is a performance vehicle equipped with ELSD on the rear axle, front differential braking, and rear differential braking. The selected control objectives for

this case are (1) enforcing the yaw rate constraint, and (2) tracking the desired yaw rate. Between ESLD and differential braking, using the former first is preferable because it does not drop the vehicle speed. Therefore, the priorities of actuators are (1) ELSD, and (2) differential braking.

In Case 3, the vehicle is an electric SUV equipped with front/rear torque shifting and differential braking capabilities. The vehicle has a high CG location, and therefore, roll-over accidents are likely to happen. Such accidents can be more dangerous than those involving spinning or skidding. Therefore, the control objectives are prioritized as: (1) enforcing the roll constraint, (2) enforcing the sideslip constraint, (3) enforcing the yaw rate constraint, and (4) tracking the desired yaw rate.

Figure 3.11 shows the prioritization control structure for the three cases. In this structure, the objective priorities and actuator priorities are combined such that differential braking, which is the low priority actuator, is activated only for the high priority objectives. The proposed structure restrains the controller from using differential braking for the low priority control objectives. There is one more condition for the activation of the rear differential braking in Case 2, which is the inability of ELSD to generate understeering yaw moments.

The prioritization model predictive control method is employed for all the above-mentioned case studies. In this design, differential braking, which is the low priority actuation, is set as the second control input, and then the matrix $\mathbf{P}$ in actuator constraints, Eq. (3.61), becomes:

$$\mathbf{P} = \begin{bmatrix} 1 & 0 \\ 0 & \rho \end{bmatrix}. \tag{3.64}$$

In the second case study, differential braking is divided to front and rear differential braking; and therefore, there are three control inputs. In this case, the matrix $\mathbf{P}$ in actuator constraints is written as:

$$\mathbf{P} = \begin{bmatrix} 1 & 0 & 0 \\ 0 & \rho & 0 \\ 0 & 0 & \rho\,\eta \end{bmatrix}. \tag{3.65}$$

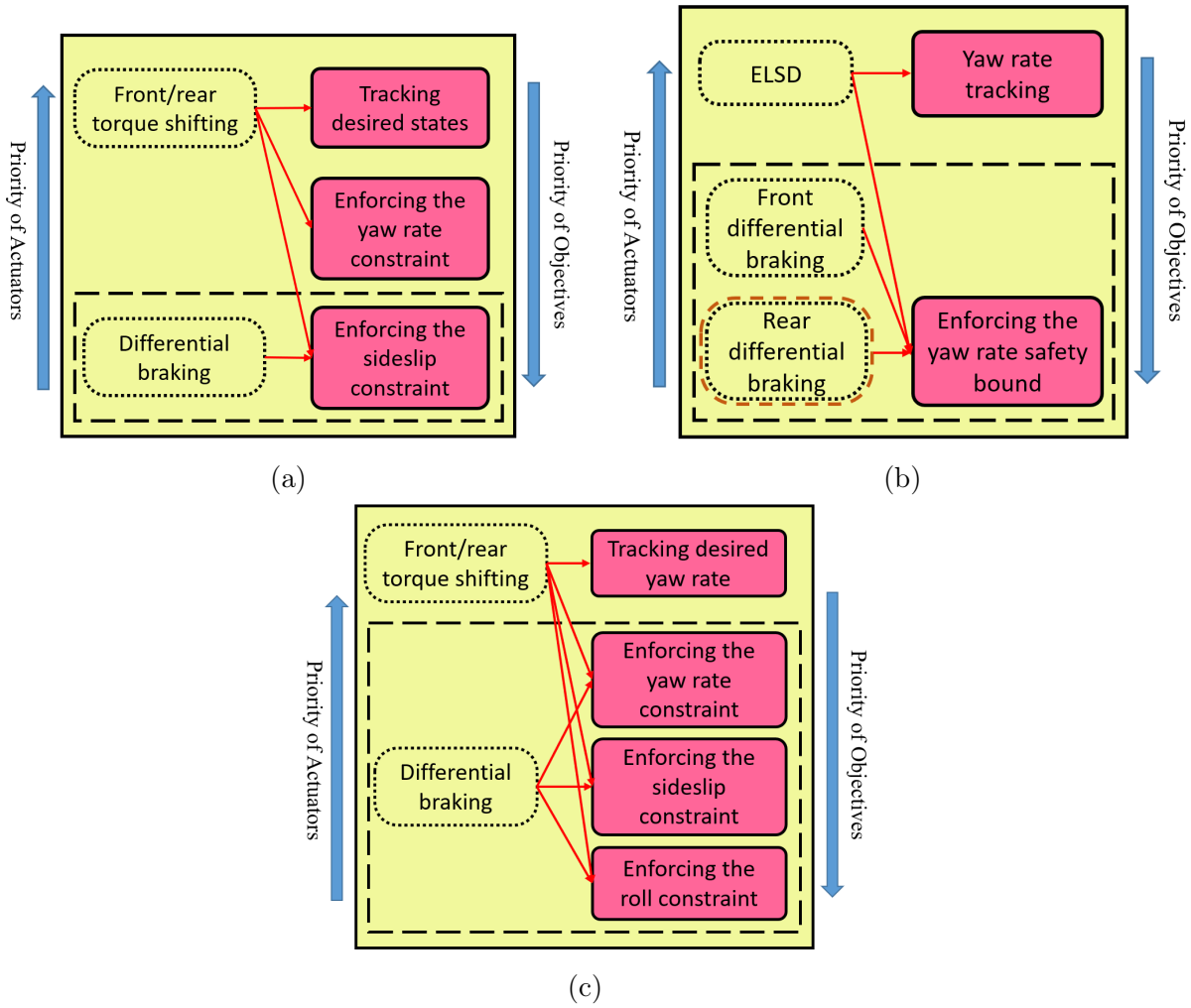

Figure 3.11: The prioritization controller is used for three case studies. (a) Case study 1, (b) Case study 2, (c) Case study 3.

The variable η is a switch variable that is $\eta = 0$ when the ELSD clutch can generate understeering yaw moments. This switch variable changes to $\eta = 1$ only when the ELSD clutch model predicts that the clutch can generate oversteering yaw moments.

The order of state constraints in Eq. (3.60) is set such that the control objective with the highest priority, enforcing the roll constraint, is set as the last constraint. Therefore, the matrices $\mathbf{H}$ and $\mathbf{G}$ for Case study 3 become $\mathbf{H} = \begin{bmatrix}\mathbf{H}_r & \mathbf{H}_\beta & \mathbf{H}_\phi\end{bmatrix}^T$ and $\mathbf{G} =$

$\begin{bmatrix}\mathbf{G}_r & \mathbf{G}_\beta & \mathbf{G}_\phi\end{bmatrix}^T$, and the vector of slack variables is similarly set as $\mathbf{s} = \begin{bmatrix}\mathbf{s}_r & \mathbf{s}_\beta & \mathbf{s}_\phi\end{bmatrix}^T$.

3.9 Summary

In this chapter, a prioritization model predictive controller was developed for multi-actuated vehicles with multiple control objectives. The control actuations and control objectives were prioritized such that the low priority actuation is engaged only for the high priority objective. In this design, the MPC controller applies the priority of control objectives and control actuations using slack variables and priority variables, respectively. The prioritization control structure was implemented for vehicle control problem in three case studies with actuations of front/rear torque shifting, ELSD, and differential braking.

The vehicle prediction model consists of the vehicle yaw dynamics, lateral dynamics, and roll dynamics and includes the effect of road angles. The prediction model considers the force coupling effect to allow for optimal control of front/rear torque shifting. An ELSD model was designed for estimating ELSD clutch torque, which is then used to properly control ELSD clutch pressure. The desired vehicle yaw rate is defined based on the steering input, speed, the vehicle understeer coefficient, and the yaw rate safety limit.

The actuator constraints and state constraints were illustrated and included in the MPC control design. The constraint of braking forces in differential braking was calculated using a geometrical analysis of the tire force vectors. The constraints defined on vehicle states were used to define the control objectives, including rollover prevention, maintaining sideslip and yaw rate within their stable limits, and yaw rate tracking. Then, the priority of control objectives was defined based on their importance.

Chapter 4

Simulation and Experimental Results

In this chapter, the controller designed in the previous chapter is employed for the three case studies described in Section 3.8. The first case study deals with controlling a vehicle's yaw rate and sideslip using front/rear torque shifting and differential braking, which is evaluated numerically as well as experimentally with implementation on an electric Chevrolet Equinox vehicle (Fig. 4.1a). In the second case study, the vehicle's yaw rate is controlled using ELSD and differential braking, and the controller's performance is assessed experimentally using a Cadillac CTS vehicle (Fig. 4.1b). The third case study focuses on the integrated control of lateral and roll motion using front/rear torque shifting and differential braking, evaluated numerically using an electric E-Class SUV vehicle in CarSim. The specifications of the test vehicles are listed in Table 4.1.

The experimental setup diagram for the tests is shown in Fig. 4.2. The controller is implemented in the Simulink environment, which is compiled on dSpace Micro-Autobox. The Micro-Autobox communicates with the vehicle actuators and sensors through CAN bus network. The vehicle IMU sensor provides the yaw rate and longitudinal and lateral accelerations. The longitudinal and lateral velocities are measured by a 6-axis GPS (RT2500) in Chevrolet Equinox. However, they are obtained by estimation in Cadillac CTS vehicle. The wheel force transducer sensors are installed at each corner to measure the torque and speed of wheels. However, the measured corner torques are only used to evaluate the closed loop performance of the ELSD clutch model, and they are not used within the controller. The control parameters for the three case studies are shown in Table 4.2.

(a)

(b)

Figure 4.1: Test vehicles used in experimental verifications, (a) the electric all-wheel-drive Chevrolet Equinox vehicle, and (b) the Cadillac CTS vehicle.

Table 4.1: Specifications of the Test Vehicles.

Parameter	Description	Value		
		Case 1	Case 2	Case 3
$m\,[kg]$	Total mass	2272	1731	1860
$I_z\,[kg.m^2]$	Vehicle moment of inertia	4600	3200	2687
$l_s\,[m]$	Track width	1.6	1.57	1.58
$l_f\,[m]$	Distance from front axle to CG	1.42	1.44	1.18
$l_r\,[m]$	Distance from rear axle to CG	1.43	1.47	1.77
$R_e\,[m]$	Effective radius	0.351	0.316	0.393
$C_{\alpha f}\,[N/rad]$	Front cornering stiffness	130000	124000	120000
$C_{\alpha r}\,[N/rad]$	Rear cornering stiffness	130000	124000	84000

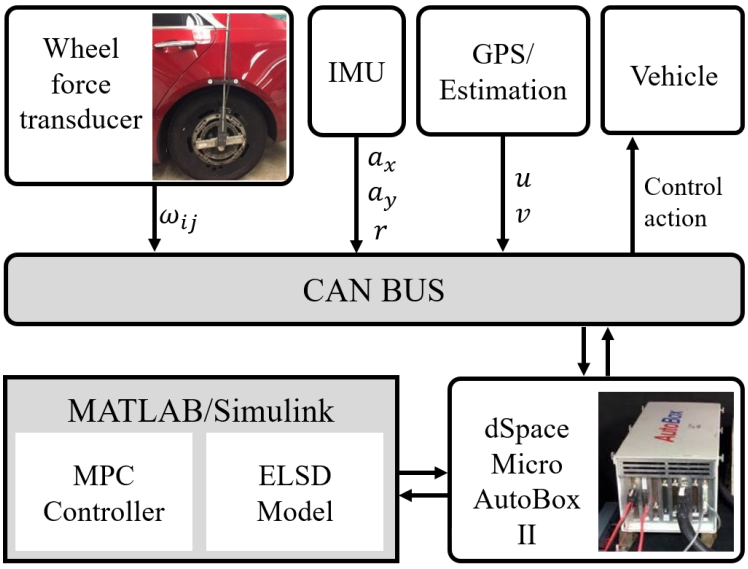

Figure 4.2: The experimental setup of the vehicle and the communication network.

Table 4.2: Controller Parameters.

Parameter	Value		
	Case 1	Case 2	Case 3
N_p	8	8	8
t_s	5 $[ms]$	5 $[ms]$	5 $[ms]$
$\mathbf{Q}$	$\text{diag}(50, 400, 0, 0)$	$\text{diag}(0, 600, 0, 0)$	$\text{diag}(50, 400, 0, 0, 0, 0)$
$\mathbf{R}_m$	$\text{diag}(2, 8) \times 10^{-7}$	$\text{diag}(3, 2 \times 10^{-7}, 2 \times 10^{-7})$	$\text{diag}(2, 8) \times 10^{-7}$
$\mathbf{R}_p$	$\text{diag}(2, 2) \times 10^{-5}$	$\text{diag}(30, 6 \times 10^{-5}, 6 \times 10^{-5})$	$\text{diag}(2, 2) \times 10^{-5}$
$\mathbf{W_s}$	$800 \times [1 \;\; 100]$	30000	$1000 \times [5 \;\; 20 \;\; 200]$
$\mathbf{W}_\rho$	8000	3000	800

4.1 Case Study 1: Differential Braking and Front/Rear Torque Shifting

In Case Study 1, the designed prioritization controller is implemented on an electric all-wheel-drive vehicle equipped with differential braking, and its powertrain includes two electric motors, each connected to an open differential on the axles. The priorities of the control actuations and control objectives of this case study are shown in Fig. 3.11a. The overall structure of the designed controller is depicted in Fig. 4.3. The baseline vehicle has a constant 40-60 front/rear torque distribution. The prioritization model predictive controller calculates the control actions to satisfy the control objectives, and then the drive torques of the front and rear axles and the corner braking torques are applied to the vehicle. The MPC controller also includes actuator constraints and state constraints. The desired values of yaw rate and sideslip are generated in the driver command interpreter (DCI).

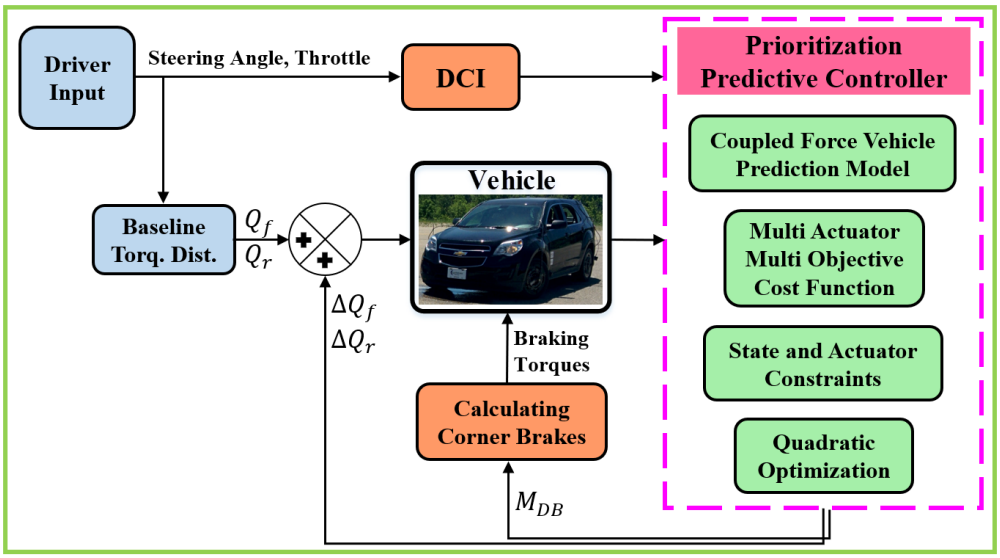

Figure 4.3: Control structure for Case 1. The controller calculates the adjustments of front/rear torque distribution and the yaw moment by differential braking, which is converted into corner brakes.

The performance of the proposed controller is evaluated numerically as well as experimentally by implementing it on an electric all-wheel-drive Chevrolet Equinox, shown in

Fig. 4.1a. The CarSim model is a high-fidelity model of the experimental test vehicle, and they have the same specifications. The numerical evaluations are performed using co-simulation in CarSim and MATLAB/Simulink.

The controller's performance is assessed first numerically in two driving maneuvers, acceleration in flick maneuver - steering to the right and quickly counter-steering - and acceleration in double-lane-change maneuver. The tests are carried out on a wet road with the friction coefficient of $\mu = 0.5$. To illustrate the performance of the proposed controller (Controller A), the results are compared with the same vehicle equipped with only differential braking and fixed front/rear torque distribution of the baseline vehicle (Controller B). Therefore, each maneuver is performed three times: (1) with Controller A, (2) with Controller B, and (3) without controller. The parameters of Controllers A and B are tuned similarly to make a fair comparison between them, except that there is no actuation priority in Controller B. The control parameters are shown in Table 4.2.

4.1.1 Acceleration in Flick Maneuver on Wet Road - Simulation

The first driving scenario is acceleration in a flick maneuver on a wet road with the initial speed of 60 kph. Figures 4.4a and 4.4b show the driver's steering input and total torque request. Figure 4.4c compares the vehicle's longitudinal velocity in uncontrolled and controlled maneuvers. Controller A's performance in longitudinal motion is better than Controller B's, with almost 4 kph less speed drop.

Figure 4.5a shows the controlled front/rear torque distribution for Controller A. The uncontrolled maneuver and Controller B have a constant baseline torque distribution, which is 40 percent to the front axle and 60 percent to the rear axle. Figure 4.5b shows the yaw moment generated by the differential braking over the maneuver period for Controllers A and B. The test results of the uncontrolled and controlled maneuvers are presented comparatively in Figs. 4.5c and 4.5d, showing respectively the vehicle's yaw rate and the rear tire slip angle. The uncontrolled maneuver shows unstable behavior, i.e., the yaw rate and the rear tire slip angle exceed safety limits. However, in the controlled maneuvers, the control actuations are activated properly with the defined priorities to improve yaw tracking and enforce the safety limits of yaw rate and sideslip. Controller A shifts torque to the front axle whenever the yaw rate or sideslip constraints are violated, to indirectly reduce the front tires' lateral force by the effect of longitudinal and lateral tire force coupling and

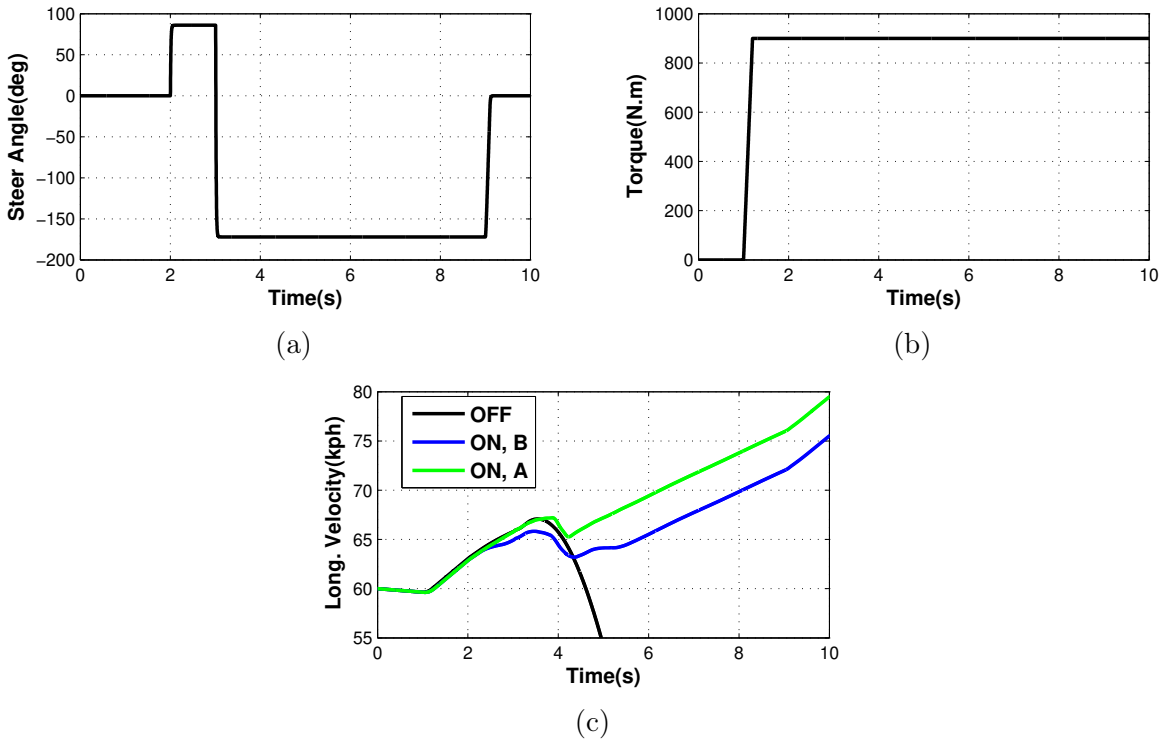

Figure 4.4: (a) The steering wheel angle, (b) driver's torque request, and (c) the vehicle longitudinal velocity in an accelerating Flick maneuver on a wet road.

consequently generate indirect understeering yaw moment. However, differential braking, which is the low priority actuation, is activated only between $t \approx 3.8\,s$ to $4.2\,s$, when it predicts that the safety limit of the rear tire slip angle, the high priority objective, is violated to prevent vehicle instability. When the vehicle trajectory is inside the safety constraints, the controller adjusts the front/rear torque distribution to improve the yaw tracking performance. For instance, to induce oversteering, the controller allocates more torque to the rear axle at around $t \approx 4.3\,s$, when the magnitude of the yaw rate is less than its desired value. Controller B uses only differential braking to satisfy the control objectives. Unlike Controller A, it uses differential braking to improve yaw tracking and enforce the safety limit of the yaw rate. When the safety limit of the rear tire slip angle is violated, the differential braking is activated with the same effort as with Controller A. The results show that Controllers A and B have almost similar performance in the yaw rate and

the rear tire slip angle. However, Controller A has a better performance in longitudinal velocity because it incorporates the available actuation of front/rear torque distribution and uses less differential braking.

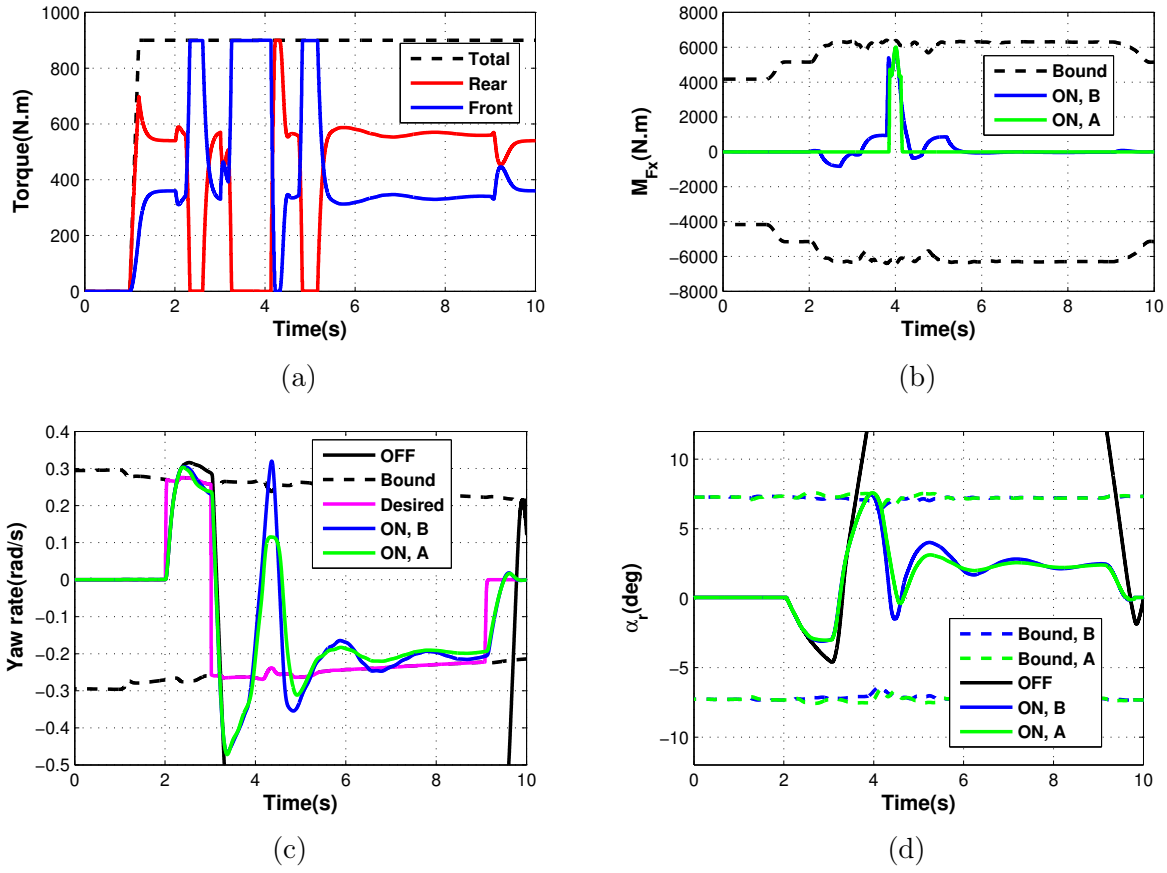

Figure 4.5: (a) The front/rear torque allocation for Controller A, (b) the yaw moment by differential braking for Controllers A and B, (c) the yaw rate, and (d) the rear tire slip angle, with controller ON (A and B) and OFF in an accelerating Flick maneuver on a wet road.

4.1.2 Acceleration in DLC Maneuver on Wet Road - Simulation

The second driving scenario is acceleration in a double-lane-change (DLC) maneuver on a wet road, with the initial speed of 62 kph. Figures 4.6a and 4.6b show the driver inputs of steering angle and acceleration torque request. Figure 4.6c shows the vehicle speed during the uncontrolled and controlled maneuvers. It can be seen that the vehicle speed in Controller A drops (by almost 3 kph) less than that in Controller B.

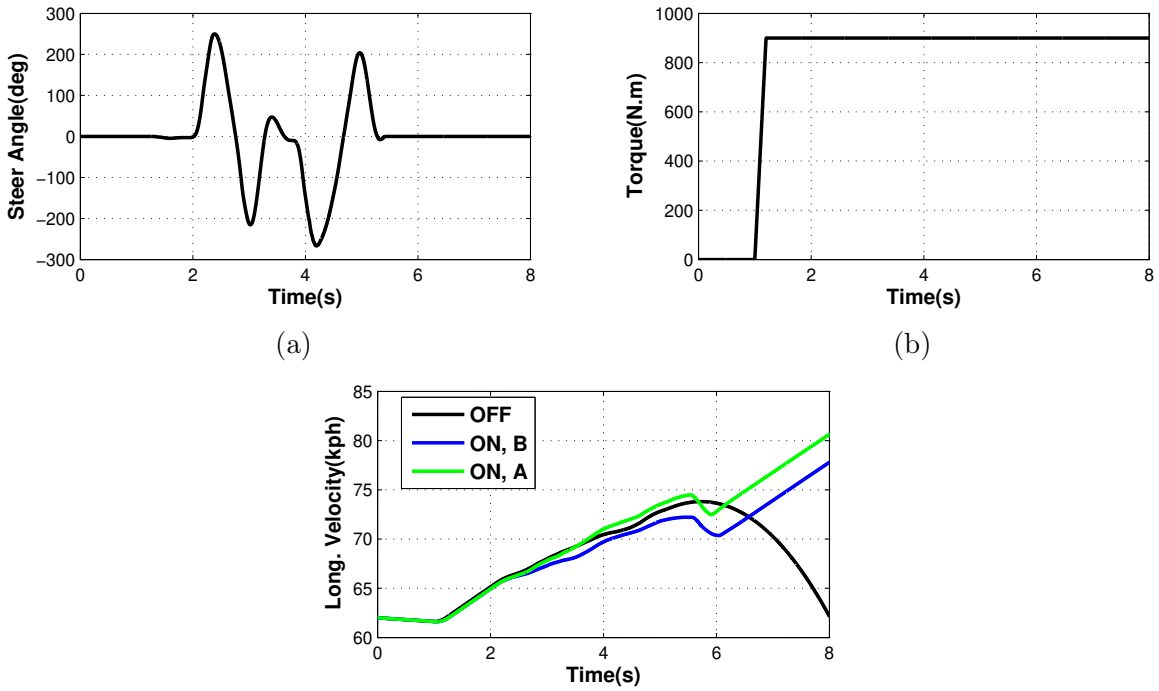

(a) (b) (c)

Figure 4.6: (a) The steering wheel angle, (b) driver's torque request, and (c) the vehicle longitudinal velocity in an accelerating DLC maneuver on a wet road.

The controlled front/rear torque distribution in Controller A is shown in Fig. 4.7a, and the yaw moment generated by differential braking for Controllers A and B is shown in Fig. 4.7b. The vehicle's yaw rate and the rear tire slip angle are respectively presented in Figs. 4.7c and 4.7d. The test results show that the uncontrolled maneuver becomes unstable, whereas the controlled maneuvers are stabilized by properly activating the control actuations. Controller A adjusts front/rear torque distribution for improving yaw tracking

performance and transfers torque to the front axle to enforce the safety limits of the yaw rate and sideslip, but differential braking is activated only to enforce the sideslip constraint. The activation of differential braking can be seen between $t \approx 5.5\,s$ to $5.9\,s$, which is associated with the violation of the sideslip limit. In Controller B, differential braking is used for satisfying all the control objectives, but with different control efforts. Controller B enforces the sideslip limit by applying as much control effort as Controller A does. There is a nearly similar performance in the vehicle's yaw rate and the rear tire slip angle of Controllers A and B. However, Controller A's performance in longitudinal motion is better than Controller B's. This capability results from the wise incorporation of the front/rear torque distribution with differential braking and the design of a priority structure that allows us to minimize the engagement of brakes because of their negative impact on longitudinal motion.

4.1.3 Acceleration in Slalom Maneuver on Wet Road - Experiment

The maneuver chosen for experiments is acceleration in slalom on a wet asphalt patch with the friction coefficient of $\mu = 0.5$. The acceleration in slalom can clearly show the effectiveness of the designed controller in the transient responses of the vehicle. This maneuver is performed first without the controller and then with the controller in the loop.

Figure 4.8 shows the driver's steering input, torque request, and the vehicle's longitudinal velocity during the test. It can be seen that the uncontrolled and controlled maneuvers are very similar; therefore, the results of the maneuvers can be compared to assess the controller's performance. Comparing the longitudinal velocities of the two maneuvers shows similar speeds during the maneuvers with the minimum of 53 kph and maximum of 60 kph, thus allowing a fair comparison of the test results.

Figure 4.9 shows the optimized control actuations, front/rear torque distribution and the yaw moment with differential braking, for the controlled maneuver, and Fig. 4.10 compares the vehicle's yaw rate and the rear tire slip angle of the uncontrolled and controlled maneuvers. The uncontrolled maneuver uses a constant 40/60 percent front/rear torque distribution, and Figs. 4.10a and 4.10c show that the vehicle's yaw rate and the rear tire slip angle diverge from their desired values and violate their safety limits. After $t \approx 6\,s$, the yaw rate and the rear tire slip angle of the uncontrolled maneuver show a very unsafe

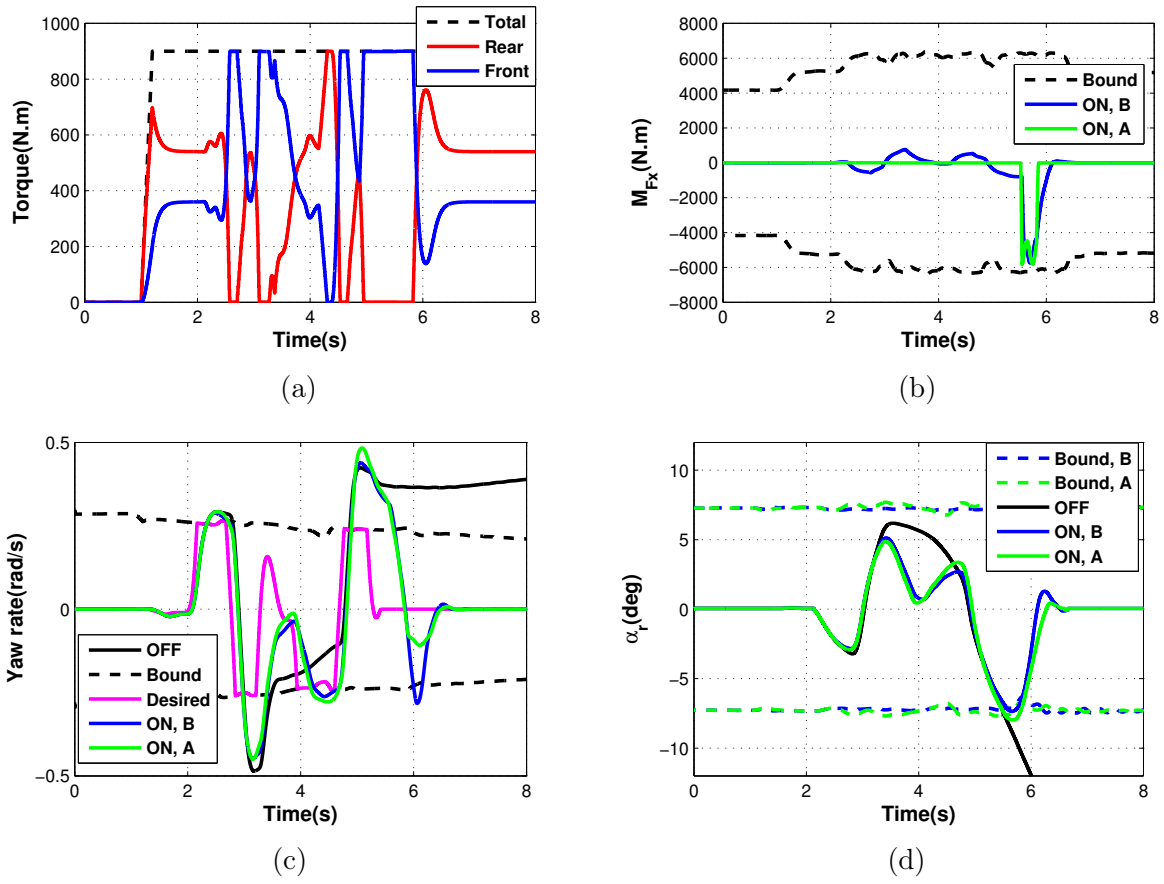

Figure 4.7: (a) The front/rear torque allocation for Controller A, (b) the yaw moment by differential braking for Controllers A and B, (c) the yaw rate, and (d) the rear tire slip angle, with controller ON (A and B) and OFF in an accelerating DLC maneuver on a wet road.

behavior, and after that, the driver skillfully drops the torque and finishes the uncontrolled slalom maneuver to avoid spinning and to keep the vehicle under control.

In the controlled maneuver, the controller optimizes the front/rear torque distribution and differential braking with the designed priority structure to improve the vehicle's performance. The controller transfers the torque to the front axle whenever the vehicle yaw rate or the rear tire slip angle exit their safety bounds, thereby decreasing the oversteer tendency by maintaining the rear tires lateral force capacity and inducing understeering

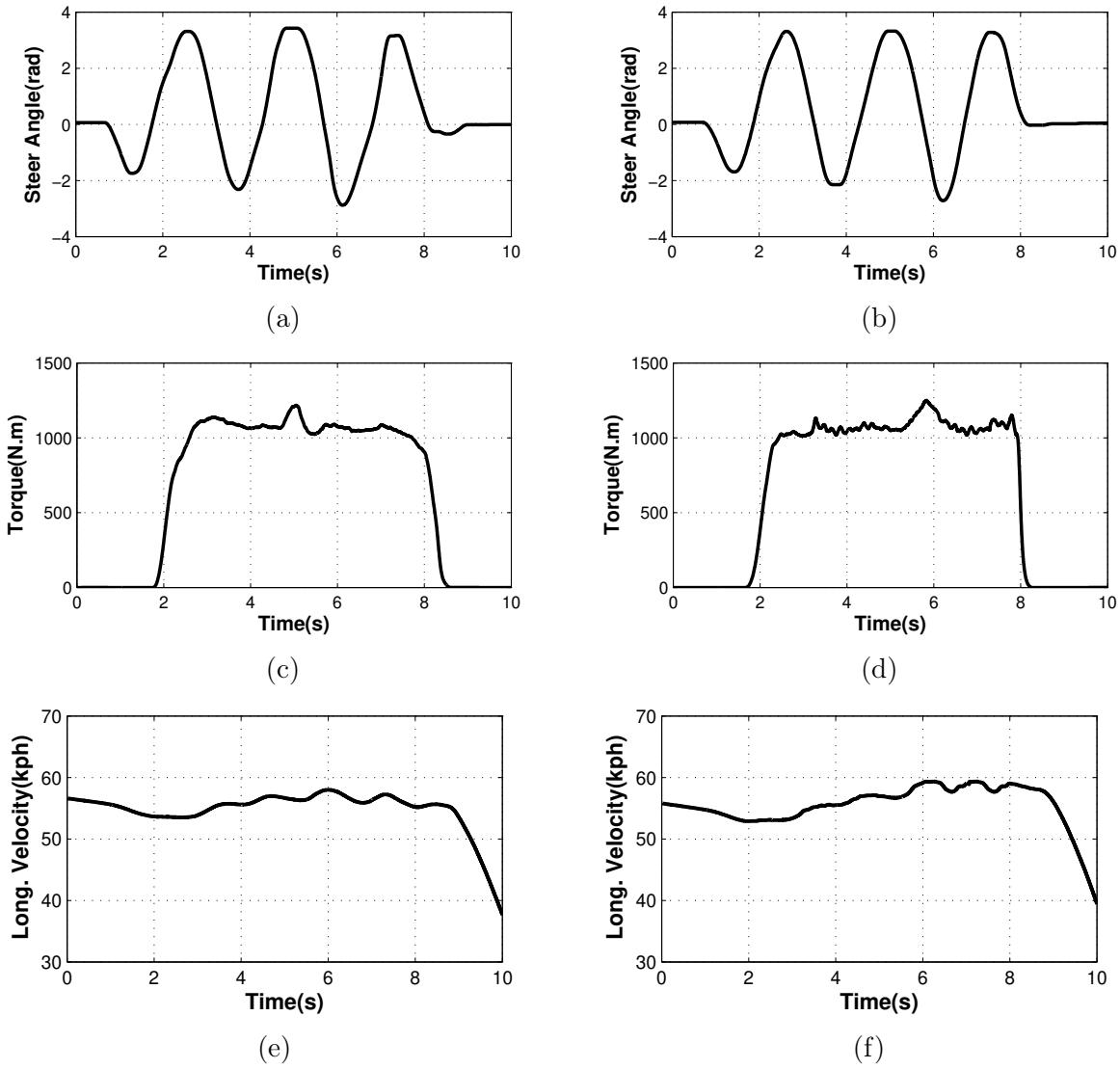

Figure 4.8: The steering wheel input, driver's torque request, and the vehicle longitudinal velocity in accelerating slalom maneuver on a wet asphalt patch, with controller OFF (a,c,e) and controller ON (b,d,f).

by decreasing the lateral force of the front axle. The driver's torque is transferred to the rear axle at $t \approx 5.5\,s$ to $6\,s$ and $t \approx 7.7\,s$ to $8\,s$, when the yaw rate becomes less than its desired value, so as to drop the rear axle's lateral force and induce oversteering. The

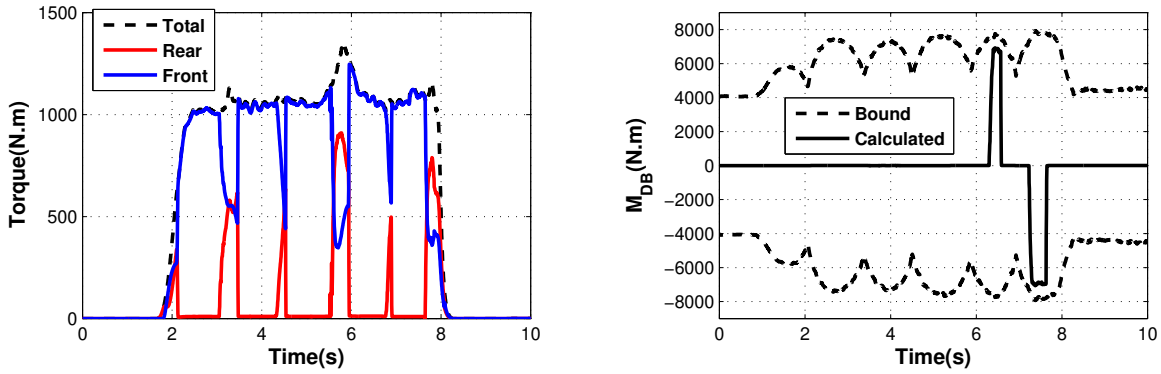

(a) (b)

Figure 4.9: (a) The front/rear torque allocation, and (b) the yaw moment by differential braking, in the controlled accelerating slalom maneuver on a wet asphalt patch.

controller activates differential braking, the low priority actuation, only at $t \approx 6.3\,s$ to $6.6\,s$ and $t \approx 7.2\,s$ to $7.7\,s$ to prevent violations of the sideslip safety limit, the high priority actuation. This combination of the objective priority and actuator priority allows us to minimize the engagement of the low priority actuator, differential braking, to decrease the negative impacts of the safety actuators on the vehicle's longitudinal motion and driver comfort. Figure 4.9b also shows the bound of the yaw moment $M_{DB,max}$, which is calculated using Eqs. (3.40) and (3.42). The optimized yaw moment M_{DB} is distributed between the front and rear corner brakes proportional to the maximum effective braking forces of each corner, and then the calculated brakes are applied to the vehicle. Finally, the comparison of the vehicle performance in the uncontrolled and controlled maneuvers clearly shows the improvement achieved by the controller in the vehicle's yaw rate and the rear tire slip angle.

4.2 Case Study 2: ELSD and Differential Braking

In Case Study 2, the designed prioritization controller is implemented on a performance Cadillac CTS, shown in Fig. 4.1b. This vehicle is rear-wheel drive and equipped with an active electro-hydraulic limited slip differential on the rear axle and differential braking capability. The priority structure of the control actuations and control objectives of this

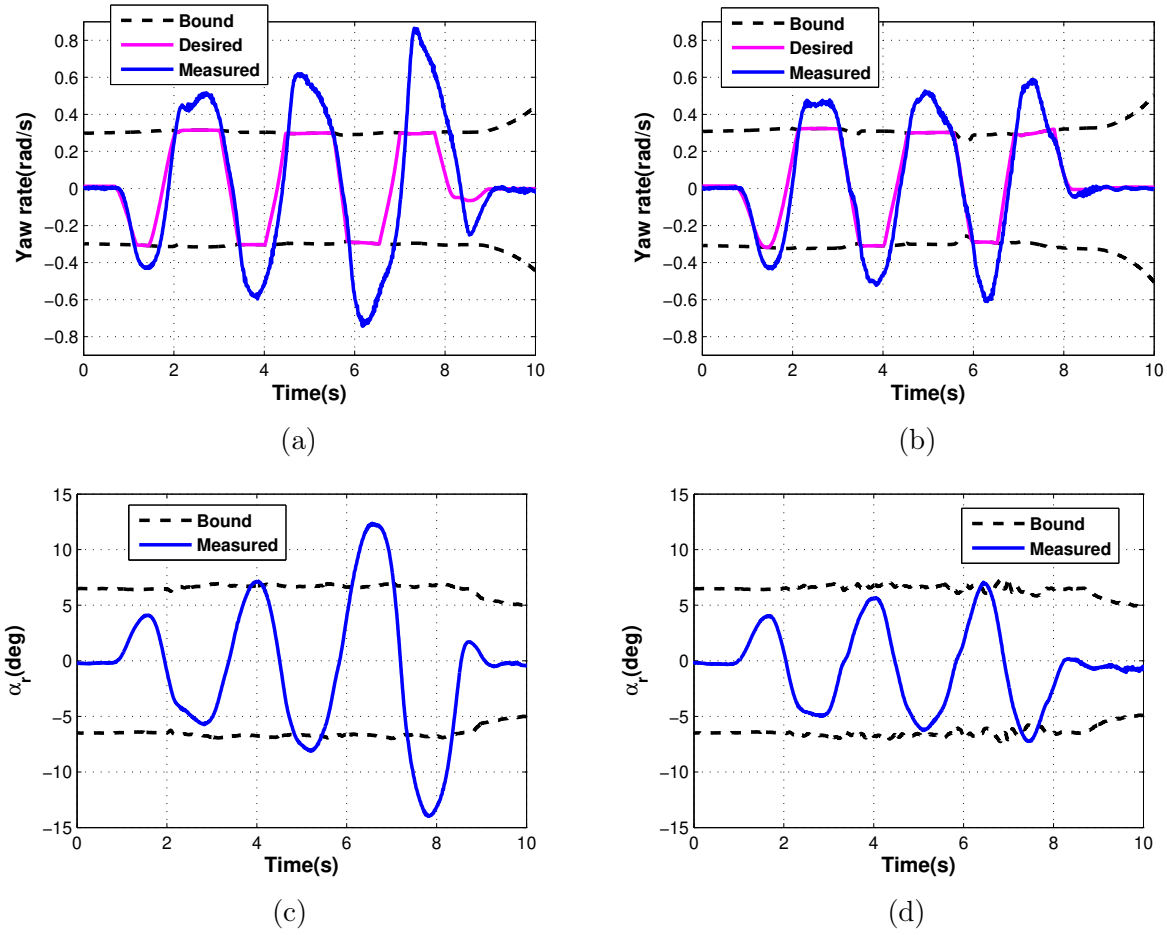

Figure 4.10: The vehicle's yaw rate and the rear tire slip angle in accelerating slalom maneuver on a wet asphalt patch, with controller OFF (a,c) and controller ON (b,d).

case study are shown in Fig. 3.11b.

The overall structure of the controller is illustrated in Fig. 4.11. The controller improves vehicle stability and handling performance by tracking the desired yaw rate generated in the driver command interpreter (DCI) and enforcing the yaw rate safety limit. The controller calculates the optimal actuations of ELSD clutch pressure and differential braking, and then the ELSD clutch pressure and the corner braking pressures are applied to the vehicle.

The differential used in the studied vehicle is a hydroelectric ELSD. As it was explained in Section 3.2, current ELSD differential controllers send a requested clutch torque com-

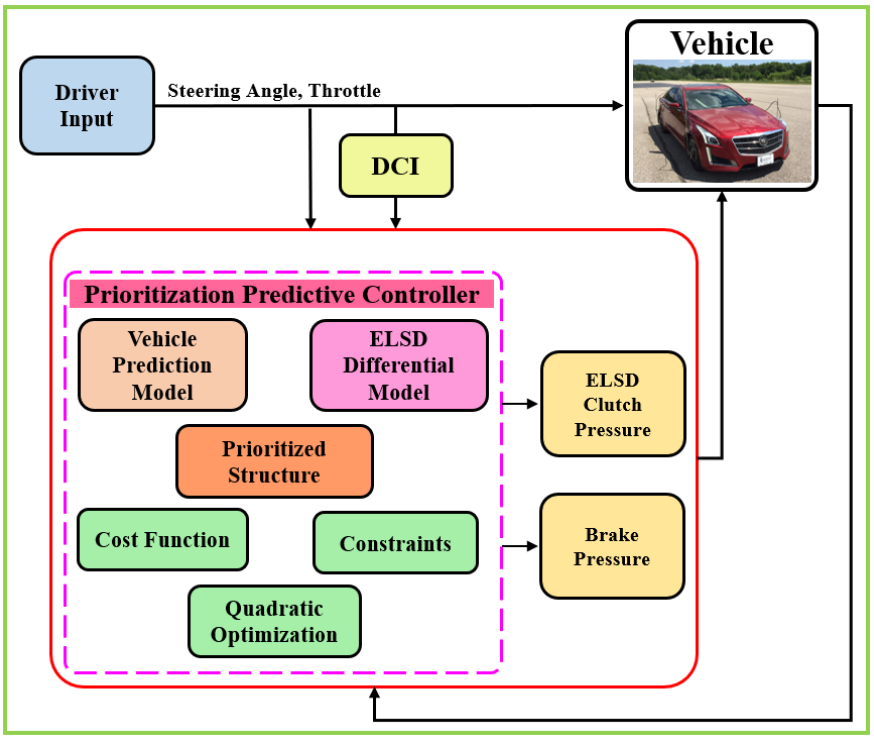

Figure 4.11: Control structure for Case 2. The controller calculates the ELSD clutch pressure and the corner braking forces.

mand to the ELSD's built-in module. However, in this research, the manufacturer's ELSD module is replaced with a controller designed to provide direct control over clutch pressure. The clutch pressure is controlled by a hydraulic pump that provides the requested pressure using a PID controller. The PID controller minimizes the error between the requested and feedback clutch pressures.

Both open loop testing, to collect test data for ELSD modelling, and closed loop testing, to assess the effectiveness of the controller, are carried out on the vehicle. The open loop test data is first used to examine the performance and accuracy of the ELSD clutch model. Various driving maneuvers with different ELSD clutch pressures are carried out to validate the proposed ELSD model.

4.2.1 ELSD Model Evaluation - Experiment

Figures 4.12 and 4.13 show the results of the ELSD clutch models in a slalom maneuver and an acceleration in turn (AIT) maneuver, respectively. Both maneuvers are performed on a dry asphalt patch with constant ELSD clutch pressures, the slalom maneuver with 40 percent pressure and the AIT maneuver with 50 percent pressure. The ELSD clutch torque is obtained by calculating the torque difference between the right and left wheels, $T_C = T_{rr} - T_{rl}$, measured using the wheel force sensors. It can be seen that although the 40 percent clutch pressure used in the slalom maneuver does not fully lock the differential, it provides a significant torque bias between the wheels. In the AIT maneuver, the acceleration pedal is suddenly activated during the turn, which results in a decrease in the wheel speed difference and subsequently chattering and change in the direction of $\Delta\omega$. The torque applied on the rear axle decreases the clutch torque and even changes its direction for a short time ($t \approx 3\,s$ to $3.5\,s$).

The predicted clutch torques using the spring-damper model (Model 1) and its modified version (Model 2), presented respectively in Eqs. (3.34) and (3.35), are compared with the measured clutch torques. Both the models properly follow the measured clutch torque, with just some small local errors at the peaks and saturations except for the end of maneuvers. In both maneuvers, the clutch torque drops to zero when the maneuver is finished, but Model 1 fails to properly follow it. The modified model (Model 2) improves the performance and converges to zero by gradually forgetting the offset error caused by the spring term in the model.

Figure 4.14 shows the results of the ELSD models for the AIT maneuver illustrated in Section 3.2 of the previous chapter (Fig. 3.6), and Fig. 4.15 demonstrates the results of an acceleration in slalom (AIS) maneuver with 40 percent clutch pressure in a wet asphalt patch. In the AIT maneuver, both the ELSD models, with nearly similar performance, reasonably follow the measured clutch torque and properly estimate the change in the direction of the clutch torque. In the AIS maneuver, the high acceleration torque applied between $t \approx 4.2\,s$ to $8.5\,s$ initiates a change in the ELSD clutch torque, which is very different with the pattern observed in the previous slalom maneuver (Fig. 4.12d). The acceleration torque changes the direction of the clutch torque from the inner wheel to the outer wheel. The comparison of the results of the ELSD models with the measured clutch torque shows a reasonable performance for this very complex and dynamic maneuver. Before $t \approx 5\,s$ and after $t \approx 10\,s$, both the models show a good prediction of the clutch

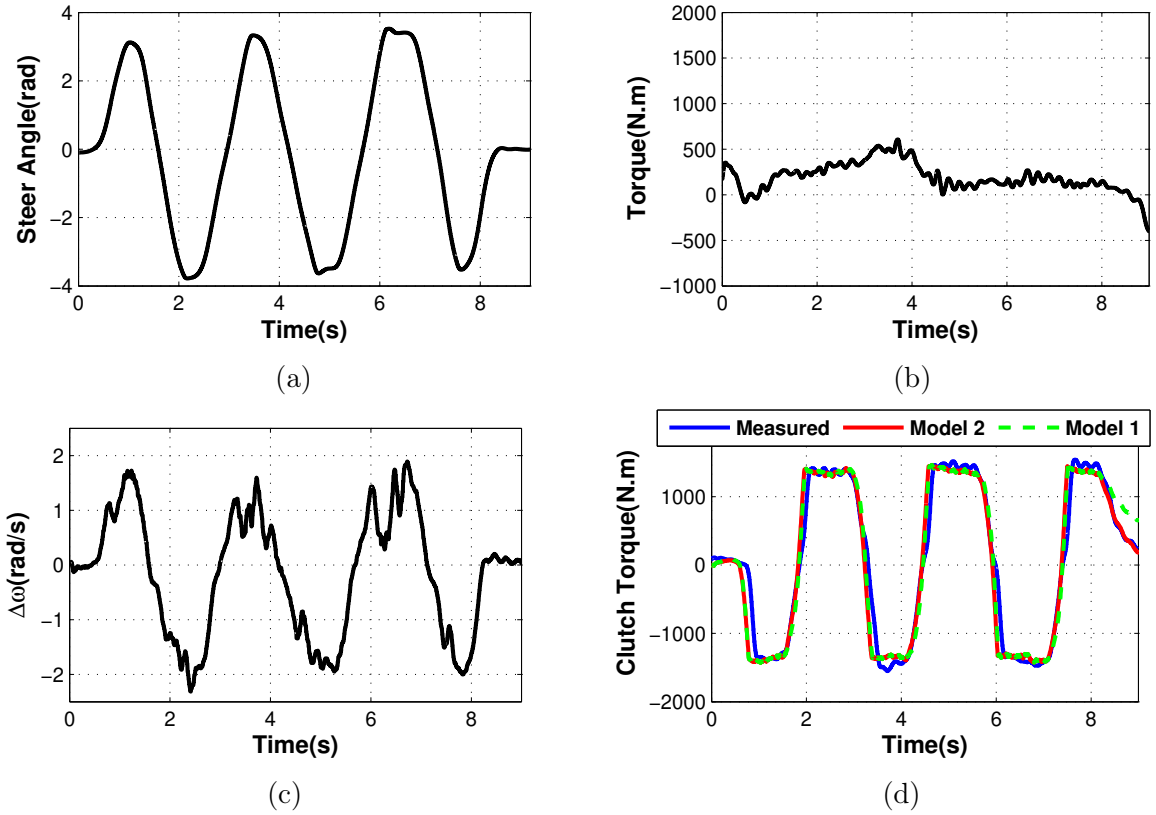

Figure 4.12: (a) The steering wheel input, (b) driver's torque request, (c) wheel speed difference, and (d) ELSD clutch torque in an slalom maneuver with 40 percent clutch pressure performed on a dry asphalt patch.

torque. Between $t \approx 5\,s$ to $10\,s$, there is a reasonable and acceptable error in the ELSD model results. However, the modified model generally has a better performance than the original spring-damper model.

The performance of the ELSD model in the performed maneuvers confirms that it can be used in the controller. This model enables intelligent control of ELSD differential, capable of working in both off-throttle and on-throttle scenarios to prevent unwanted oversteering yaw moments. To evaluate the controller's performance, different maneuvers are conducted including double lane change (DLC), acceleration in turn (AIT), and acceleration in slalom (AIS). The tests are performed on both dry and wet asphalt patches with the friction

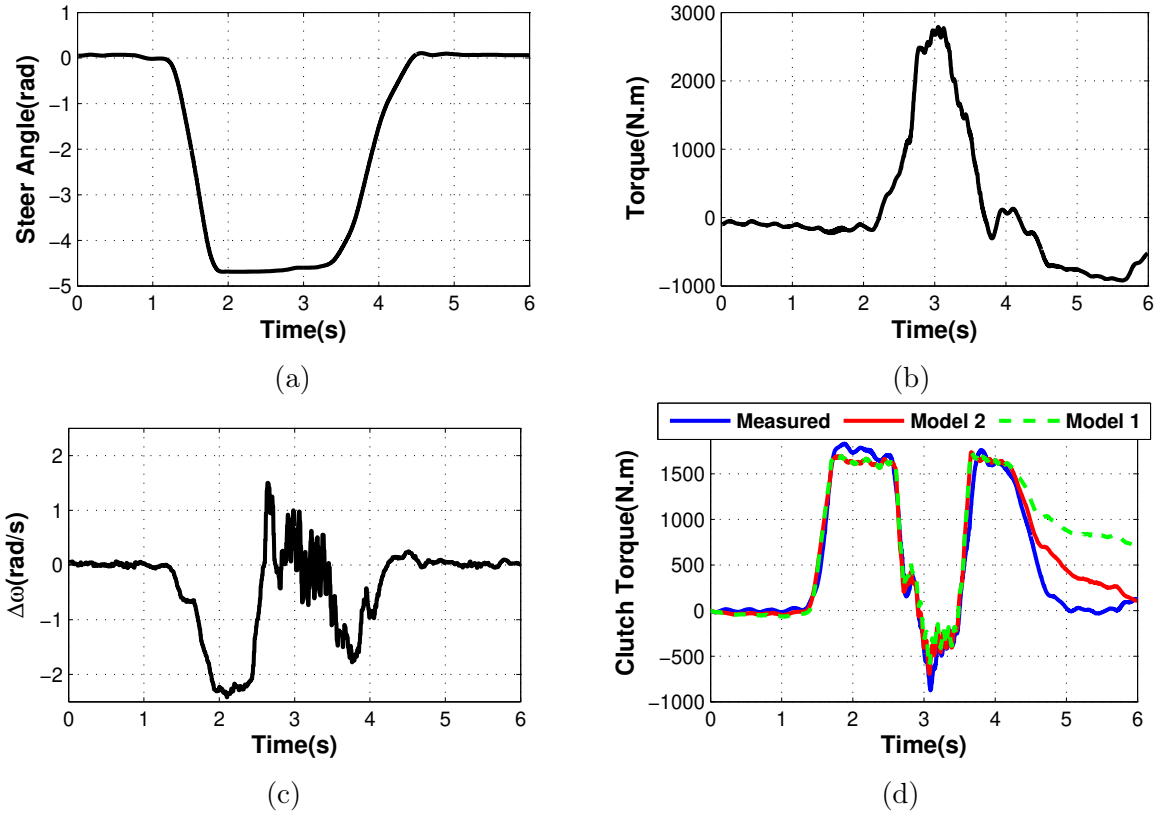

Figure 4.13: (a) The steering wheel input, (b) driver's torque request, (c) wheel speed difference, and (d) ELSD clutch torque in an AIT maneuver with 50 percent clutch pressure performed on a dry asphalt patch.

coefficients of $\mu = 0.9$ and $\mu = 0.6$, respectively.

4.2.2 DLC Maneuver on Wet Road - Experiment

The first driving scenario is a double lane change on a wet asphalt patch ($\mu = 0.6$), with the initial speed of 55 kph. This maneuver is performed with and without the controller. To illustrate the controller's contribution, which consists of ELSD and differential braking, on the vehicle's longitudinal motion, the maneuver is repeated one more time with differential braking only. The parameters of the integrated controller and the differential braking

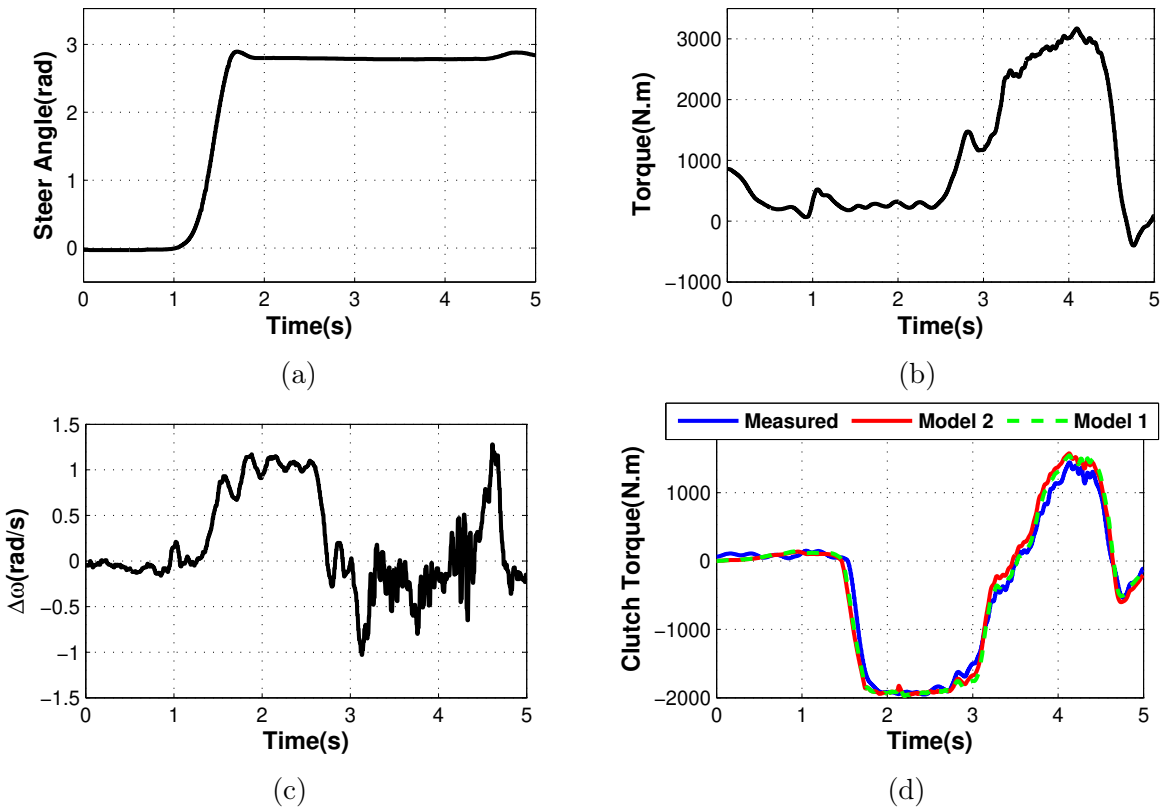

Figure 4.14: (a) The steering wheel input, (b) driver's torque request, (c) wheel speed difference, and (d) ELSD clutch torque in the AIT maneuver shown in Fig. 3.6.

controller are the same, except that ELSD is off in the latter. The driver's steering angle and torque are illustrated in Fig. 4.16. The uncontrolled and controlled maneuvers are very similar; therefore, the maneuvers are suitable for a comparison to assess the controller's performance.

Figure 4.17 compares the vehicle's yaw rate and the longitudinal velocity of the uncontrolled and controlled maneuvers, and Fig. 4.18 shows the controlled ELSD clutch pressure, front differential braking, and rear differential braking in the controlled maneuvers. In the uncontrolled maneuver, the yaw rate rises to $|r_{max}| = 0.91$ and shows a large deviation from the desired value, thereby indicating oversteer and unsafe yaw performance. In the controlled maneuvers, the control actuations are activated properly with the defined priorities

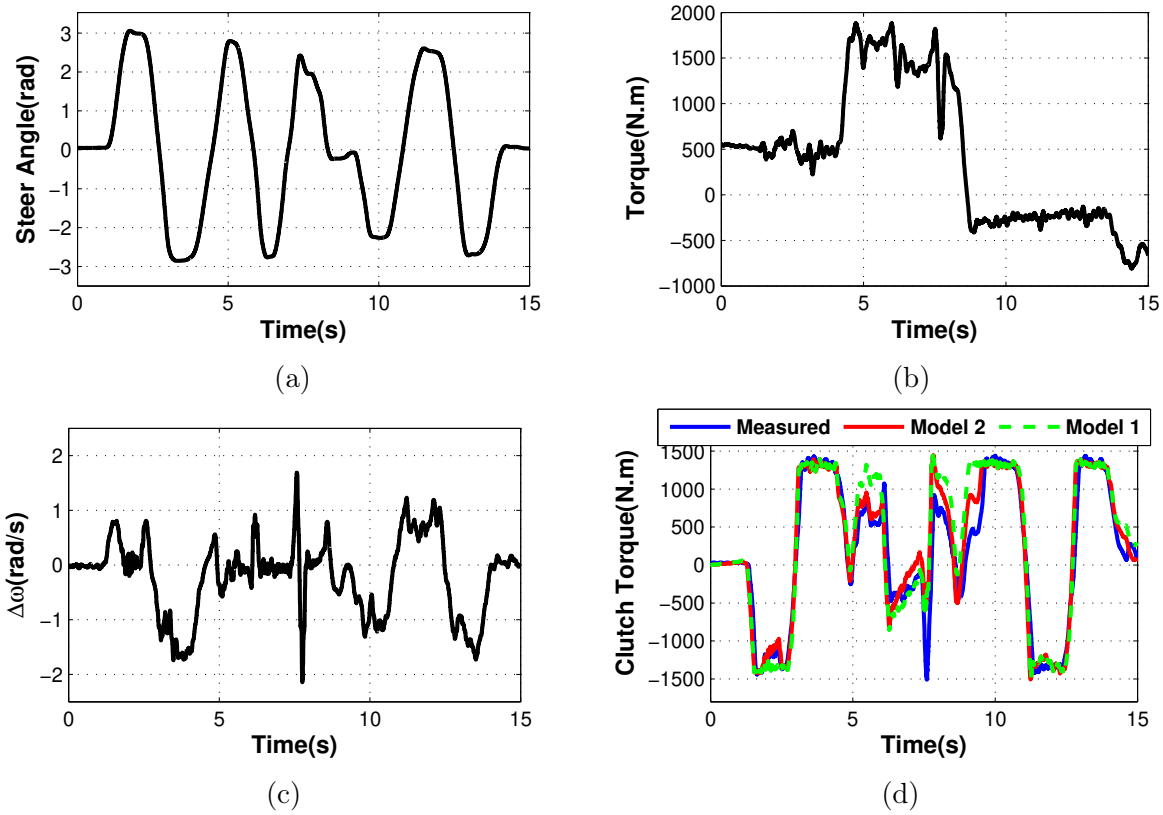

Figure 4.15: (a) The steering wheel input, (b) driver's torque request, (c) wheel speed difference, and (d) ELSD clutch torque in an AIS maneuver with 40 percent clutch pressure on a wet asphalt patch

to improve yaw tracking and enforce the yaw rate's safety limit. The integrated controller activates the ELSD whenever the yaw rate response shows oversteering behavior. This activation of the ELSD generates the clutch torque T_C, calculated as $T_C = T_{rr} - T_{rl}$. Figure 4.18b compares the clutch torque estimated by the ELSD model with the measured clutch torque and shows that the ELSD model has a reasonable closed-loop performance. The front differential braking, which is the low priority actuation, is activated whenever the yaw rate constraint, the high priority objective, is violated to prevent vehicle instability. The rear differential braking is not activated because the ELSD, which has a higher priority on the rear axle, maintains its capability to provide understeering yaw moments throughout the maneuver.

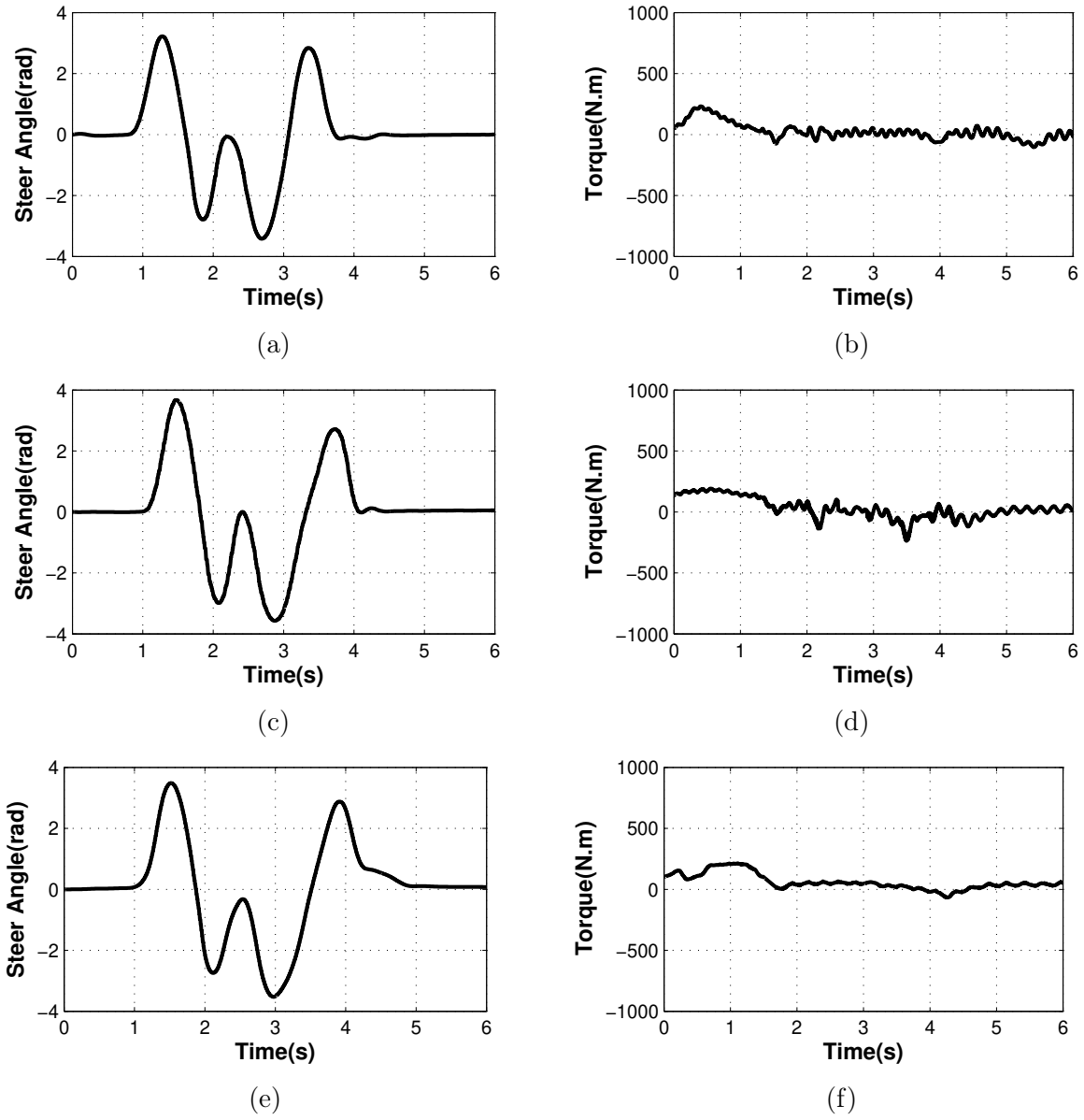

Figure 4.16: The driver's steering wheel and torque in a double lane change maneuver on a wet asphalt patch, with controller OFF (a,b), controller ON (c,d), and differential braking (e,f).

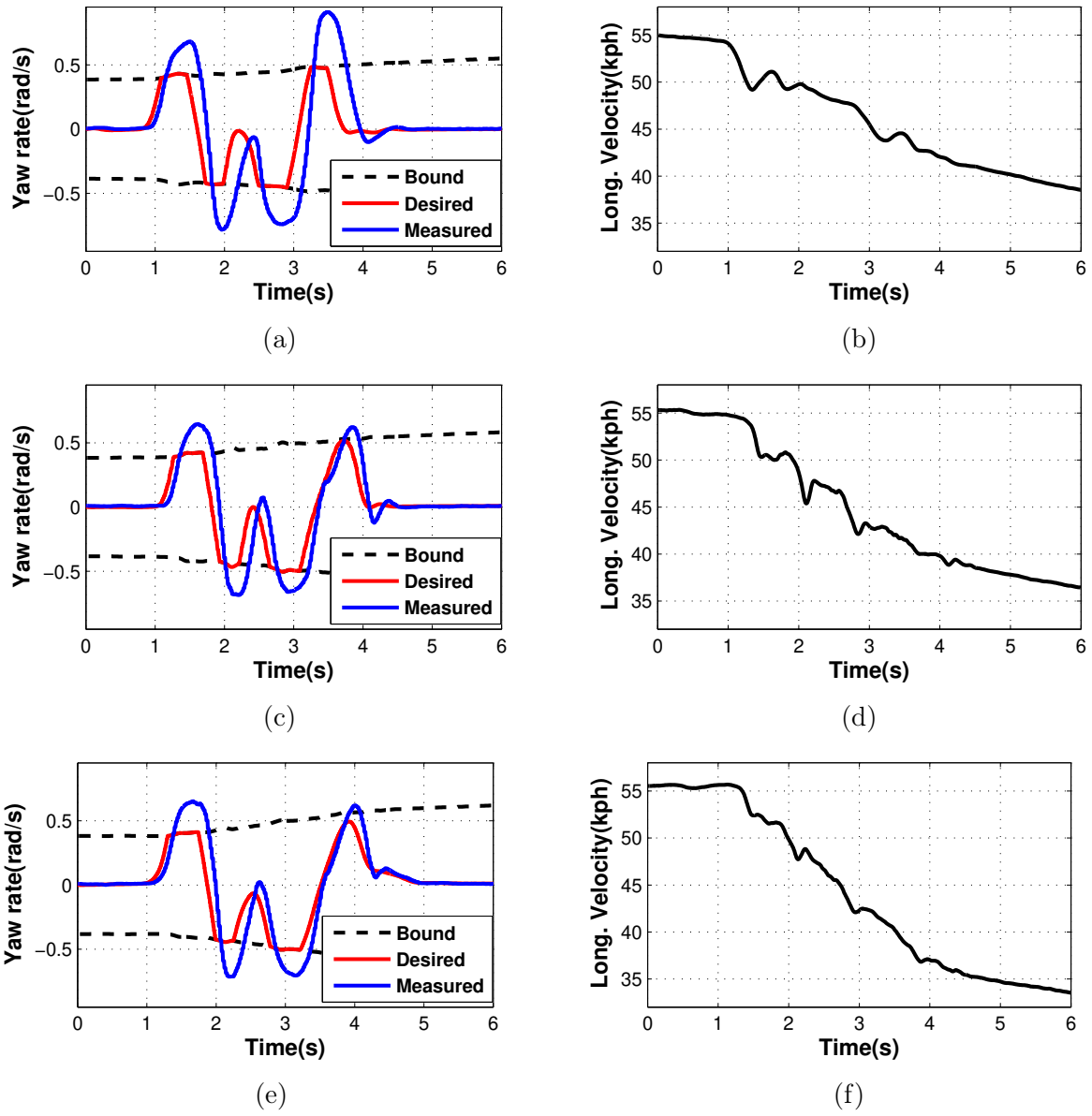

Figure 4.17: The vehicle's yaw rate and longitudinal velocity in a double lane change maneuver on a wet asphalt patch, with controller OFF (a,b), controller ON (c,d), and differential braking (e,f).

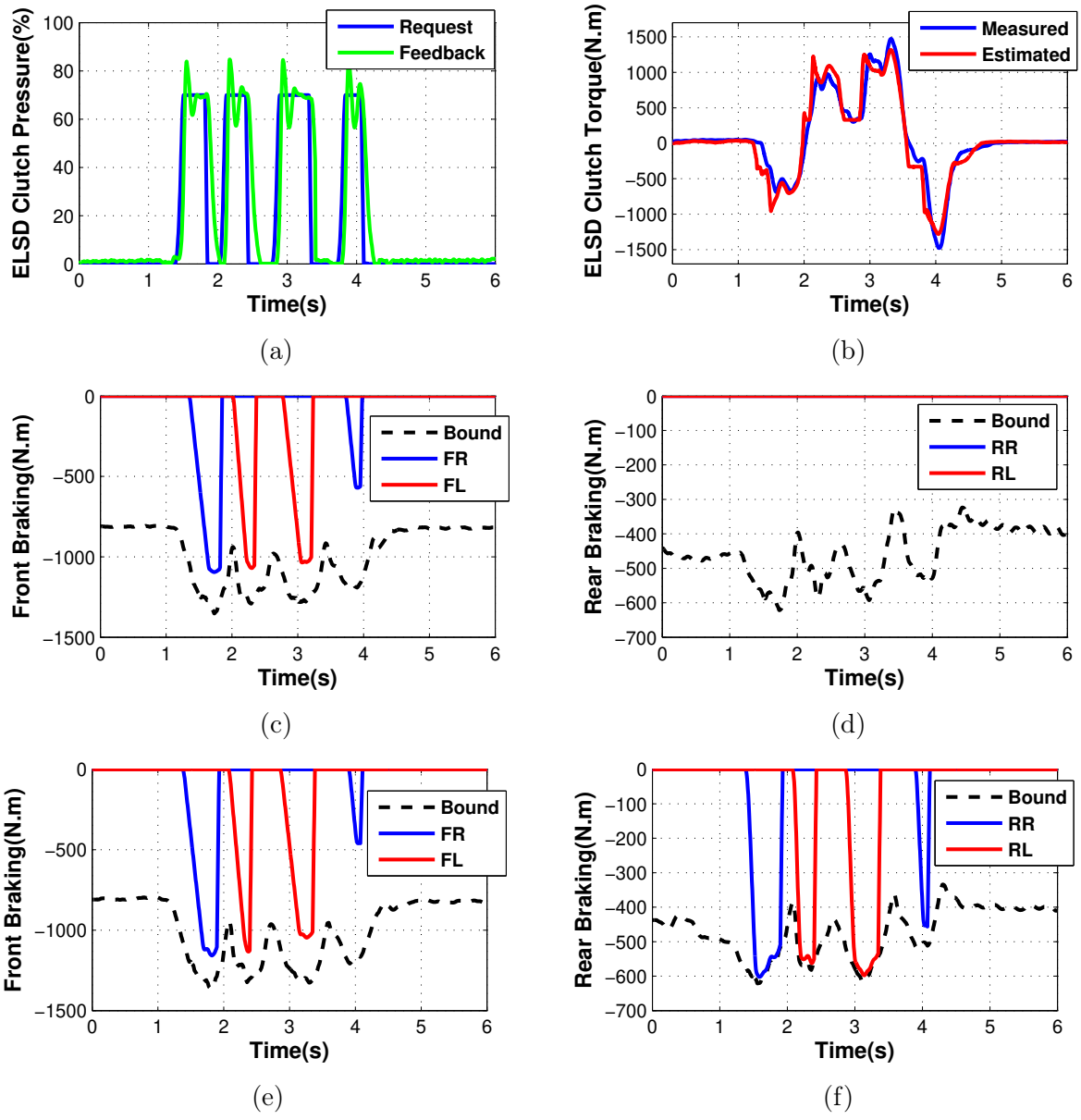

Figure 4.18: (a) Controlled ELSD clutch pressure, (b) controlled ELSD clutch torque. Front and rear differential braking with controller ON (c,d) and differential braking only (e,f) in a double lane change maneuver on a wet asphalt patch.

The differential braking controller activates the front and rear differential braking when the yaw rate's safety limit is violated. The results show that both the integrated controller and the differential braking controller significantly improve the yaw rate response, with almost similar performance and with the maximum yaw rate of $|r_{max}| = 0.7$, which is much less than that in the uncontrolled maneuver. However, the integrated controller has a better performance in longitudinal velocity (with almost 4 kph less speed drop) because it incorporates the available actuation of ELSD with the prioritization control structure and uses less differential braking.

4.2.3 Acceleration in Slalom Maneuver on Dry Road - Experiment

The second driving scenario is accelerating during a slalom maneuver on dry asphalt ($\mu = 0.9$), which is performed with the controller in the loop to evaluate the closed loop performance of the ELSD model and the actuator prioritization in an on-throttle maneuver. Figure 4.19 shows the driver inputs of steering and throttle torque along with the vehicle's longitudinal velocity and yaw rate. The initial vehicle speed is 35 kph, with acceleration to 53 kph.

Figure 4.20 presents the ELSD clutch pressure, the ELSD clutch torque, the front differential braking, and the rear differential braking during the test. The hydraulic pump controller design is intended to ensure that the clutch pressure feedback closely follows any changes in clutch pressure request. Apart from a few minor local errors, the ELSD model is able to follow the measured clutch torque. The controller activates the ELSD clutch whenever the clutch torque can generate a yaw moment contributing to the yaw tracking objective. Before $t \approx 6\,s$, the ELSD clutch has the capability of generating understeering yaw moment, as predicted by the ELSD model. Thus, whenever the desire yaw rate is exceeded, the ELSD clutch is activated and damps the excess yaw rate. Between $t \approx 6\,s$ to $9\,s$, the ELSD clutch model detects that the direction of the torque biasing capability of the ELSD clutch has changed. Thus, the controller makes the ELSD inactive to avoid generating oversteer yaw moments that could jeopardize the stability of the vehicle. The change in the torque biasing direction is due to the sudden high acceleration torque and the resultant increase in vehicle speed saturating the inner wheels. During this time, the yaw rate increases whereas its safety bound drops, causing the yaw rate to violate the safety limit. As a result, to improve vehicle stability, the controller activates the front differential braking whenever the yaw rate's bound is violated. It also involves the rear differential

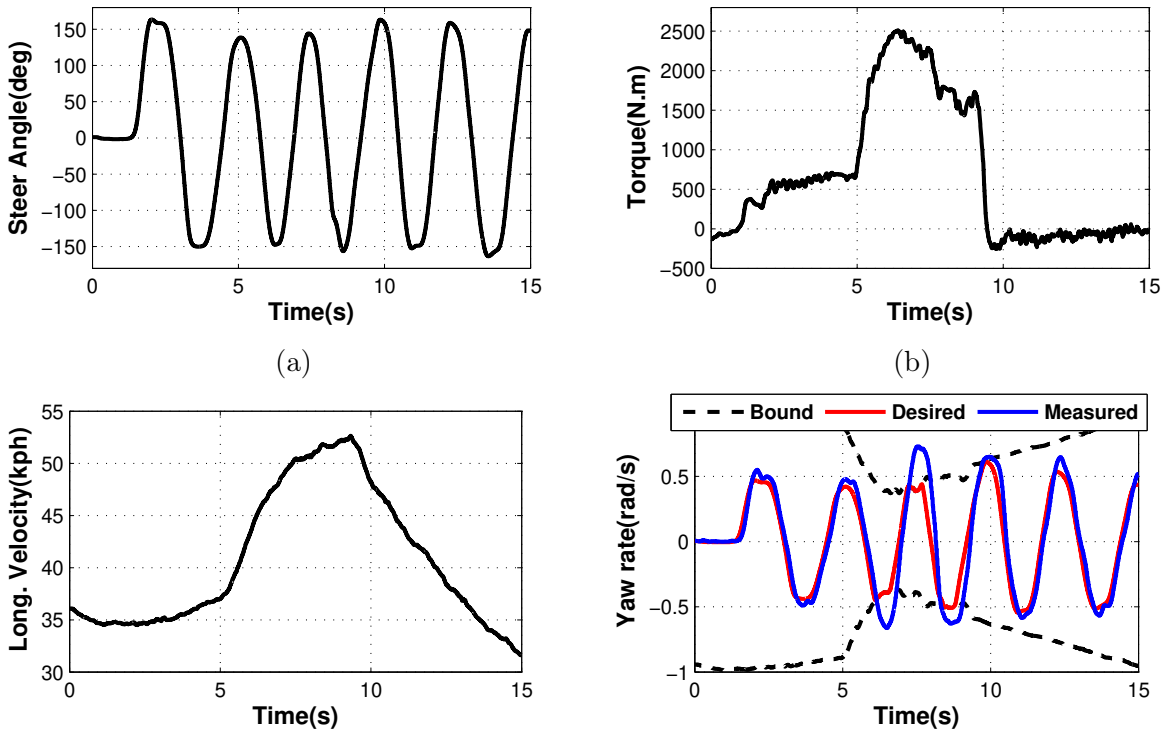

Figure 4.19: The driver's steering wheel and torque (a,b), and the vehicle's longitudinal velocity and yaw rate (c,d) in an acceleration in slalom maneuver on a dry asphalt patch with controller in the loop.

braking because of the safety limit's violation and the inability of the ELSD to generate understeering yaw moments during this time ($t \approx 6\,s$ to $9\,s$). When after $t \approx 9\,s$, the ELSD model detects that the differential can generate understeering yaw moment again. Thus, the ELSD clutch is activated if the yaw rate exceeds the desired value.

4.2.4 Acceleration in Turn Maneuver on Dry Road - Experiment

The third driving scenario is an acceleration in turn maneuver on dry asphalt ($\mu = 0.9$), and this maneuver is carried out 1) with the controller OFF, and 2) with it ON. In Fig. 4.21, the similarity of the driver inputs (steering angle and torque) of the uncontrolled and

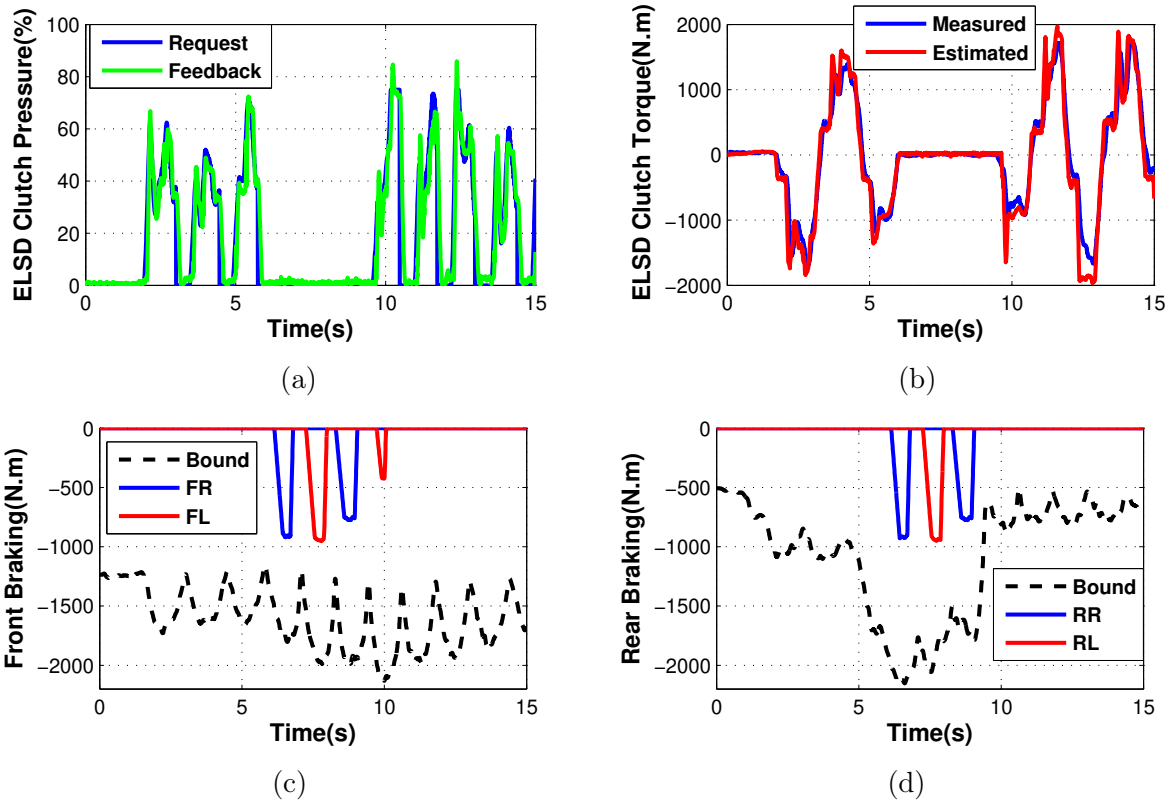

Figure 4.20: (a) ELSD clutch pressure, (b) ELSD clutch torque, (c) front differential braking, and (d) rear differential braking in an acceleration in slalom maneuver on a dry asphalt patch with controller in the loop.

controlled maneuvers indicates that they are suitable for a comparative evaluation of the controller's performance.

Figures 4.22a and 4.22b show the yaw rate of the uncontrolled and controlled maneuvers. The yaw rate response shows that the uncontrolled maneuver becomes unstable, whereas the controlled maneuver is stabilized by properly controlling the ELSD clutch pressure (Fig. 4.22c), the front differential braking (Fig. 4.22e), and the rear differential braking (Fig. 4.22f). The ELSD model properly estimates clutch torque (Fig. 4.22d). The controller activates the ELSD clutch at $t \approx 1.4\,s$ to damp the excessive yaw rate by generating an understeering yaw moment. The driver's acceleration torque on the rear axle reduces the yaw rate's safety limit. At $t \approx 3.2\,s$, the yaw rate violates its safety bound, causing the

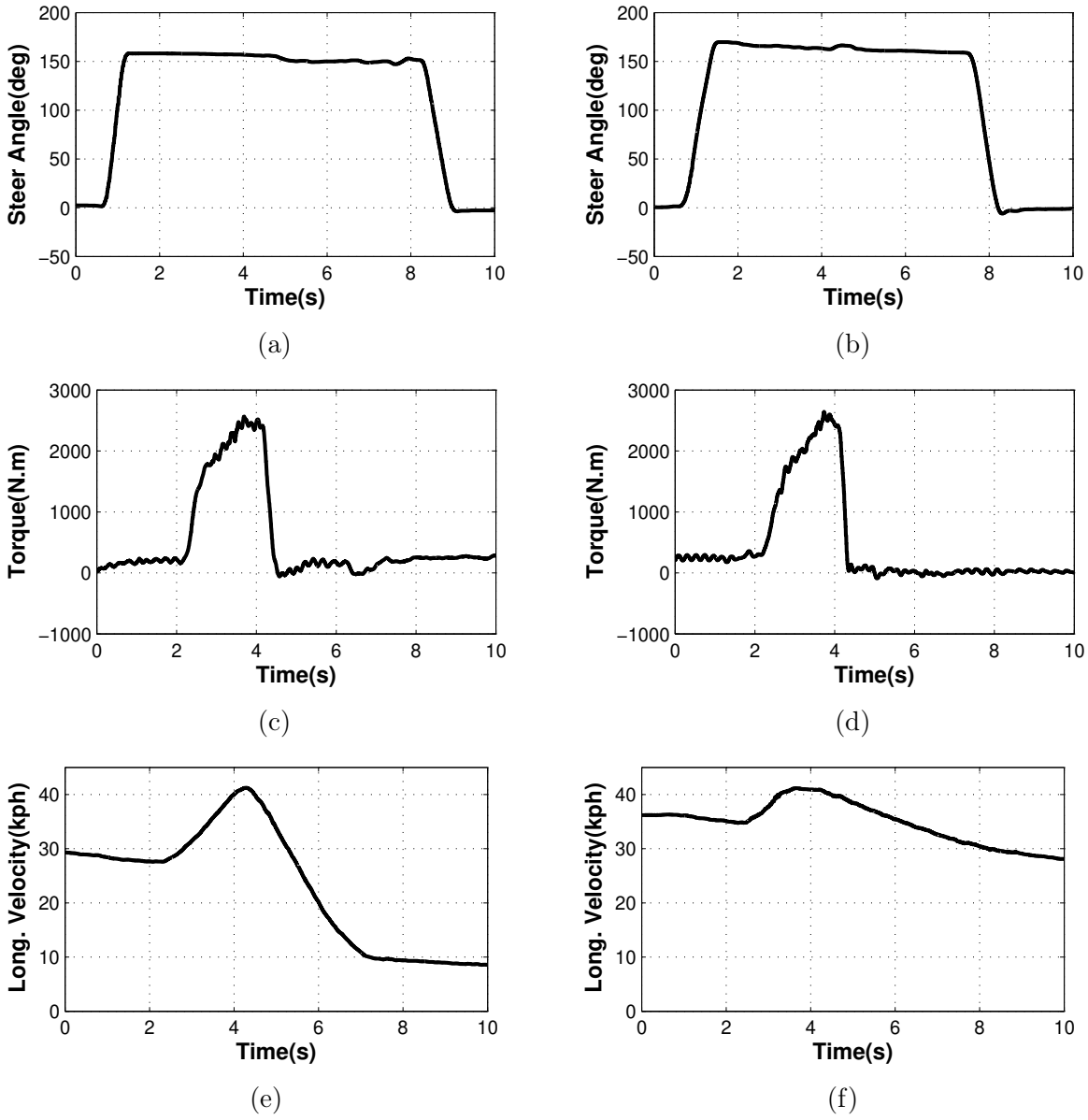

Figure 4.21: The steering wheel input, driver's torque request, and the vehicle's longitudinal velocity in an acceleration in turn maneuver on a dry asphalt patch, with controller OFF (a,c,e) and controller ON (b,d,f).

controller to activate front differential braking to enforce the yaw safety limit. At $t \approx 3.5\,s$, the direction of the clutch torque transfer changes because of the high acceleration torque, making the ELSD unable to generate understeering yaw moment. Therefore, the controller disengages the ELSD clutch to avoid producing unwanted oversteering yaw moment and endangering vehicle stability, and instead activates the rear differential braking to generate understeering yaw moment and improve vehicle stability. At $t \approx 4.2\,s$, the driver suddenly drops the acceleration torque, thus increasing the yaw rate safety bound. Consequently, the controller deactivates the differential braking because the yaw rate becomes less than its safety limit. The reduction of the acceleration torque also results in a change in the torque biasing capability of the ELSD clutch to the desired direction. Therefore, the controller again activates the ELSD clutch to provide understeering yaw moment and improve the yaw tracking performance. This test clearly shows the effectiveness of the controller design and its intelligent control of the ELSD clutch and actuation prioritization structure (activating the low priority actuation only when the high priority objective demands doing so).

4.3 Case Study 3: Integrated Lateral and Roll Stability

In Case Study 3, the prioritization controller is implemented on an electric E-Class SUV vehicle in CarSim equipped with actuations of differential braking and front/rear torque shifting. The prioritization structure of the control actuations and control objectives is shown in Fig. 3.11c. Similar to Case Study 1, a constant 40-60 front/rear torque distribution is used for the baseline vehicle. The controller's performance is evaluated numerically using co-simulation in CarSim and MATLAB/Simulink in different driving maneuvers with different road frictions and road angles. Each maneuver is performed two times: (1) with the controller OFF, (2) with the controller ON.

4.3.1 Acceleration in Turn Maneuver on Dry Road - Simulation

The first driving scenario is an acceleration in turn maneuver on a dry road ($\mu = 1$) with the initial speed of 80 kph. Figure 4.23 shows the driver's steering input and total torque request. Figure 4.24a shows the controlled front/rear torque distribution. The uncontrolled maneuver has a constant baseline torque distribution, which is 40 percent to the front axle and 60 percent to the rear axle. Figure 4.24b shows the differential braking

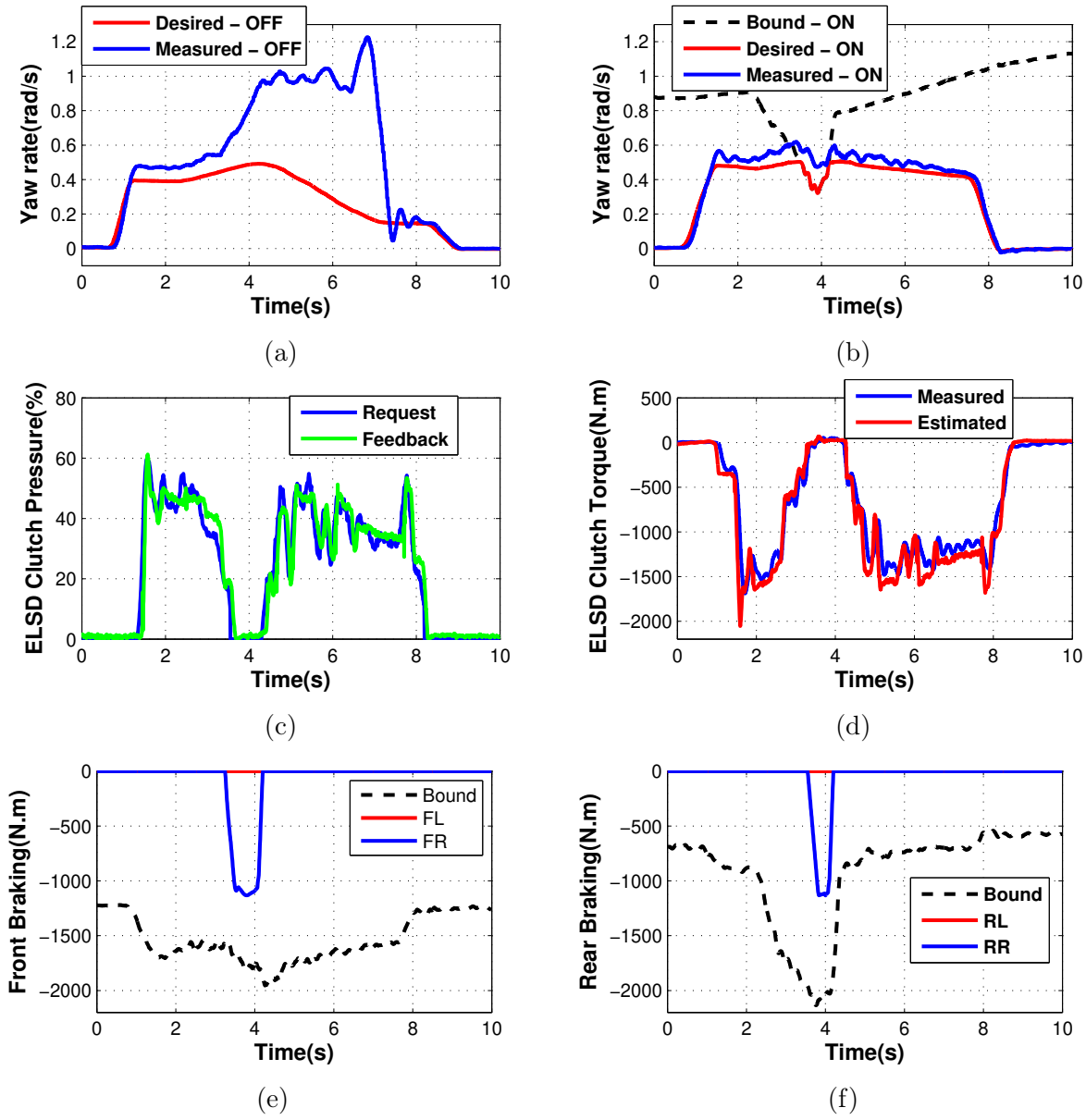

Figure 4.22: (a) The yaw rate of uncontrolled vehicle, (b) the yaw rate of controlled vehicle; (c) ELSD clutch pressure, (d) ELSD clutch torque, (e) front differential braking, and (f) rear differential braking in an acceleration in turn maneuver on a dry asphalt patch.

is not activated in this maneuver and remains unused. The vehicle's yaw rate, the rear tire slip angle, and the roll index of the uncontrolled and controlled maneuvers are presented comparatively in Fig. 4.25. In this maneuver, the yaw rate, sideslip, and roll index of both the uncontrolled and controlled maneuvers are within their safety limits. Therefore, the prioritization controller properly decides not to activate the differential braking (the low priority actuation) because the stability limits (the high priority objectives) do not demand it. However, the controller uses the front/rear torque shifting (the high priority actuation) to improve the vehicle's handling performance (the low priority objective). The yaw rate of the uncontrolled maneuver is less than the desired yaw rate and the vehicle shows understeer behavior. In the controlled maneuver, the controller allocates more torque to the rear axle to reduce the rear axle's lateral forces and induce oversteering, thereby improving the yaw tracking performance. Therefore, the yaw tracking performance is improved by simply adjusting the front/rear torque distribution and without engaging the differential braking, which shows the advantage of the proposed prioritization control structure.

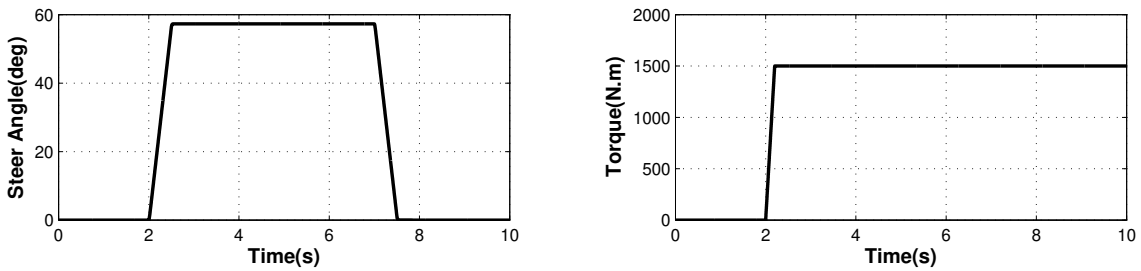

(a) (b)

Figure 4.23: (a) Steering wheel angle, and (b) driver's torque request in an acceleration in turn maneuver on a dry road.

4.3.2 Acceleration in Flick Maneuver on Sticky Road - Simulation

The first driving scenario is acceleration in a flick maneuver on a sticky (high friction) road with the initial speed of 80 kph. Figure 4.26 shows the driver's steering input and total torque request. Figure 4.27a shows the controlled front/rear torque distribution. The uncontrolled maneuver has a constant baseline torque distribution, which is 40 percent

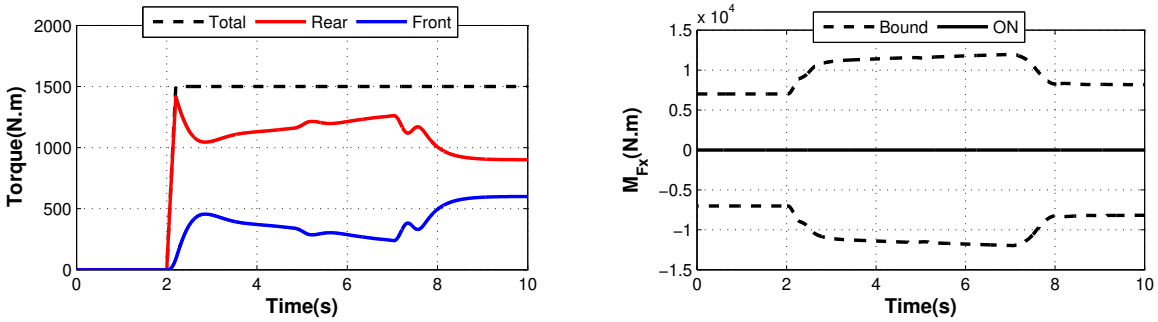

(a) (b)

Figure 4.24: (a) Front/rear torque allocation, and (b) the yaw moment M_{F_x}, in the controlled AIT maneuver on a dry road.

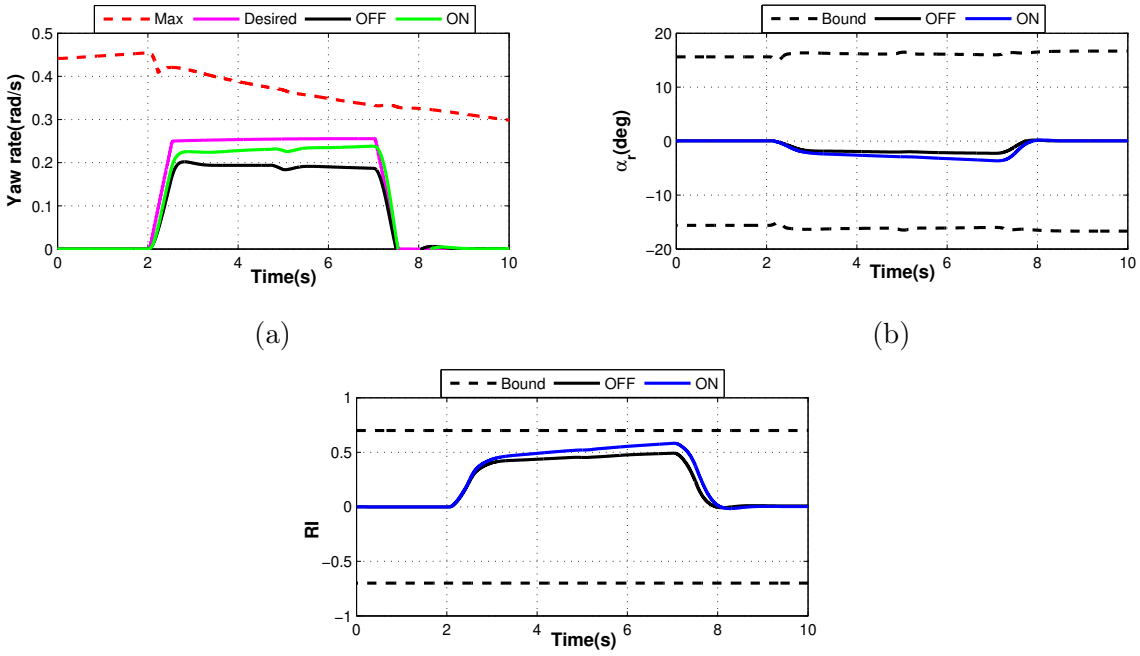

(a) (b)

(c)

Figure 4.25: (a) The yaw rate, (b) the rear tire slip angle, and (c) the roll index, with controller ON and OFF in an acceleration in turn maneuver on a dry road.

to the front axle and 60 percent to the rear axle. Figure 4.27b shows the yaw moment generated by the differential braking in the controlled maneuver. The vehicle's yaw rate, the rear tire slip angle, and the roll index of the uncontrolled and controlled maneuvers are presented comparatively in Fig. 4.28. The roll index of the uncontrolled vehicle exceeds the defined safety zone and endangers the roll stability of the vehicle. However, in the controlled mamneuver, the control actuations are activated properly to enforce the roll constraint and prevent the vehicle's roll over. Whenevr the safety constraints are violated, the controller activates the differential braking and shifts torque to the front axle to indirectly reduce the lateral forces of the front tires by the tire force coupling effect and consequently generate understeering yaw moment. The uncontrolled maneuver's sideslip is within the safety limits, and its yaw rate violates the yaw rate's safety bound only for a short period of time. In fact, this maneuver excites mostly the vehicle's roll dynamic and endangers the roll stability, which is controlled properly with the designed controller.

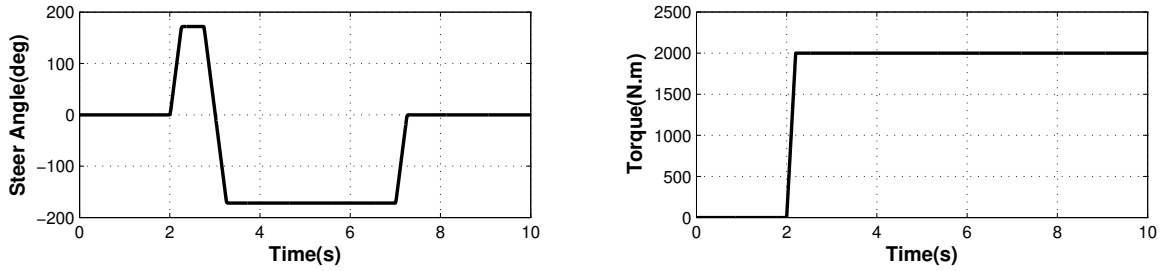

(a) (b)

Figure 4.26: (a) The steering wheel angle, and (b) driver's torque request in an acceleration in a flick maneuver on a sticky road.

4.3.3 Acceleration in Slalom Maneuver on Wet Banked Road - Simulation

The second driving scenario is acceleration in a slalom maneuver on a wet banked road with the friction coefficient of $\mu = 0.5$ and the bank angle of $\phi_r = -20\%$ with the initial speed of 50 kph. Figure 4.29 shows the driver inputs of steering angle and acceleration torque request. The controlled actuations, front/rear torque distribution and differential braking, are shown in Fig. 4.30. The test results of the uncontrolled and controlled maneuvers

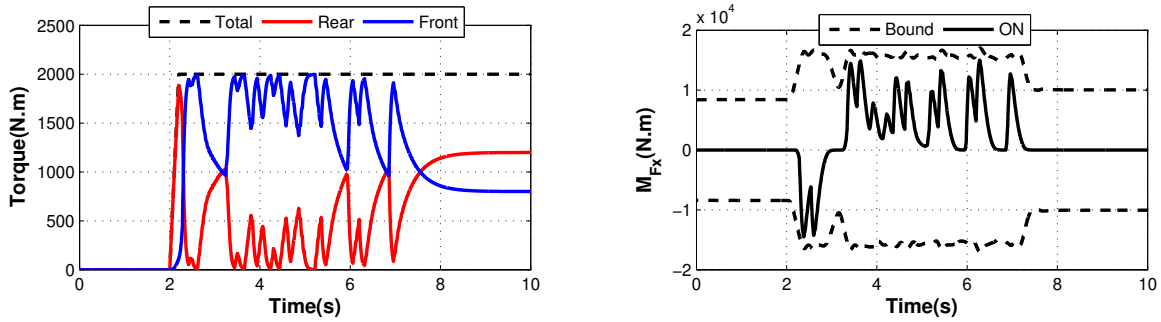

(a) (b)

Figure 4.27: (a) The front/rear torque allocation, and (b) the yaw moment by differential braking, in the controlled acceleration in flick maneuver on a sticky road.

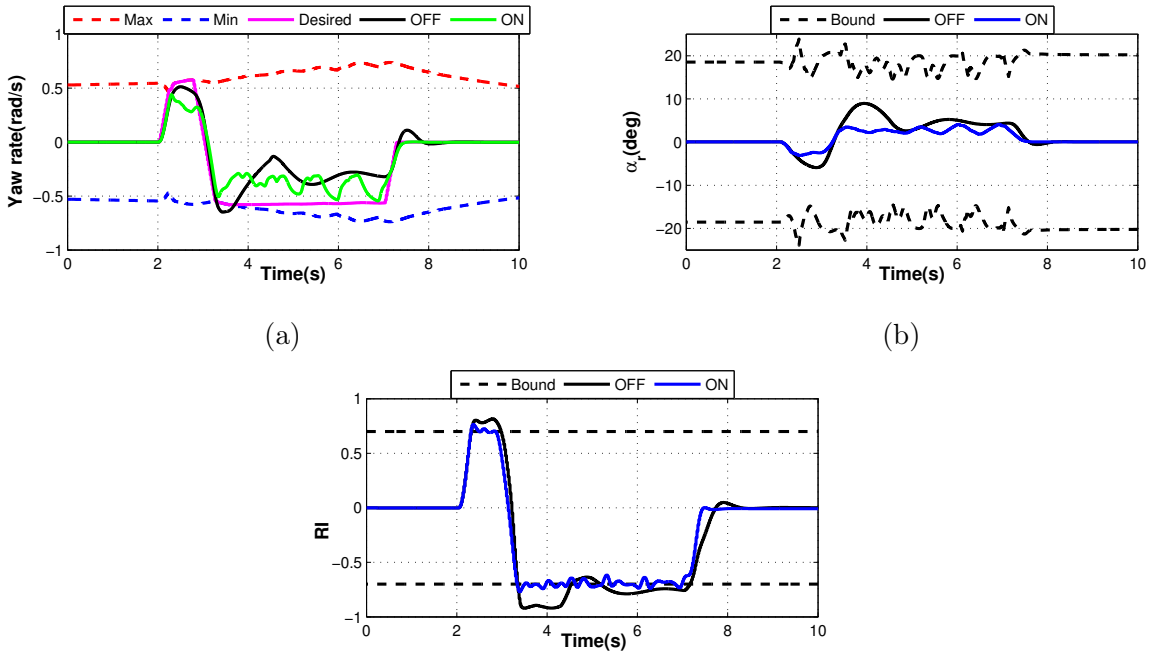

(a) (b)

(c)

Figure 4.28: (a) The yaw rate, (b) the rear tire slip angle, and (c) the roll index, with controller ON and OFF in an acceleration in flick maneuver on a sticky road.

are compared in Fig. 4.31. The yaw rate and the rear tire slip angle of the uncontrolled vehicle violate the defined safety limits and show unstable behavior, whereas the controlled maneuver is stabilized by properly activating the control actuations. The controller adjusts front/rear torque distribution for improving yaw tracking performance and enforcing the defined safety limits, but differential braking is activated only to enforce the safety limits. The adjustment of torque distribution between $t \approx 2\,s$ to $4.8\,s$ is related to improving the yaw tracking performance within the safety limits. It should be noted that the roll indexes of both uncontrolled and controlled maneuvers are within its safety limits because the low friction surface cannot significantly excite the roll dynamic and endanger roll stability. However, the low friction surface can be more dangerous for the vehicle's lateral and yaw stability. In the controlled maneuver, differential braking is activated whenever the yaw rate's limit is violated to maintain vehicle stability.

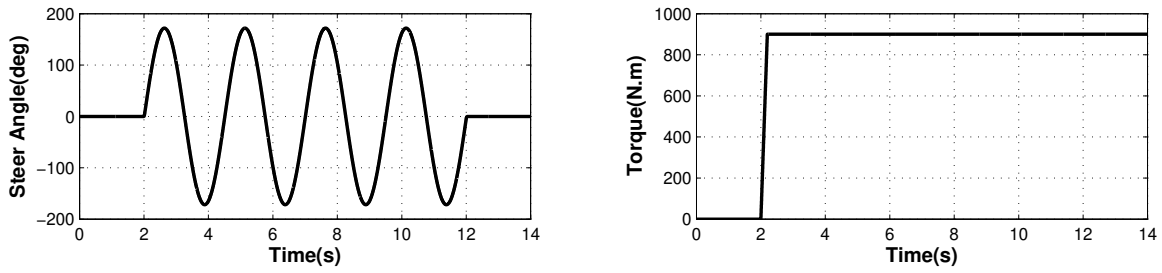

(a) (b)

Figure 4.29: (a) The steering wheel angle, and (b) driver's torque request in an acceleration in a slalom maneuver on a wet banked road.

4.3.4 Acceleration in Slalom Maneuver on Dry Banked Road - Simulation

The third driving scenario is acceleration in a slalom maneuver on a dry banked road with the friction coefficient of $\mu = 1$ and the bank angle of $\phi_r = -20\%$ with the initial speed of 80 kph. The driver inputs are shown in Fig. 4.32. The steering angle is the same as the previous maneuver, but the acceleration torque is increased to 1500 N.m. Figure 4.33 shows the controlled front/rear torque shifting and differential braking, and Fig. 4.34 compares the test results of the uncontrolled and controlled maneuvers. In the

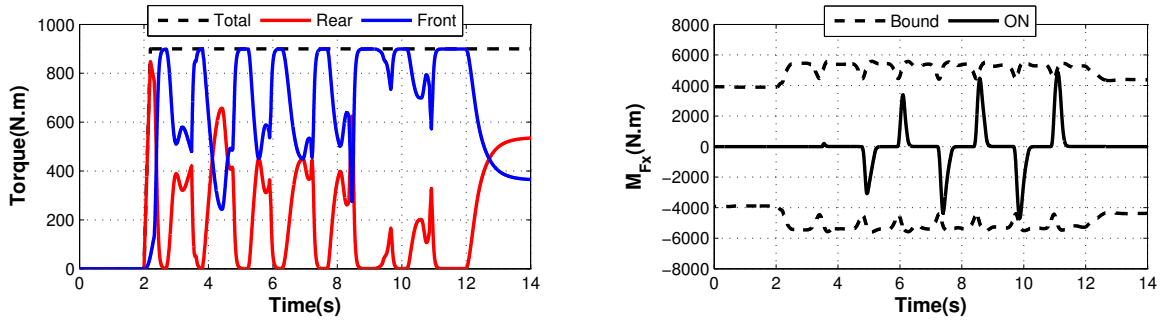

(a) (b)

Figure 4.30: (a) The front/rear torque allocation, and (b) the yaw moment by differential braking, in the controlled acceleration in a slalom maneuver on a wet banked road.

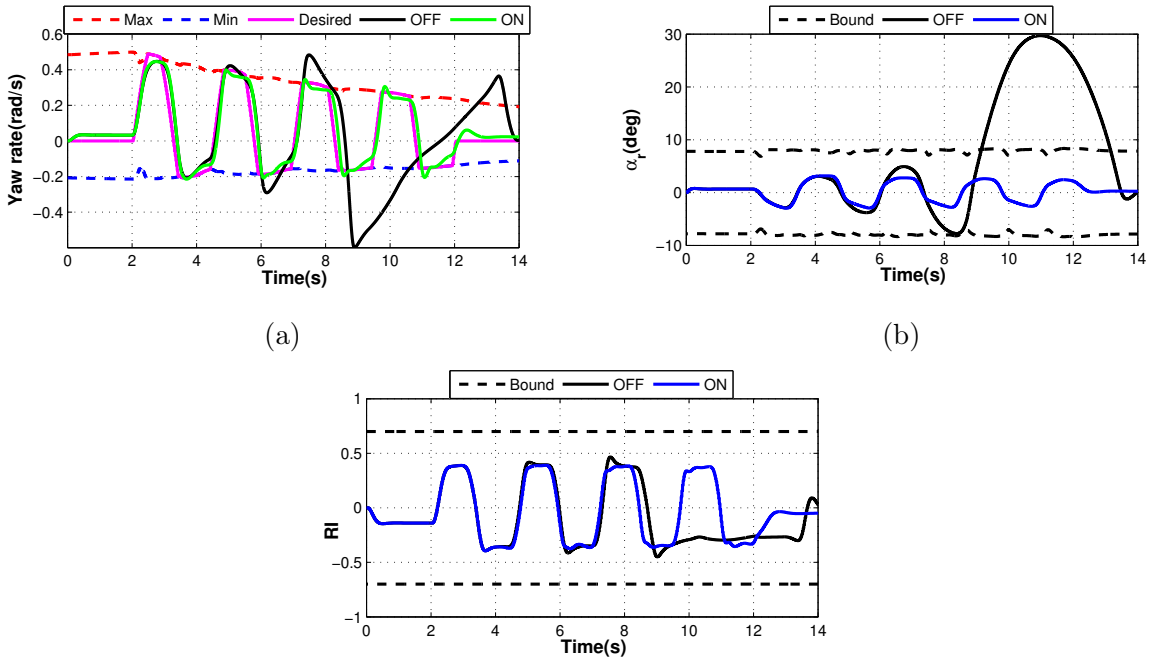

(a) (b)

(c)

Figure 4.31: (a) The yaw rate, (b) the rear tire slip angle, and (c) the roll index, with controller ON and OFF in an acceleration in a slalom maneuver on a wet banked road.

uncontrolled maneuver, all the defined safety limits for the vehicle's yaw rate, sideslip, and roll index are violated and the vehicle shows a very dangerous behavior. In the controlled maneuver, the controller properly adjusts the front/rear torque distribution and activates differential braking to enforce the safety limits. In the uncontrolled maneuver, the safety limits of both the vehicle's yaw rate and the roll index are violated at around $t \approx 3\,s$. Comparing the results of this maneuver to those of the previous maneuver shows that performing a similar maneuver on a road with higher friction increased the excitation of roll dynamics and resulted in a higher roll index. While the lateral stability is usually more important in low friction surfaces, the roll stability can be critical in high friction roads. Therefore, the integration of the lateral stability, yaw stability, and roll stability systems enables the controller to ensure that all these safety limits are addressed.

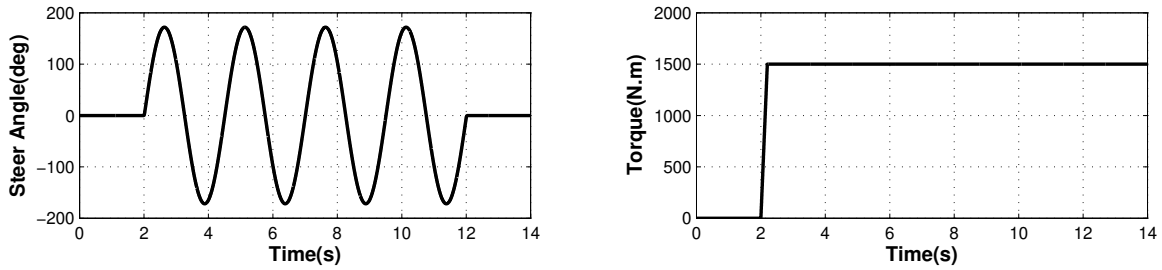

(a) (b)

Figure 4.32: (a) The steering wheel angle, and (b) driver's torque request in an acceleration in a slalom maneuver on a dry banked road.

4.4 Summary

In this chapter, the performance of the prioritization model predictive controller developed in Chapter 3 was evaluated numerically as well as experimentally for the three case studies described in Section 3.7. In the first case study, implemented on an electric Chevrolet Equinox, the closed-loop vehicle performance was compared with the uncontrolled vehicle response. The numerical and experimental tests showed that the axle torque distribution combined with the differential braking can effectively improve vehicle stability and handling. In addition, to illustrate the benefit of the proposed prioritization controller (Controller A), the results were compared with those of the same vehicle equipped with

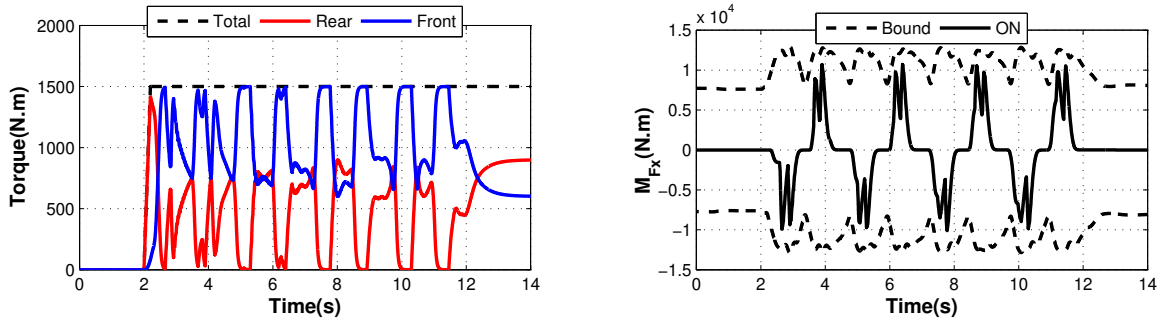

(a) (b)

Figure 4.33: (a) The front/rear torque allocation, and (b) the yaw moment by differential braking, in the controlled acceleration in a slalom maneuver on a dry banked road.

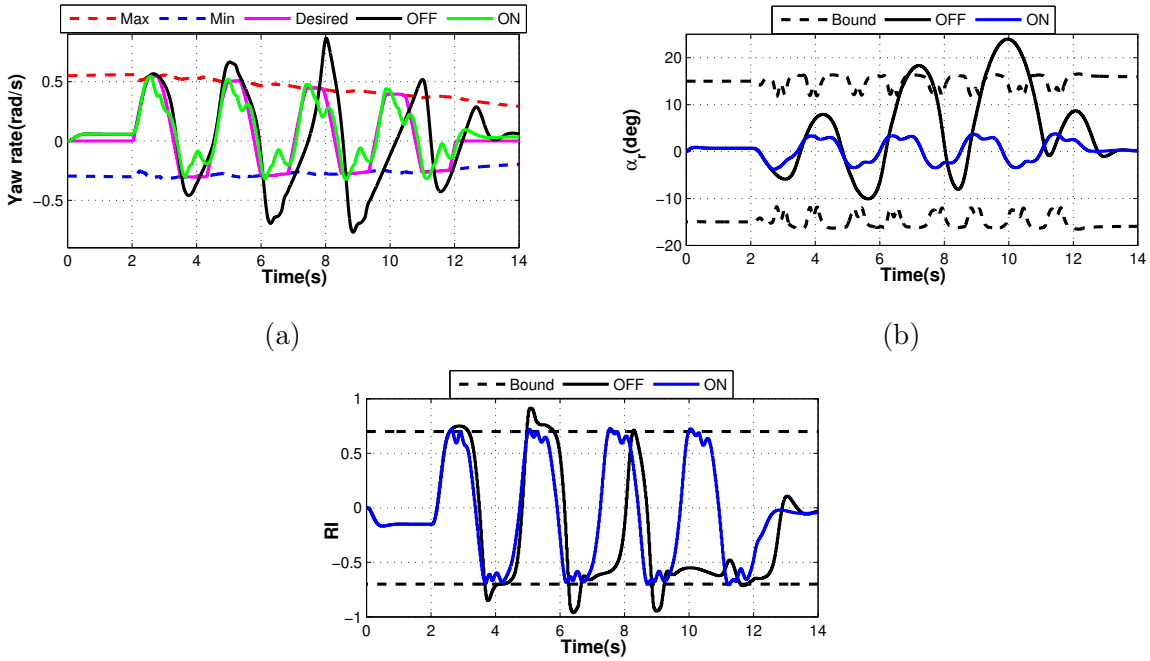

(a) (b)

(c)

Figure 4.34: (a) The yaw rate, (b) the rear tire slip angle, and (c) the roll index, with controller ON and OFF in an acceleration in a slalom maneuver on a dry banked road.

only differential braking (Controller B). The comparison showed that the actuation prioritization enables the controller to enhance the vehicle's performance in longitudinal motion by decreasing the use of differential braking.

In the second case study, implemented on a Cadillac CTS vehicle, the accuracy of the designed ELSD model was validated experimentally in different maneuvers and with different ELSD excitation levels. The designed ELSD model was used in the controller to properly control ELSD clutch pressure and to allow for correctly switching the control actions on the rear axle. Experimental evaluation during a range of driving maneuvers on various road surfaces confirms the proposed controller's performance. To control the vehicle's yaw rate, it properly engages and disengages the control actions while considering their capabilities and the defined priorities. Similar to Case 1, the prioritization scheme resulted in decreasing the use of differential braking, with a consequent lessening of the controller's impact on the vehicle's longitudinal motion.

In the third case study, the controller performance was evaluated numerically using an E-Class SUV vehicle in CarSim. The designed controller activates differential braking to ensure roll, lateral, and yaw stabilities. Its performance, evaluated in different driving maneuvers with different road frictions on flat and non-flat roads, illustrates the importance of integrating roll dynamics with lateral dynamics. The results show that maneuvers performed on high friction roads mostly excite the roll dynamics thereby endangering roll stability, whereas those performed on low friction roads mostly excite the lateral dynamics.

Chapter 5

Integrated Vehicle Stability and Path Planning/Tracking Control Design

In this chapter, the stability controller designed in the previous chapters is extended to act as a path planning/tracking controller through the addition of two new control objectives - tracking a desired path and collision avoidance - within the model predictive control design. The controller considers a short prediction horizon for vehicle stability and a long prediction horizon for path planning/tracking. When a sudden obstacle appears on the road, autonomous steering may not be able to respond fast enough to prevent a collision or instability. Therefore, the controller may employ torque/brake vectoring conservatively when needed, to produce an additional yaw moment, thereby improving a vehicle's lateral agility and responsiveness. Another challenge that an autonomous vehicle needs to tackle is uncertain road condition. To this end, the designed path planner is extended to a contingency path planner to ensure avoidance maneuvers, while still following the given path as closely as possible.

This chapter describes the following in the order given: the system modeling, which includes the vehicle model and its discretization; the system constraints, including the environmental and actuation constraints; the control design, with its lateral and longitudinal controllers; the extension of the designed controller to a contingency MPC controller capable of handling sudden events; and finally, the simulations performed to evaluate the effectiveness of the designed controllers.

5.1 System Modelling

The control-oriented model is created using a planar bicycle model with two velocity states, lateral velocity, v, and yaw rate, r, and two position states, heading deviation, $\Delta\psi$, and lateral deviation, e, from the desired path, illustrated in Fig. 5.1. The vehicle is front-wheel drive and is equipped with active front steering and differential braking. The desired longitudinal velocity of the vehicle along the path is given, and a longitudinal controller is used to calculate the drive/brake torque to follow the desired speed. Therefore, the longitudinal velocity, u, is considered to be known by the lateral controller. Using the small angle assumption, the lateral dynamics of the vehicle are as follows:

$$\dot{v} = \frac{F_{yf} + F_{yr}}{m} - ur - g\left(\cos\theta_r \sin\phi_r + \sin\theta_r\, \Delta\psi\right), \tag{5.1}$$

$$\dot{r} = \frac{M_{F_y} + M_{F_x}}{I_z}, \tag{5.2}$$

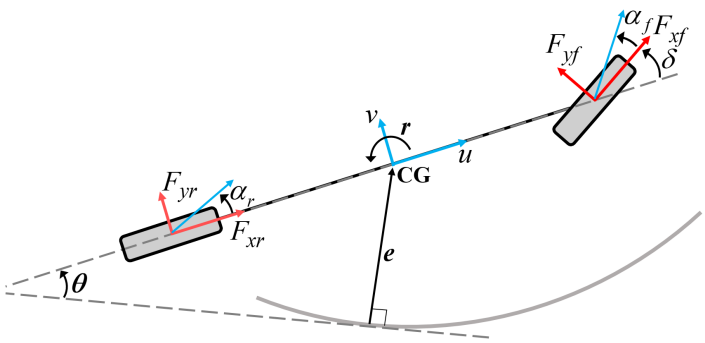

Figure 5.1: Bicycle model diagram.

where m and I_z are the vehicle's mass and moment of inertia, respectively; F_{yf} and F_{yr} are the front and rear lateral tire forces; ϕ_r and θ_r are respectively the road bank and grade angles; M_{F_x} and M_{F_y} are the yaw moment produced by longitudinal forces and lateral forces, respectively.

Lateral agility of a vehicle is defined as how fast the vehicle's heading and lateral position can be changed. In autonomous path tracking problems, it is accepted that front steering can have full authority for guiding a vehicle along its path. Front steering produces lateral

forces on tires, resulting in the yaw moment $M_{F_y} = aF_{yf} - bF_{yr}$. In emergency situations if the yaw moment M_{F_y} cannot provide an appropriate reaction to avoid collision, the yaw moment provided by longitudinal forces (differential braking for instance), M_{F_x}, is added to M_{F_y} to improve the vehicle's lateral agility and allow faster responses, thereby facilitating collision avoidance.

To avoid collision, the vehicle may need to operate up to its handling limits, reaching its maximum lateral acceleration capacity. In this regard, assuming the front and rear tires saturate at the same time, the maximum limit of lateral acceleration, $a_{y,max}$, can be written as:

$$a_{y,max} = \frac{1}{m}(F_{yf,max} + F_{yr,max}), \tag{5.3}$$

where $F_{yf,max} = \sqrt{(\mu F_{zf})^2 - F_{xf}^2}$ and $F_{yr,max} = \sqrt{(\mu F_{zr})^2 - F_{xr}^2}$ are obtained based on the friction limit circle. This equation shows that the maximum limit of lateral acceleration decreases when the longitudinal forces increase. Therefore, incorporating the yaw moment M_{F_x} is a trade-off between increasing the lateral agility and decreasing the maximum lateral acceleration capacity due to tire force coupling effect. Figure 5.2 uses the friction limit circle to show that constraining the applied longitudinal forces within a certain limit of the tire capacity causes only a negligible reduction in lateral force, but produces a considerable yaw moment that improves lateral responsiveness.

Additionally, it should be noted that the front and rear tires will not always saturate at the same time. Considering a front wheel drive vehicle, the front tires may saturate before the rear ones if the longitudinal controller applies drive torque to the front axle. In this situation, when the vehicle tends toward understeering and the front tires are saturated, the remaining capacity of the rear tires can provide an additional yaw moment by longitudinal forces, with only minimal effect on the maximum lateral acceleration. This additional yaw moment can compensate for the reduction in yaw moment of the lateral forces caused by the longitudinal force applied to the front axle.

Although the yaw moment from differential braking M_{F_x} improves the yaw rate responsiveness to prevent collision, it can endanger the vehicle's stability. This risk of instability also occurs because of the lateral force drop due to tire force coupling effect. This problem can be resolved by constraining the limit of differential braking, especially when the lateral velocities violate a predefined stability constraint. When the vehicle's trajectory exits the

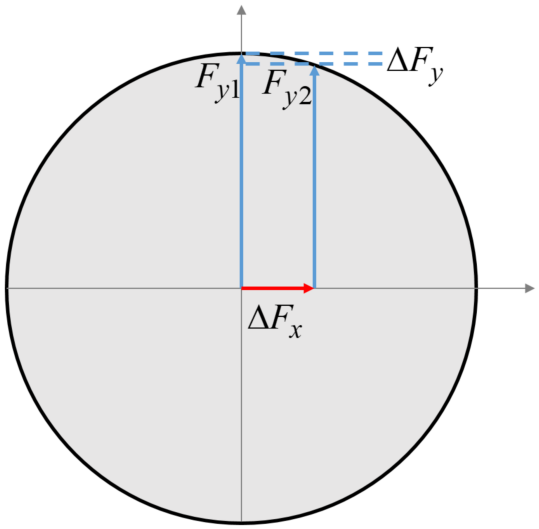

Figure 5.2: Friction force circle. Applying a limited longitudinal force has minimal effect on the lateral force capacity.

defined stable region (stability parallelogram), the tires are on the nonlinear and saturation region, and the vehicle is prone to instability. Therefore, the limit of differential braking needs to be constrained properly to avoid instability. This constrained or limited use of differential braking is called conservative differential braking in our study.

The tire forces F_{yf} and F_{yr} are obtained using the brush tire model presented in Eq. (3.20). The rear lateral force F_{yr} is modeled by repeatedly linearizing the tire force model at each time step around the current rear slip angle $\bar{\alpha}_r$. Also, the front lateral force F_{yf} is considered as the first control input instead of the steering angle, and then is mapped to δ. Finally, the lateral dynamics of the vehicle can be written as affine functions of the velocity states and the inputs F_{yf} and M_{F_x}:

$$\dot{v} = \frac{F_{yf} + \bar{F}_{yr} + \bar{C}_{\alpha_r}\left(\alpha_r - \bar{\alpha}_r\right)}{m} - ur - g\left(\cos\theta_r \sin\phi_r + \sin\theta_r\, \Delta\psi\right), \tag{5.4}$$

$$\dot{r} = \frac{l_f F_{yf} - l_r\left(\bar{F}_{yr} + \bar{C}_{\alpha_r}\left(\alpha_r - \bar{\alpha}_r\right)\right)}{I_z} + M_{F_x}. \tag{5.5}$$

The position states - heading deviation, θ, and lateral deviation, e - are local to a path

with given curvature, $\kappa(s)$, and specify the equations of motion as:

$$\Delta\dot{\psi} = r - u\kappa(s)\cos\phi_r \cos\theta_r, \tag{5.6}$$

$$\dot{e} = u\Delta\psi + v. \tag{5.7}$$

The resulting continuous-time vehicle model containing the vehicle dynamics and position states can now be expressed as:

$$\dot{\mathbf{x}} = \mathbf{A}_t^k \mathbf{x} + \mathbf{B}_t^k \mathbf{u} + \mathbf{d}_t^k, \tag{5.8}$$

with $\mathbf{x} = [v, r, \Delta\psi, e]^T$, $\mathbf{u} = [F_{yf}, M_{F_x}]^T$, and

$$\mathbf{A}_t^k = \begin{bmatrix} \frac{\bar{C}_{\alpha r}}{mu} & -\frac{l_r \bar{C}_{\alpha r}}{mu} - u & -g\sin\theta_r & 0 \\ -\frac{l_r \bar{C}_{\alpha r}}{I_z u} & \frac{l_r^2 \bar{C}_{\alpha r}}{I_z u} & 0 & 0 \\ 0 & 1 & 0 & 0 \\ 1 & 0 & u & 0 \end{bmatrix},$$

$$\mathbf{B}_t^k = \begin{bmatrix} \frac{1}{m} & 0 \\ \frac{l_f}{I_z} & 1 \\ 0 & 0 \\ 0 & 0 \end{bmatrix}, \; \mathbf{d}_t^k = \begin{bmatrix} \frac{\bar{F}_{yr} - \bar{C}_{\alpha r}\bar{\alpha}_r}{m} - g\cos\theta_r \sin\phi_r \\ -\frac{l_r\left(\bar{F}_{yr} - \bar{C}_{\alpha r}\bar{\alpha}_r\right)}{I_z} \\ -u\kappa(s)\cos\phi_r\cos\theta_r \\ 0 \end{bmatrix}.$$

The continuous-time model should be discretized to form a discrete time model that can be implemented in an MPC controller. To properly predict the vehicle behavior along the prediction horizon, an appropriate discretization method and sampling time t_s are chosen. To accurately model vehicle stability and capture the propagation of the velocity states, v and r, at a high frequency, the sampling time is chosen to be small enough for the initial time steps. However, longer time steps are used later in the prediction horizon to make the horizon long enough. Doing so gives the vehicle sufficient time to react to upcoming dangerous situations. Thus, the sampling time t_s^k for discretization, including intermediate time steps linearly elongated, can be written as:

$$t_s^k = \begin{cases} t_{short} & 1 \leq k \leq N_1, \\ t_{short} + (t_{long} - t_{short}) \frac{k-N_1}{N_2-N_1} & N_1 < k \leq N - N_2, \\ t_{long} & N - N_2 < k \leq N, \end{cases} \tag{5.9}$$

where N_1, N_2, and N are the number of short, long, and total time steps, respectively.

The most common discretization method for MPC is zero-order hold (ZOH). This method assumes a constant control input between time steps, which is not accurate enough for a path planning problem with long time steps. To improve the accuracy of discretization, first-order hold (FOH) method can be employed [111]. In first-order hold method, a linear variation is assumed between $\mathbf{u}(k)$ and $\mathbf{u}(k+1)$ as $\mathbf{u}(k+1) = \mathbf{u}(k) + t_s^k \dot{\mathbf{u}}(k)$. To calculate discrete-time model, first the following augmented matrix $\mathbf{\Lambda}^k$ is constructed.

$$\mathbf{\Lambda}^k = \begin{bmatrix} \mathbf{A}_t^k & \mathbf{B}_t^k & \mathbf{d}_t^k & \mathbf{0}_{4\times 3} \\ \mathbf{0}_{3\times 4} & \mathbf{0}_{3\times 2} & \mathbf{0}_{3\times 1} & (1/t_s^k)\mathbf{I}_{3\times 3} \\ \mathbf{0}_{3\times 4} & \mathbf{0}_{3\times 2} & \mathbf{0}_{3\times 1} & \mathbf{0}_{3\times 3} \end{bmatrix}. \tag{5.10}$$

Then, taking the matrix exponential of $\mathbf{\Lambda}^k t_s^k$ gives:

$$e^{\mathbf{\Lambda}^k t_s^k} = \begin{bmatrix} \mathbf{A}^k & \mathbf{\Phi}_1^k & \mathbf{\Phi}_2^k \\ \mathbf{0}_{3\times 4} & \mathbf{I}_{3\times 3} & \mathbf{I}_{3\times 3} \\ \mathbf{0}_{3\times 4} & \mathbf{0}_{3\times 3} & \mathbf{I}_{3\times 3} \end{bmatrix}. \tag{5.11}$$

Defining $\mathbf{B}_1^k = (\mathbf{\Phi}_1^k - \mathbf{\Phi}_2^k) \times [\mathbf{I}_{2\times 2}; \mathbf{0}_{1\times 2}]$, $\mathbf{B}_2^k = \mathbf{\Phi}_2^k \times [\mathbf{I}_{2\times 2}; \mathbf{0}_{1\times 2}]$, and $\mathbf{d}^k = \mathbf{\Phi}_1^k \times [\mathbf{0}_{2\times 1}; 1]$, the discrete-time model can be written as:

$$\mathbf{x}(k+1) = \mathbf{A}^k \mathbf{x}(k) + \mathbf{B}_1^k \mathbf{u}(k) + \mathbf{B}_2^k \mathbf{u}(k+1) + \mathbf{d}^k. \tag{5.12}$$

5.2 System Constraints

To ensure vehicle stability, the stability constraints on vehicle yaw rate and sideslip, as defined in Eqs. (3.48) and (3.50), are considered in this system. In addition, another safety

constraint can be defined for the vehicle to ensure that the planned path does not collide with any obstacle or road edges. Since the longitudinal velocity is known in the prediction horizon, the vehicle distance along the path is known over the horizon. The lateral deviation of the vehicle at each time step in the prediction horizon can be constrained between a maximum and a minimum value, which are set to be within the road edges and free of obstacles. Figure 5.3 shows the vehicle in the road with two pop-up obstacles. The first and second obstacles are observed by the vehicle when it passes the first and second lateral dashed lines, respectively. To create a convex region for lateral deviation, one of the two areas between the obstacle and the road edges is ignored, maintaining the safer tube for path planning problem. This safety constraint on the lateral deviation is defined as:

$$e_{min}(k) + \left(\frac{l_s}{2} + e_s\right) < e(k) < e_{max}(k) - \left(\frac{l_s}{2} + e_s\right), \tag{5.13}$$

where l_s is the vehicle width and e_s is a minimum safe distance to the boundaries of the safe region. The safe region on position states can be written as:

$$\mathbf{H}_e \mathbf{x}(k) \leq \mathbf{G}_e, \tag{5.14}$$

where $\mathbf{H}_e = \begin{bmatrix} 0 & 0 & 0 & 1 \\ 0 & 0 & 0 & -1 \end{bmatrix}$, and $\mathbf{G}_e = \begin{bmatrix} e_{max}(k) - \left(\frac{l_s}{2} + e_s\right) \\ -e_{min}(k) - \left(\frac{l_s}{2} + e_s\right) \end{bmatrix}$.

The maximum capacity of the control actuations F_{yf} and M_{F_x} are constrained based on the maximum physical capability of the actuators and the maximum friction force capacity between tires and road. These actuator constraints can be written as:

$$|F_{yf}| \leq F_{yf,max}, \tag{5.15}$$

$$|\Delta F_{yf}| \leq \Delta F^k_{yf,max}, \tag{5.16}$$

$$|M_{F_x}| \leq M_{F_x,max}, \tag{5.17}$$

$$|\Delta M_{F_x}| \leq \Delta M^k_{F_x,max}, \tag{5.18}$$

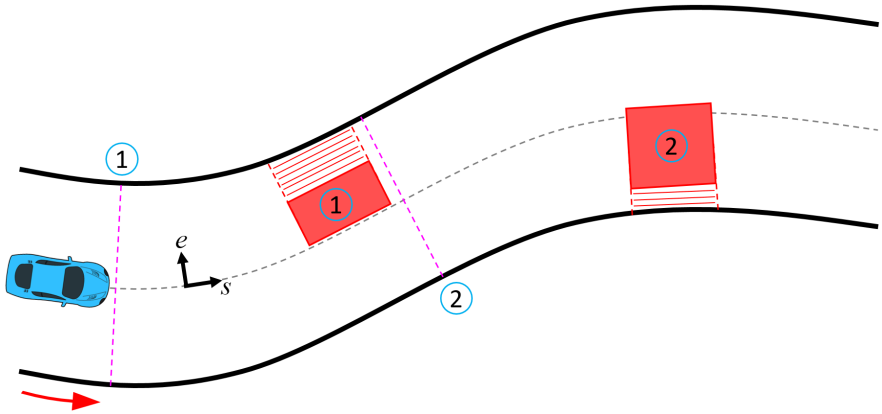

Figure 5.3: The safe region for position states is represented by defining a constraint on the lateral deviation.

where $\Delta F^k_{yf,max}$ and $\Delta M^k_{F_x,max}$ are respectively the maximum allowable change in front lateral force and the yaw moment generated by differential braking. These maximum slew rates are dependent on the time step size. Indeed, the variations of the control actions can get larger for the longer time steps.

$$\Delta F^k_{yf,max} = \frac{t^k_s}{t_{short}} \Delta F^0_{yf,max}, \tag{5.19}$$

$$\Delta M^k_{F_x,max} = \frac{t^k_s}{t_{short}} \Delta M^0_{F_x,max}, \tag{5.20}$$

To protect the vehicle's lateral force capacity, the maximum yaw moment allowed by differential braking is set to be limited by a portion of the tire force capacity, as illustrated in Section 5.1. However, to improve the effectiveness of the controller design, the maximum allowable yaw moment gradually decreases when a vehicle's trajectory exits the handling stability region. This modification decreases the contribution of differential braking and prevents fast changes of yaw rate out of the stability parallelogram, thus reducing the vehicle's tendency to instability. Therefore, $M_{F_x,max}$ can be modified as:

$$M_{F_x,max} = \chi \bar{M}_{F_x,max}, \tag{5.21}$$

where $\bar{M}_{F_x,max}$ is the maximum allowable yaw moment inside the stable region and $\chi \in [0, 1]$ is obtained by $\chi = \min(\chi_1, \chi_2)$ with χ_1 and χ_2 defined as:

$$\chi_1 = \begin{cases} 1 & |r| \leq r_{max}, \\ 1 - \frac{|r| - r_{max}}{\rho_1 r_{max}} & r_{max} < |r| \leq (1+\rho_1) r_{max}, \\ 0 & |r| > (1+\rho_1) r_{max}, \end{cases} \tag{5.22}$$

$$\chi_2 = \begin{cases} 1 & |\alpha_r| \leq \alpha_{r,max}, \\ 1 - \frac{|\alpha_r| - \alpha_{r,max}}{\rho_2 \alpha_{r,max}} & \alpha_{r,max} < |\alpha_r| \leq (1+\rho_2) \alpha_{r,max}, \\ 0 & |\alpha_r| > (1+\rho_2) \alpha_{r,max}, \end{cases} \tag{5.23}$$

where ρ_1 and ρ_2 are scaling parameters for the transition region width out of the stability region.

The optimized yaw moment M_{F_x} is distributed between the front and rear axles at a constant ratio unless the vehicle trajectory leaves the stable region. If it does so, the braking distribution is adjusted so that the rear braking is less involved. This manipulation contributes to vehicle stabilization because of tire force coupling effect. This idea arises from the fact that the lateral force of the rear axle drops when the rear brakes are activated, pushing the vehicle towards oversteer. Shifting the rear braking to the front axle indirectly increases the rear lateral force and decreases the front lateral force, assisting in instability avoidance. Therefore, the modified distribution of the differential braking between the front and rear axles can be modeled using the following equation, with η representing the ratio of the allocated differential braking on the front axle [143]:

$$\eta = \eta_f - \chi(\eta_f - \eta_e), \tag{5.24}$$

where η_e and η_f are defined as the ratios of the allocated brakes on the front axle for $\chi = 1$ and $\chi = 0$, respectively. Therefore, η is linearly increasing from η_e to η_f as the vehicle trajectory leaves the stable region and χ moves from one to zero.

Figure 5.4 shows the variations of the maximum yaw moment $M_{F_{x,max}}$ and the ratio η in the phase plane. The performed modifications provide a conservative differential braking structure that improves the vehicle's responsiveness in emergency situations so as to prevent collisions and instability.

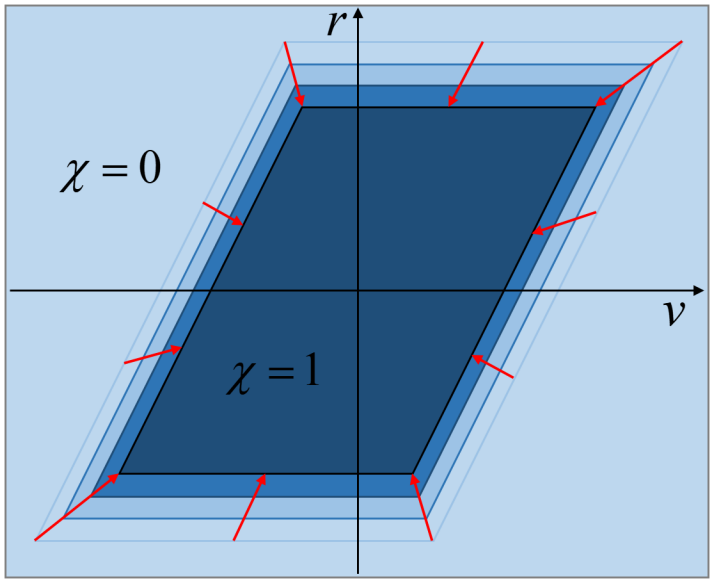

Figure 5.4: The maximum yaw moment $M_{F_{x,max}}$ and the braking distribution ratio η are adjusted out of the stable region using the scaling variable χ.

5.3 Emergency Path Planning/Tracking Controller

The control objectives that are addressed in our control design are: tracking the desired path, enforcing vehicle stability, and avoiding collisions. To satisfy these objectives, a model predictive controller has been developed to determine the optimal control inputs of the front lateral force F_{yf} and the yaw moment M_{F_x}. The calculated M_{F_x} is provided by applying brakes on the left or right wheels (both axles) to produce the yaw moment in the desired direction. Longitudinal velocity is adjusted using a separate speed controller by applying a positive longitudinal command to the electric motor or a negative command to the brakes. The overall control structure is depicted in Fig. 5.5.

5.3.1 Longitudinal Controller

The vehicle speed is controlled by calculating the required longitudinal command to track the desired speed. The net force required in the longitudinal direction, $F_{x,net}$, is obtained

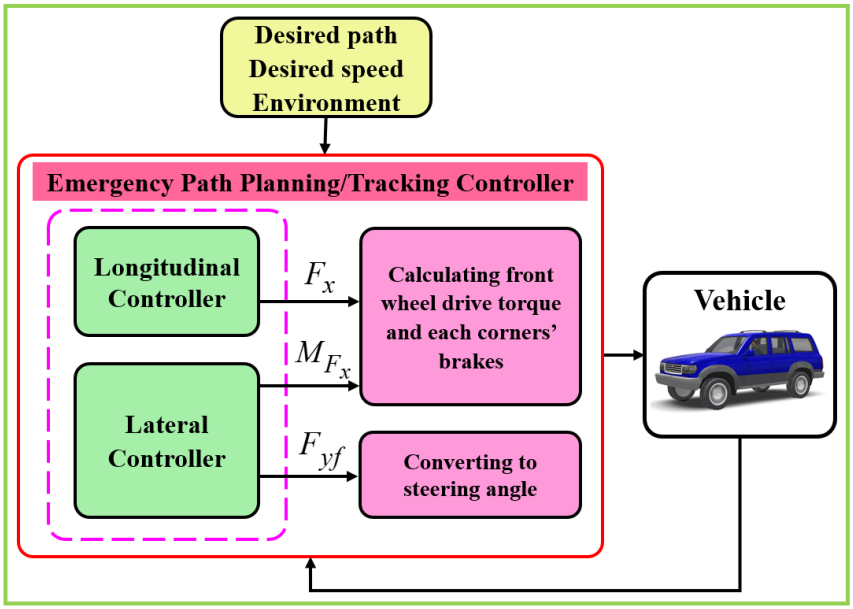

Figure 5.5: Control structure. The designed controller calculates longitudinal and lateral control inputs, based on which drive, brake, and steering commands are obtained.

using a proportional controller as follows:

$$F_{x,net} = ma_{x,des} + k_p(u_{des} - u), \tag{5.25}$$

where u_{des} and $a_{x,des}$ are the desired longitudinal velocity and acceleration, and k_p is a speed tracking gain. Since the lateral controller uses differential braking to produce yaw moment, the brake forces applied by differential braking are compensated for by the longitudinal controller. Therefore, the drive torque applied to the vehicle ensures that the desired longitudinal velocity is achieved.

The global path planning module in autonomous vehicles needs to plan an appropriate longitudinal velocity along the path. To approximately calculate the maximum safe driving velocity for a curved non-flat road, the force limit circle can be used as:

$$F_x^2 + F_y^2 \leq \mu^2 N^2. \tag{5.26}$$

Neglecting the longitudinal forces, F_x, simplifies the above equation to:

$$|F_y| \leq \mu N. \tag{5.27}$$

Substituting Eqs. (3.15), (3.45), and (5.1) in Eq. (5.27), making steady state assumption ($\dot{v} \approx 0$ and $\Delta\dot{\psi} \approx 0$), and assuming $\theta_r \approx 0$, $\Delta\psi \approx 0$, and $v/u \approx 0$ gives:

$$|\kappa u^2 \cos\phi_r + g \sin\phi_r| \leq \mu \left(g \cos\phi_r - \kappa u^2 \sin\phi_r\right). \tag{5.28}$$

The above inequality gives the vehicle's maximum speed as:

$$u_{max} = \sqrt{\frac{g\left(\mu\cos\phi_r - \sin\phi_r\right)}{\kappa\left(\cos\phi_r + \mu\sin\phi_r\right)}}. \tag{5.29}$$

The calculated maximum speed, u_{max}, can be used as a constraint in longitudinal path planning on a curved banked road.

5.3.2 Lateral Controller

The lateral dynamics of the vehicle is controlled using an MPC controller. The following optimization problem calculates the optimized control inputs at each time step, generating a trajectory that can best follow a desired path while satisfying the constraints related to stability and position.

$$\begin{aligned} J = \textstyle\sum_{k=1}^{N} \mathbf{x}^T(k)\mathbf{Q}\mathbf{x}(k) + \mathbf{u}^T(k)\mathbf{R}\mathbf{u}(k) + \boldsymbol{\Delta}\mathbf{u}^T(k)\mathbf{P}\boldsymbol{\Delta}\mathbf{u}(k) \\ + \mathbf{W_s}\mathbf{s}_s(k) + \mathbf{W_e}\mathbf{s}_e(k), \end{aligned} \tag{5.30}$$

subject to the discrete-time vehicle model Eq. (5.12) for $(k = 1, ..., N)$, and

$$|\mathbf{u}(k)| \leq \mathbf{u}^k_{max}, \tag{5.31}$$

$$|\boldsymbol{\Delta}\mathbf{u}(k)| \leq \boldsymbol{\Delta}\mathbf{u}^k_{max}, \tag{5.32}$$

$$\mathbf{H}_s\mathbf{x}(k) \leq \mathbf{G}^k_s + \mathbf{s}_s(k), \tag{5.33}$$

$$\mathbf{H}_e\mathbf{x}(k) \leq \mathbf{G}_e^k + \mathbf{s}_e(k), \tag{5.34}$$

$$\mathbf{s}_s(k) \geq 0, \tag{5.35}$$

$$\mathbf{s}_e(k) \geq 0, \tag{5.36}$$

where $\mathbf{\Delta u}(k) = \mathbf{u}(k) - \mathbf{u}(k-1)$, $\mathbf{u}_{max}^k = [F_{yf,max}^k, M_{F_x,max}^k]^T$, and $\mathbf{\Delta u}_{max}^k = [\Delta F_{yf,max}^k, \Delta M_{F_x,max}^k]^T$. The first term in the cost function is for tracking the desired path. This term penalizes heading and lateral deviations with respect to the desired path. The second term penalizes the magnitude of control actuations. The magnitude of the front lateral force is not penalized, but the magnitude of the yaw moment from differential braking is penalized in the objective function. This measure enables the controller to rely on front steering and activate differential braking only when an additional yaw moment is needed. The third term penalizes the proximity of the control actuations, allowing the vehicle to hold a constant steering angle and change smoothly during differential braking. The fourth and fifth terms assign costs for the non-negative slack variables that are used to ensure a feasible solution for the optimization problem. The first slack variable $\mathbf{s}_s(k)$ is used for the stability constraint on yaw rate and lateral velocity states. The second slack variable $\mathbf{s}_e(k)$ is used for the position constraint. The positive semi-definite weight matrices $\mathbf{Q}^k$, $\mathbf{W}_s^k$, and $\mathbf{W}_e^k$ determine the priority between the control objectives. These weights are set such that the priority is given first to collision avoidance and then stability. Therefore, the designed MPC controller performs optimal path planning to prevent collisions and instability by deviating from the desired path. The optimized yaw moment along with the calculated longitudinal force for longitudinal controller and the updated distribution ratio η determine the drive or brake commands at each corner.

5.4 Contingency Path Planning/Tracking Controller

The wide acceptance of autonomous vehicles in the future requires their ability to handle the surprises and challenges that a human driver would routinely encounter, such as children suddenly running out into traffic or unanticipated icy surfaces. One solution for improving their capability to avoid collisions is to improve their lateral agility and responsiveness. To this end, the incorporation of conservative torque/brake vectoring was

suggested in the previous section. Another solution for enhancing the safety of autonomous vehicles is to make the path planning/tracking controller robust to possible variations of system parameters. One of the unexpected events that is challenging to predict is the sudden loss of road friction. Several studies in the literature propose robust control methods to handle road friction uncertainties [96, 144, 145]. However, a path planner needs reliable information about upcoming road conditions to be able to plan a safe path in emergency scenarios. Even though the effect of varying road conditions on vehicle dynamics has been well studied and included in robust control designs for improving vehicle handling and stability, it has only recently been considered in the context of motion planning at the limits of handling [146, 147, 148, 149].

Although accurately determining what road friction conditions a vehicle may encounter in the immediate future (i.e., a few dozen meters) is not possible, the perception module in autonomous vehicles may be able to anticipate changes in road friction using the data available about the upcoming road surface. This capability enables a path planner to prepare for contingency events.

To properly plan a safe path in contingency events, a contingency model predictive controller is designed to ensure the path planner's robustness to road friction uncertainties. In contingency MPC, a prediction horizon tree is built, which branches from a single stage-node at x_0 [148]. At this stage, a nominal horizon and a contingency horizon are employed that share their first control action as illustrated in Fig. 5.6. With this equality constraint in the CMPC control design, the vehicle will adhere to its desired path as closely as possible, while maintaining the ability to maneuver to avoid a contingency event.

The contingency path planner is designed by extending the deterministic path planner developed in the previous section. The system model, Eq. (5.12), is duplicated to include both $\mathbf{x}_{nom}$ and $\mathbf{x}_c$ state vectors and support both the nominal and contingency prediction horizons as follows:

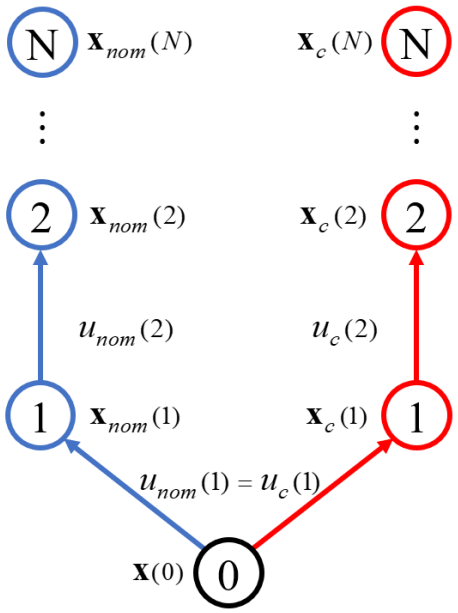

Figure 5.6: Contingency MPC prediction horizon. A nominal and contingency trajectory are computed, which have equal control action at the first step.

$$\begin{aligned}\mathbf{x}(k+1) &= \begin{bmatrix}\mathbf{x}_{nom}(k+1)\\ \mathbf{x}_c(k+1)\end{bmatrix}\\ &= \begin{bmatrix}\mathbf{A}^k_{nom} & 0\\ 0 & \mathbf{A}^k_c\end{bmatrix}\mathbf{x}(k) + \begin{bmatrix}\mathbf{B}^k_{1,nom} & 0\\ 0 & \mathbf{B}^k_{1,c}\end{bmatrix}\begin{bmatrix}u_{nom}(k)\\ u_c(k)\end{bmatrix}\\ &\quad + \begin{bmatrix}\mathbf{B}^k_{2,nom} & 0\\ 0 & \mathbf{B}^k_{2,c}\end{bmatrix}\begin{bmatrix}u_{nom}(k+1)\\ u_c(k+1)\end{bmatrix} + \begin{bmatrix}\mathbf{d}^k_{nom}\\ \mathbf{d}^k_c\end{bmatrix}.\end{aligned} \tag{5.37}$$

The following optimization problem is extended from the deterministic MPC controller illustrated in Eqs. (5.30) to (5.36). In this section, the conservative differential braking is not employed, and front steering is the only control input.

$$
\begin{aligned}
J = \sum_{k=1}^{N} \mathbf{x}^T(k) \begin{bmatrix} \mathbf{Q}_{nom} & 0 \\ 0 & \mathbf{Q}_c \end{bmatrix} \mathbf{x}(k) + \mathbf{\Delta u}^T(k) \begin{bmatrix} \mathbf{R}_{p,nom} & 0 \\ 0 & \mathbf{R}_{p,c} \end{bmatrix} \mathbf{\Delta u}(k) \\
+ \begin{bmatrix} W_{r,nom} & W_{r,c} \end{bmatrix} \begin{bmatrix} s_{r,nom}(k) \\ s_{r,c}(k) \end{bmatrix} + \begin{bmatrix} W_{\beta,nom} & W_{\beta,c} \end{bmatrix} \begin{bmatrix} s_{\beta,nom}(k) \\ s_{\beta,c}(k) \end{bmatrix} \\
+ \begin{bmatrix} W_{e,nom} & W_{e,c} \end{bmatrix} \begin{bmatrix} s_{e,nom}(k) \\ s_{e,c}(k) \end{bmatrix},
\end{aligned} \tag{5.38}
$$

subject to the discrete-time system model Eq. (5.37) for $(k = 1, \cdots, N)$, and

$$
|\mathbf{u}(k)| \leq \begin{bmatrix} u^k_{max,nom} \\ u^k_{max,c} \end{bmatrix}, \tag{5.39}
$$

$$
|\mathbf{\Delta u}(k)| \leq \begin{bmatrix} \Delta u^k_{max,nom} \\ \Delta u^k_{max,c} \end{bmatrix}, \tag{5.40}
$$

$$
\begin{bmatrix} \mathbf{H}_{r,nom} & 0 \\ 0 & \mathbf{H}_{r,c} \end{bmatrix} \mathbf{x}(k) \leq \begin{bmatrix} \mathbf{s}_{r,nom}(k) \\ \mathbf{s}_{r,c}(k) \end{bmatrix}, \tag{5.41}
$$

$$
\begin{bmatrix} \mathbf{H}_{\beta,nom} & 0 \\ 0 & \mathbf{H}_{\beta,c} \end{bmatrix} \mathbf{x}(k) \leq \begin{bmatrix} \mathbf{s}_{\beta,nom}(k) \\ \mathbf{s}_{\beta,c}(k) \end{bmatrix}, \tag{5.42}
$$

$$
\begin{bmatrix} \mathbf{H}_{e,nom} & 0 \\ 0 & \mathbf{H}_{e,c} \end{bmatrix} \mathbf{x}(k) \leq \begin{bmatrix} \mathbf{s}_{e,nom}(k) \\ \mathbf{s}_{e,c}(k) \end{bmatrix}, \tag{5.43}
$$

$$
u_{nom}(1) = u_c(1), \tag{5.44}
$$

where all the slack variables are non-negative. Diagonal matrices are used in the optimization problem to penalize and constrain the contingency and nominal trajectories independently. As with the deterministic MPC controller, under the contingency controller, the weight matrices are tuned so as to give the highest priority to collision avoidance.

It should be noted that the yaw rate's safety constraint is in fact based on the maximum lateral acceleration, which is limited by the maximum available friction force. Therefore, the designed CMPC controller can properly address the contingency events with uncertain road frictions and plan a conservative path to ensure safety.

For instance, in the contingency event shown in Fig. 5.7, there are possible icy patches near an obstacle on a wet road. A deterministic path planner that is unaware of the potential loss of friction in the path may end up with a collision. On the other hand, the contingency path planner can anticipate the potential friction drop and react more conservatively to plan a safer path that avoids a collision.

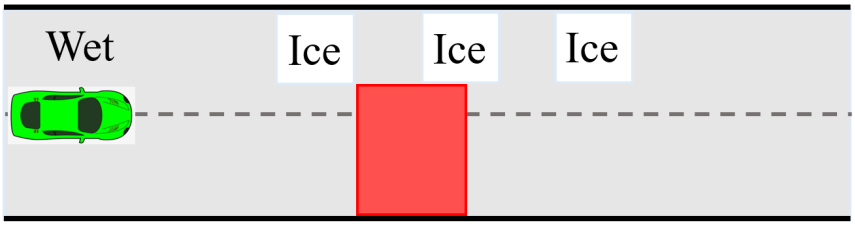

Figure 5.7: A contingency event with possible icy patches on a wet road.

Another type of contingency events is related to road angle uncertainties. Road bank affects the maximum lateral acceleration capacity and consequently the yaw rate's stability limit. In fact, road bank shifts the stability parallelogram upward or downward. The CMPC controller can properly respond to identified potential changes of road bank angle and plan a conservative path that ensures collision avoidance.

5.5 Numerical Study

In this section, the performance of the designed controller is evaluated numerically using co-simulation in CarSim and MATLAB/Simulink. The test vehicle is a high fidelity CarSim model of a Chevrolet Equinox, with the specifications listed in Table 4-1.

The performance of the path planning controller in improving lateral agility using conservative differential braking is assessed in two driving scenarios with pop-up obstacles appearing on the road. The tests, carried out on a road with the friction coefficient of $\mu = 0.5$ and the desired longitudinal velocity of 60 kph, are performed twice: (1) with

differential braking OFF (Controller A) and (2) with differential braking ON (Controller B). In other words, Controller A uses front steering only, but controller B employs integrated front steering and differential braking. The parameters of Controllers A and B are the same except that differential braking is off in Controller A.

The performance of the contingency path planning controller is evaluated in three contingency scenarios that push the limits of vehicle handling. Each scenario was performed three times: (1) with the deterministic path planner and assuming that the contingency event does not happen, (2) with the deterministic path planner and assuming that the contingency event happens, (3) with the contingency path planner and assuming that the contingency event happens. The controller parameters are shown in Table 5.1.

Table 5.1: Path Planning/Tracking Controller Parameters.

Parameter	Value		
	Emergency Controller	Contingency Controller Nominal Horizon	Contingency Controller Contingency Horizon
N, N_1, N_2	40, 10, 20	70, 10, 50	70, 10, 50
t_{short}, t_{long}	0.01, 0.2 $[ms]$	0.01, 0.2 $[ms]$	0.01, 0.2 $[ms]$
$\mathbf{Q}$	$\text{diag}(0, 0, 200, 4)$	$\text{diag}(0, 0, 4, 4)$	$\text{diag}(0, 0, 2, 2)$
$\mathbf{R}_m$	$\text{diag}(0, 4 \times 10^{-5})$	0	0
$\mathbf{R}_p$	$\text{diag}(3 \times 10^{-5}, 8 \times 10^{-5})$	6×10^{-5}	6×10^{-5}
$\mathbf{W}_r$	3000	50	50
$\mathbf{W}_\beta$	3000	50	50
$\mathbf{W}_e$	50000	400	400

5.5.1 Emergency Scenario 1: Straight Road with a Sudden Obstacle

The first scenario is a straight road with the centerline as the desired path (Fig. 5.8). A pop-up obstacle suddenly shows up when the vehicle passes from $x = 30\,m$. It is assumed

that the obstacle extends to the bottom edge (boundary) of the road ($e = -6\,m$), indicated in Fig. 5.8a by dashed red lines, leaving the easier and more feasible tube for path planning. The result is a convex region for lateral deviation at each distance along the path. The blue and green lines respectively represent the vehicle track path optimized by Controllers A and B. In Fig. 5.8, Controller A fails to respond fast enough and to properly change the heading of the vehicle, thus collides with the road boundary after avoiding the pop-up obstacle. With Controller B, however, the conservative differential braking intervenes and improves the yaw rate response to prevent a collision with the road boundaries. Figure 5.8b shows a 3D result of the scenario 1, where the blue and green cars are respectively related to Controllers A and B.

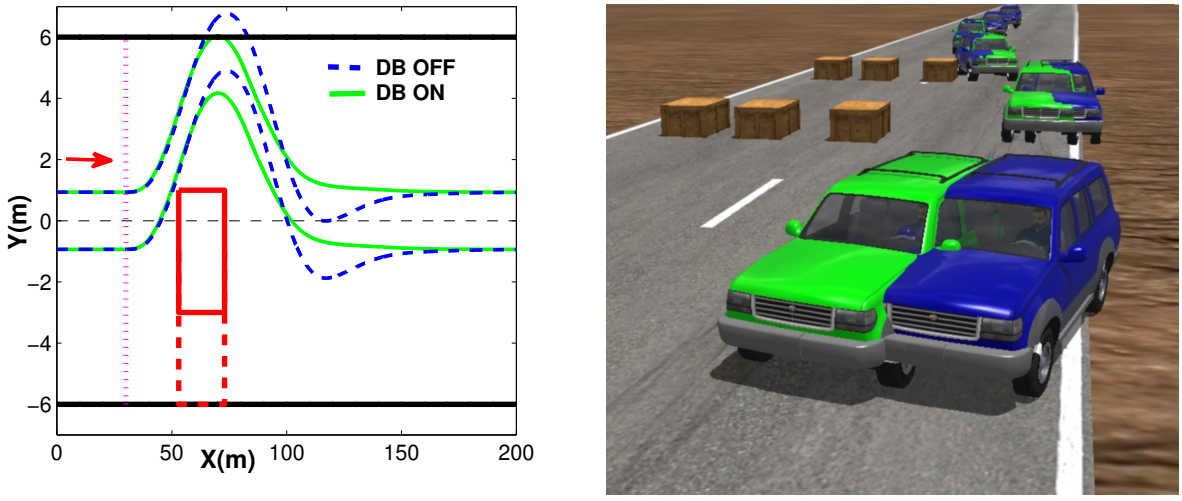

(a) (b)

Figure 5.8: (a) The optimized paths and (b) 3D results for Controllers A (blue) and B (green) confronting a pop-up obstacle suddenly introduced (magenta dashed in (a)) in a straight road (scenario 1). The red rectangle in (a) and the crates in (b) indicate the obstacle area to be avoided.

Figure 5.9 shows the closed-loop trajectories of the vehicle in the $v - r$ phase plane for Controllers A and B. In contrast to Controller A, Controller B can change the yaw rate sign faster and keep it outside the parallelogram for a little longer, which turns the vehicle's heading faster, enabling the controller to avoid a collision.

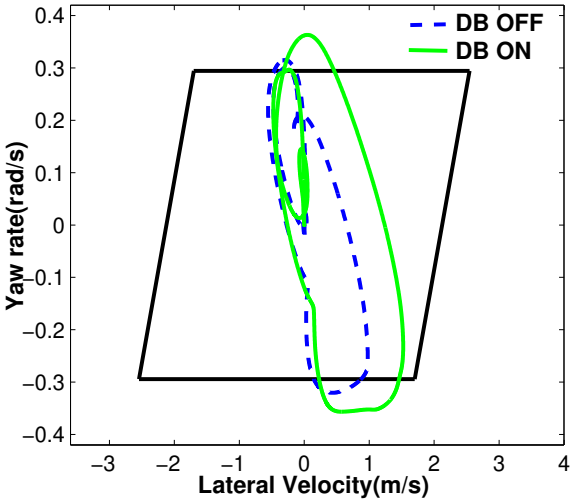

Figure 5.9: The vehicle trajectory in the phase plane of lateral velocity and yaw rate for Controllers A (blue) and B (green) in scenario 1.

The optimized control inputs of steering and differential braking are shown in Fig. 5.10, and the vehicle yaw rate, lateral acceleration, and longitudinal velocity are presented in Fig. 5.11. Figure 5.10b shows how controller B uses the yaw moment M_{F_x} to better react to dangerous situations. The first intervention of the yaw moment M_{F_x} happens at around $2\,s$, to assist in avoiding the obstacle by providing a positive yaw moment. The major contribution of the differential braking, however, can be seen between $3\,s$ to $4\,s$, when the vehicle is about to collide with the road edges. This additional yaw moment results in a faster response in yaw rate, that can be seen in Fig. 5.11a, to change the vehicle's heading. The maximum lateral acceleration of the vehicle during the maneuver (Fig. 5.11b) indicates that the controller operates up to the vehicle's handling limits ($a_{y,max} \simeq \mu g \simeq 5$). Figure 5.11c shows that the vehicle's longitudinal velocity follows the desired value of $60\,kph$ for Controllers A and B, meaning that both have the same speed during the maneuver. The improvement in collision avoidance by Controller B is achieved without compromising longitudinal velocity.

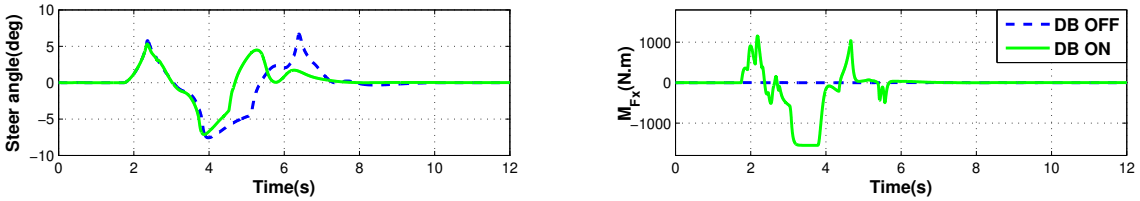

(a) (b)

Figure 5.10: (a) The steer angle and (b) M_{F_x} for Controllers A (blue) and B (green) in scenario 1.

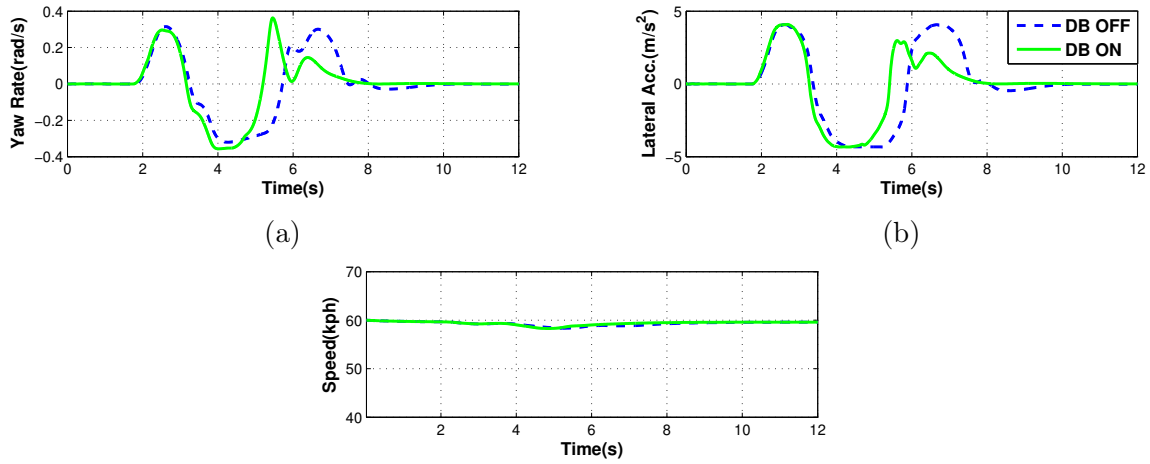

(a) (b)

(c)

Figure 5.11: Vehicle response (a) yaw rate, (b) lateral acceleration, (c) speed for Controllers A (blue) and B (green) in scenario 1.

5.5.2 Emergency Scenario 2: Curved Road with Two Sudden Obstacles

The second scenario is a curved road with two pop-up obstacles. As shown in Fig. 5.12, the first and second obstacles are observed at $s = 30\,m$ and $s = 62\,m$, respectively. Both controllers A and B successfully avoid the first obstacle with no collision with the road boundary. However, controller A is unable to pass the second obstacle, and collides with the boundary. This collision happens because the controller is unable to rapidly change the vehicle's heading. With Controller B, the additional yaw moment from differential

braking improves the yaw rate responsiveness, enabling the controller to mitigate any collisions. Figure 5.12b shows the 3D result of this scenario, where the blue and green cars are respectively related to Controllers A and B.

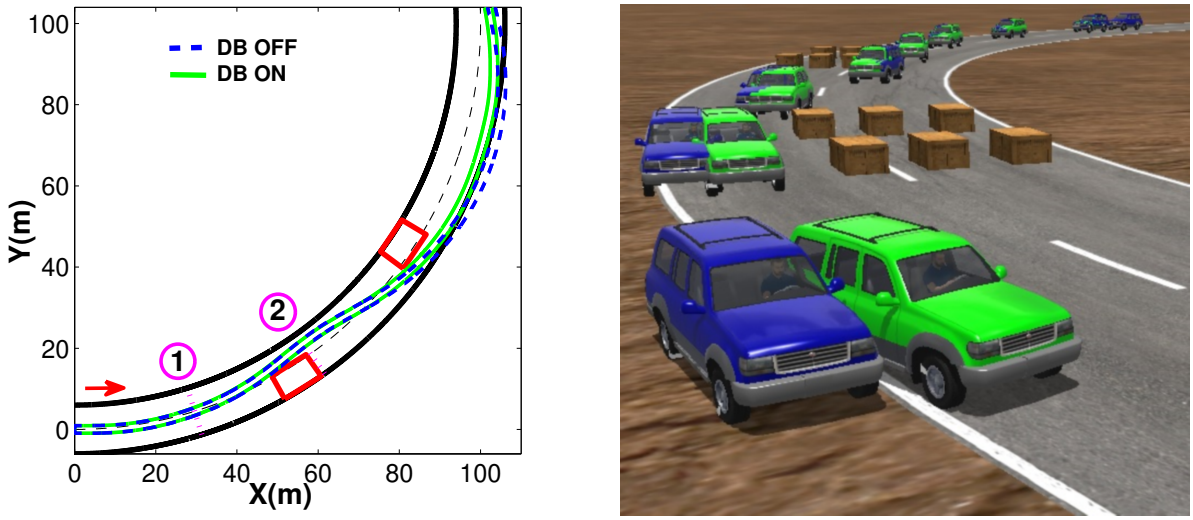

(a) (b)

Figure 5.12: (a) The optimized paths and (b) 3D results for Controllers A (blue) and B (green) confronting two pop-up obstacles suddenly introduced at distances 1 and 2 (magenta dashed in (a)) in a curved road (scenario 2). The red rectangles in (a) and the crates in (b) indicate the obstacle area to be avoided.

The closed-loop trajectory of the vehicle in the $v - r$ phase plane (Fig. 5.13) shows how Controller B's superior responsiveness provides the short-term higher yaw rate needed to mitigate collisions. The vehicle trajectory exits the stable region through the yaw rate channel and then a negative lateral velocity builds up, due to the domination of the negative term $-ru$ over the positive term $(F_{yf} + F_{yr})/m$ in Eq. (5.1). Finally, the trajectory returns to the stable region after a transition period. The trajectory generated by controller A is unable to provide a fast enough yaw rate response to prevent collision with the road boundary.

Figure 5.14 shows the optimized control inputs of steering and differential braking, and Fig. 5.15 shows the vehicle yaw rate, lateral acceleration, and longitudinal velocity. In Fig. 5.14b, the main intervention of differential braking happens after the vehicle passes the

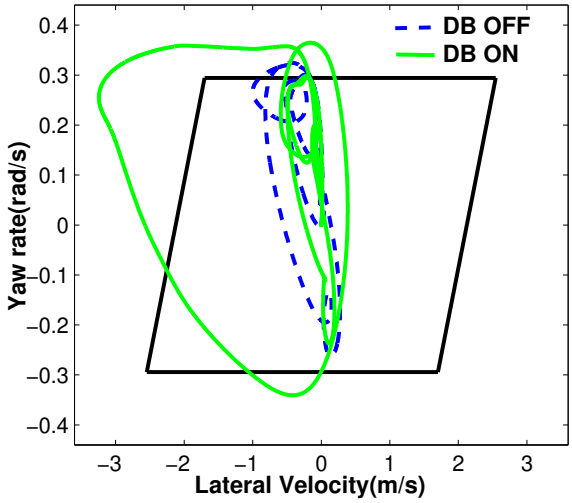

Figure 5.13: The vehicle trajectory in the phase plane of lateral velocity and yaw rate for Controllers A (blue) and B (green) in scenario 2.

first obstacle and when the second obstacle appears. In this moment, the controller needs to avoid a collision with the second obstacle as well as the road boundary. Both controllers A and B can properly avoid the second obstacle, but Controller A fails to provide enough yaw moment to avoid collision with the road boundary. Controller B uses differential braking and applies a positive yaw moment between $4\,s$ to $5\,s$. This yaw moment results in a faster yaw dynamic, as shown in Fig. 5.15b, and mitigates collision. Figure 5.15c indicates that the vehicle reaches its maximum lateral acceleration limit ($a_{y,max} \simeq \mu g \simeq 5\,m/s^2$) when avoiding the obstacles. In Fig. 5.15d, the longitudinal velocities for Controllers A and B are almost the same during the maneuver. Therefore, the improvement in collision avoidance by Controller B is achieved without compromising the longitudinal velocity.

The simulation results show the effectiveness of the controller in satisfying the three control objectives in the prioritized structure. In other words, the controller tracks the desired path when there is no violation of the stability and collision avoidance constraints, but it deviates from the desired path when it is necessary to avoid instability or collision. Also, since the priority is given to collision avoidance over vehicle stability, the controller may temporarily violate stability criteria, if necessary, to avoid a collision.

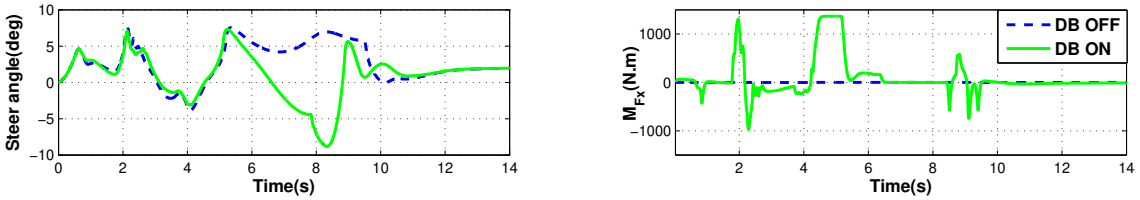

Figure 5.14: (a) The steer angle and (b) M_{F_x} for Controllers A (blue) and B (green) in scenario 2.

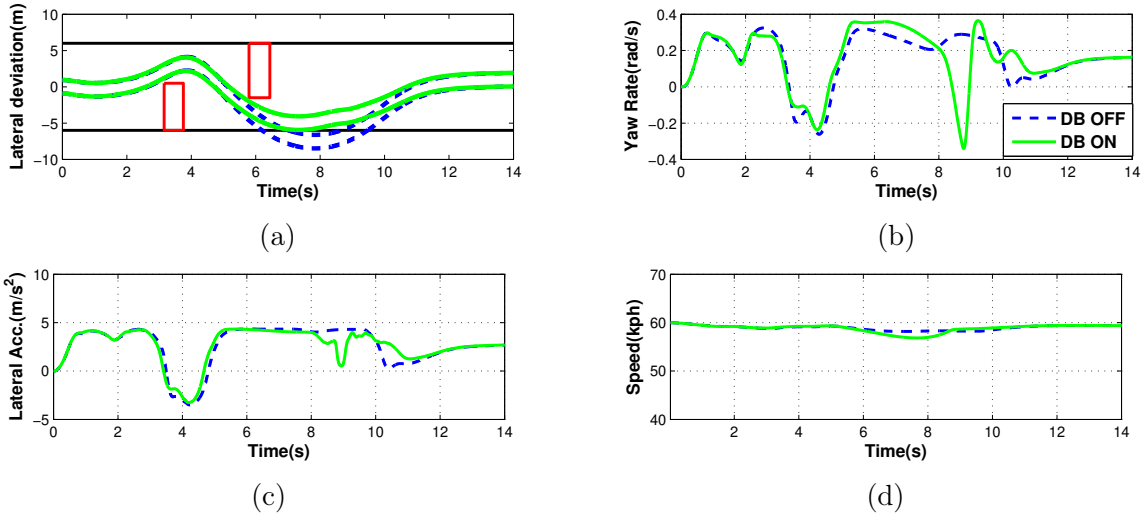

Figure 5.15: Vehicle response (a) lateral deviation, (b) yaw rate, (c) lateral acceleration, and (d) speed for Controllers A (blue) and B (green) in scenario 2.

5.5.3 Contingency Scenario 1: Mixed Wet and Icy Road with Two Obstacles

The first contingency scenario is a straight road with the centerline as the desired path and two obstacles in the road. For comparing how the two path planners perform in response to road friction, two roads are considered: Roads A and B. Road A is totally wet, and Road B is wet in the middle and icy near the sides, as shown in Fig. 5.16. The desired longitudinal velocity is assumed to be $u = 36\,kph$ constant. Figures 5.17a and 5.17b show the vehicle track paths optimized by the deterministic and contingency path planners respectively for

Road A and Road B. Figure 5.18 shows the results of the steer angle, yaw rate, and lateral acceleration for the three simulated cases. On Road A, the deterministic path planner properly and minimally deviates from the desired path and prevents a collision with the obstacles and road edges. However, on Road B, the deterministic path planner collides with the road edges because it was unaware of the ice on the sides and consequently started to deviate very late. This failure occurs because it assumes the lateral acceleration capacity of a wet road everywhere on the road and catches the friction drop when it is too late to avoid collision. In contrast, the contingency path planner, which anticipates the presence of ice on the sides, steers earlier to manage the low lateral acceleration capacity of the sides and make the curve gentler and more conservative.

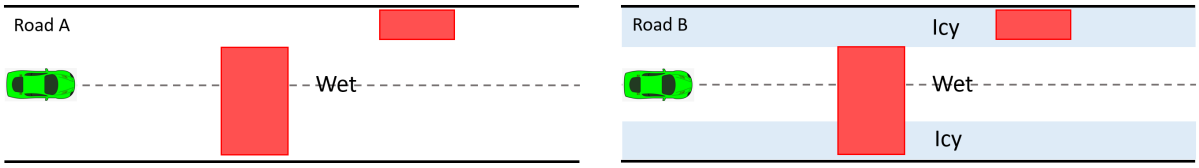

(a) (b)

Figure 5.16: The first contingency scenario is a straight road with two obstacles. (a) Road A is totally wet, and (b) Road B is wet in the middle and icy near the sides.

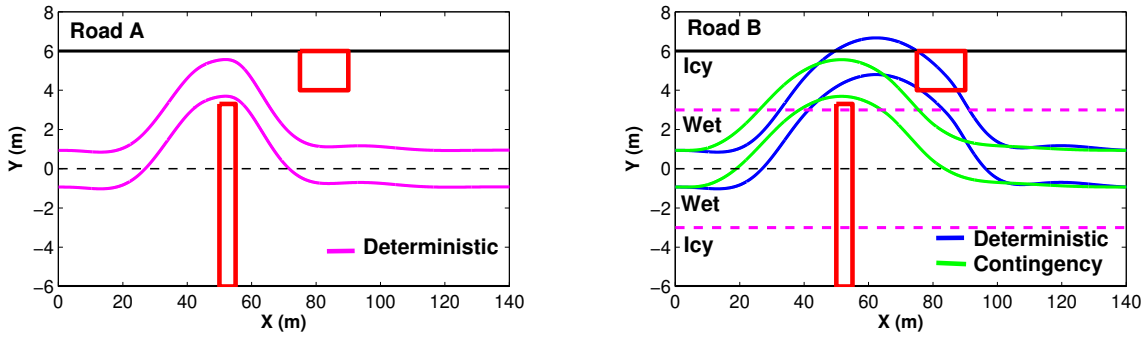

(a) (b)

Figure 5.17: The vehicle track paths calculated by the deterministic and contingency path planners on (a) Road A and (b) Road B in the first contingency scenario.

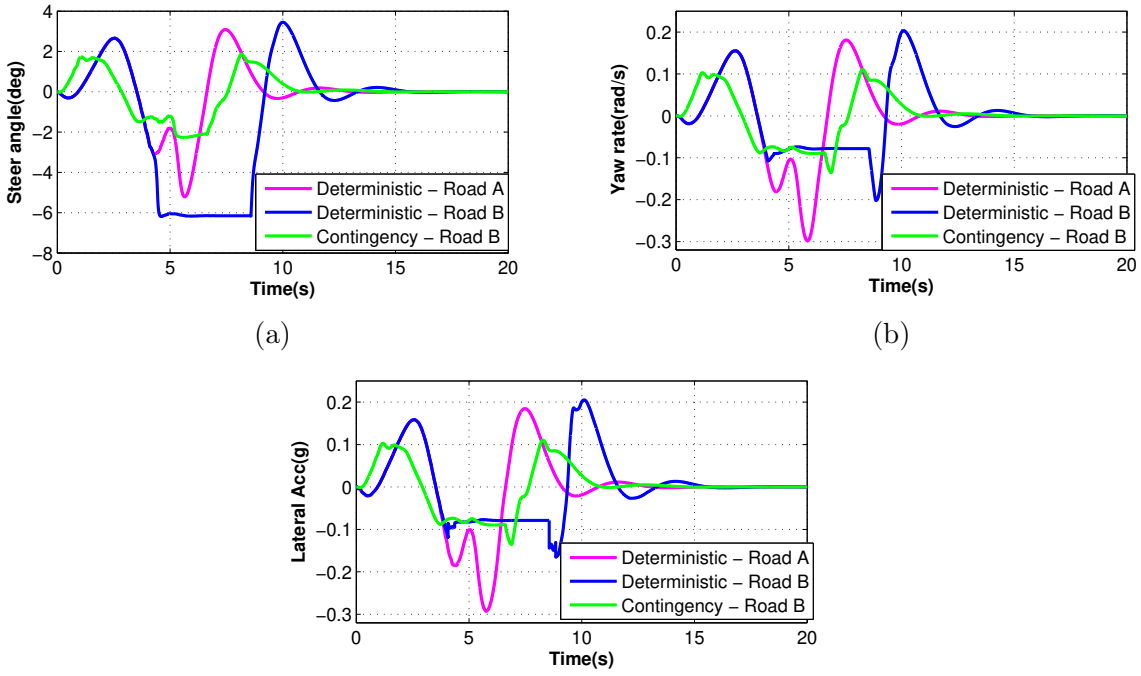

Figure 5.18: (a) The steer angle, (b) yaw rate, and (c) lateral acceleration for the deterministic and contingency controllers on Road A and Road B in the first contingency scenario.

5.5.4 Contingency Scenario 2: Left Turn on Mixed Snowy and Icy Road

The second contingency scenario is a 90-degree turn with the centerline as the desired path. Two roads with different conditions are considered for the simulations. Road A is totally snowy, whereas Road B is assumed to be snowy before the turn and icy after that, as shown in Fig. 5.19. The desired longitudinal velocity is assumed to be $u = 18\,kph$ constant. Figure 5.20a shows the vehicle track path controlled by the deterministic path planner for Road A, and Fig. 5.20b depicts the path optimized by the deterministic and contingency path planners for Road B. The steer angle, yaw rate, and lateral acceleration of the three simulated cases are shown in Fig. 5.21. Comparing the results of the deterministic path planner on Road A with those on Road B shows that although the deterministic path

planner/tracker can properly track the desired path with minimum deviation on Road A, it fails to keep the vehicle within the road boundaries on Road B. In fact, the deterministic path planner/tracker was unaware of the ice ahead on Road B and followed the centerline. Consequently, it could not provide the lateral forces needed for tracking the path when it comes to the icy part of the road. Once the vehicle is on the ice, nothing can ensure safety. To escape collision, the vehicle should have behaved differently before the turn. On the other hand, the contingency path planner/tracker did anticipate the presence of ice on Road B and therefore steered earlier to increase the radius of curvature, making the vehicle's behavior look like the outside-inside-outside behavior of professional race car drivers.

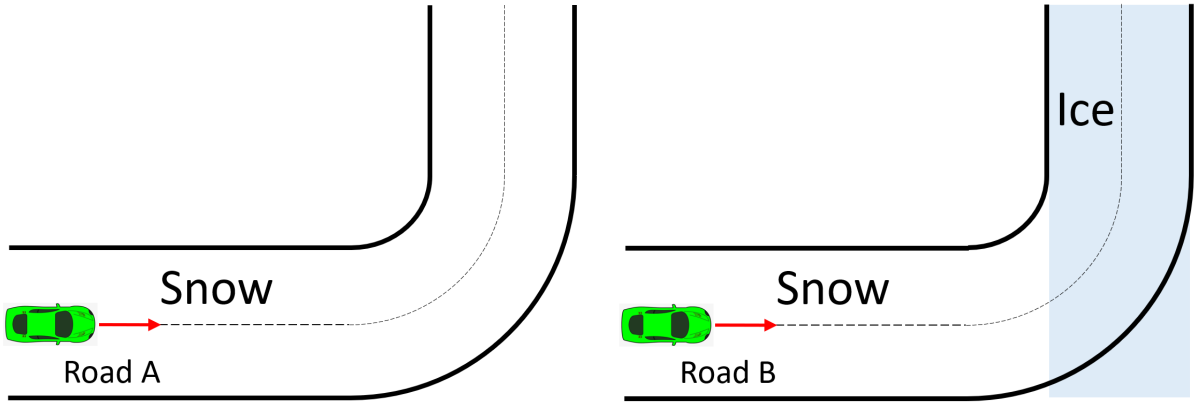

(a) (b)

Figure 5.19: The second contingency scenario is a 90-degree turn. (a) Road A is totally snowy, and (b) Road B is snowy before the turn and icy after that.

5.5.5 Contingency Scenario 3: Potential Change in Road Bank in a Curved Road

The third contingency scenario is an icy road ($\mu = 0.14$) with the centerline as the desired path and two obstacles in the road. The road is straight before $s = 50\,m$ and curved after that. To compare how the two path planners perform in response to road bank, two roads are considered: Roads A and B. Road A is totally flat, and Road B is flat in the straight part and banked ($\phi_r = -6\,\%$) in the curved part, as shown in Fig. 5.22. The

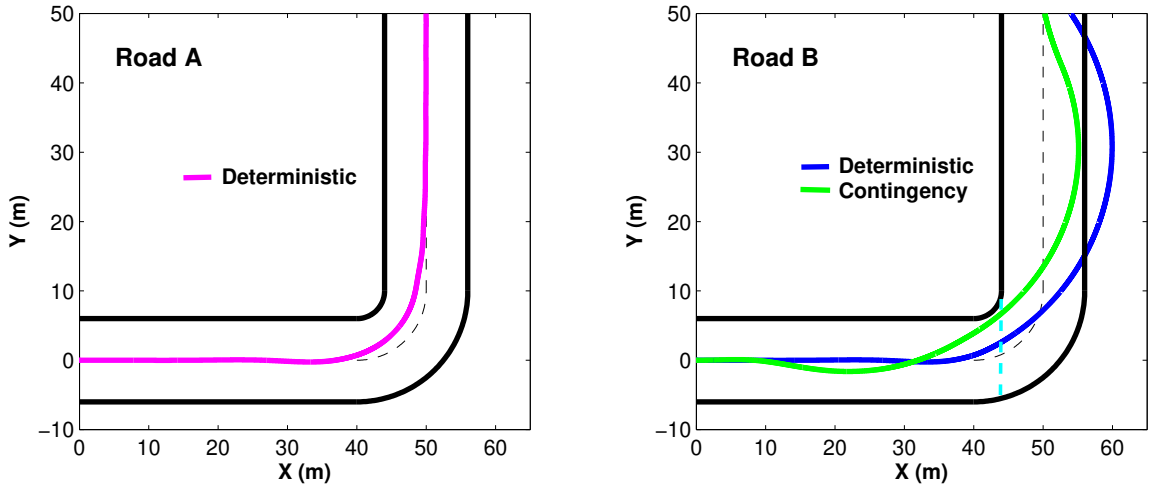

(a) (b)

Figure 5.20: The vehicle paths controlled with the deterministic and contingency path planners on (a) Road A and (b) Road B in the second contingency scenario.

desired longitudinal velocity is assumed to be $u = 36\,kph$ constant. Figure 5.23a shows the vehicle track path controlled by the deterministic path planner for Road A, and Fig. 5.23b depicts the path optimized by the deterministic and contingency path planners for Road B. The steer angle, yaw rate, and lateral acceleration of the three simulated cases are shown in Fig. 5.24. Comparing the results of the deterministic path planner on Road A with those on Road B shows that although the deterministic path planner/tracker can properly deviate from the centerline to avoid collision with the obstacles, it fails to maintain collision avoidance on Road B. The deterministic path planner/tracker was unaware of the road bank ahead on Road B and consequently did not prepare for the reduced lateral acceleration capacity in the negative direction. On the other hand, the contingency path planner/tracker anticipated the change in road bank in the curved section of the road and reacted more conservatively to ensure collision avoidance.

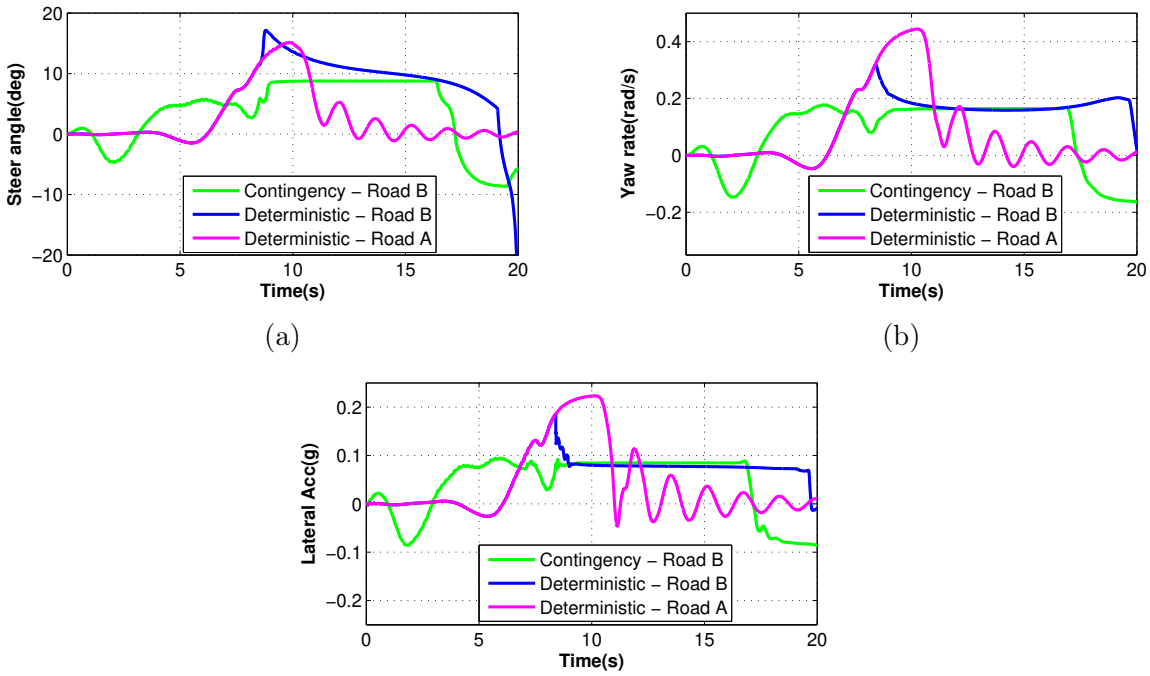

Figure 5.21: (a) The steer angle, (b) yaw rate, and (c) lateral acceleration for the deterministic and contingency path planners on Road A and Road B in the second contingency scenario.

5.6 Summary

In this chapter, an integrated vehicle stability and path planning/tracking controller was designed for emergency collision avoidance in autonomous vehicles. The designed controller is in fact an extension of the vehicle stability controller developed in Chapter 3, achieved by integrating a vehicle stability objective with the collision avoidance and path tracking objectives within the model predictive control design.

The integrated controller uses a combination of steering and differential braking to improve yaw rate responsiveness and mitigate collisions. The integrated controller constrains the use of differential braking so as to decrease the chance of instability. It should be noted that differential braking can be simply replaced with torque vectoring or any other actuation that can provide an additional corrective yaw moment to the system. This MPC

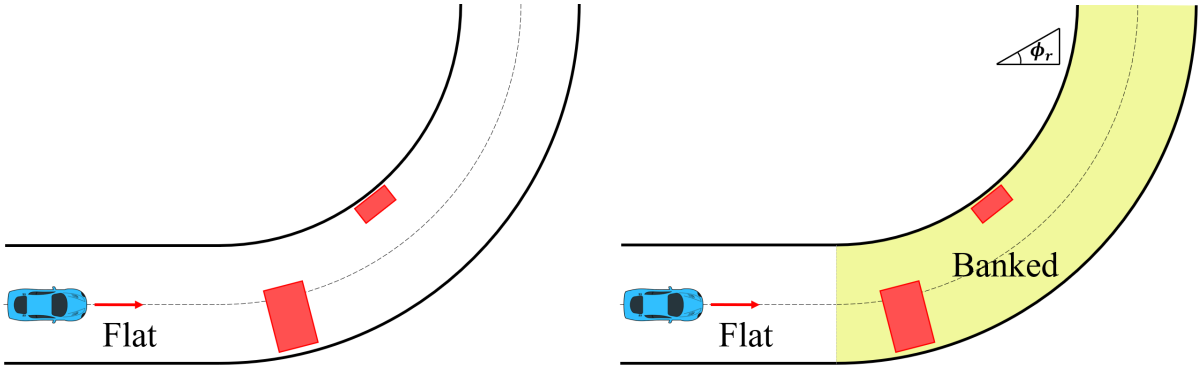

(a) (b)

Figure 5.22: The third contingency scenario is a curved road with potential change road bank. (a) Road A is totally flat, and (b) Road B is flat in the straight section and banked in the curved section.

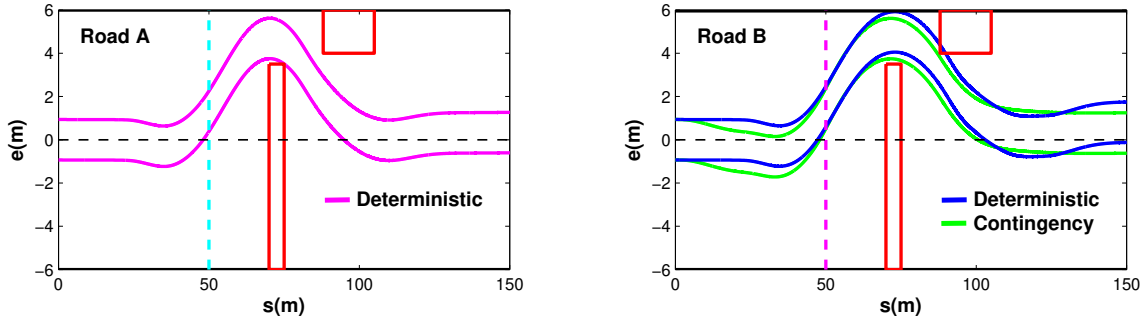

(a) (b)

Figure 5.23: The vehicle paths controlled with the deterministic and contingency path planners on (a) Road A and (b) Road B in the third contingency scenario.

controller uses slack variables to combine the control objectives with the priorities of (1) collision avoidance, (2) vehicle stability, and (3) path tracking. The designed controller has also been extended to a contingency MPC controller to handle uncertain road conditions. The CMPC controller uses a nominal prediction horizon and an emergency prediction horizon that share their first action.

A high fidelity CarSim model was used to demonstrate the effectiveness of the designed controllers in emergency scenarios. The path planning controller's performance in

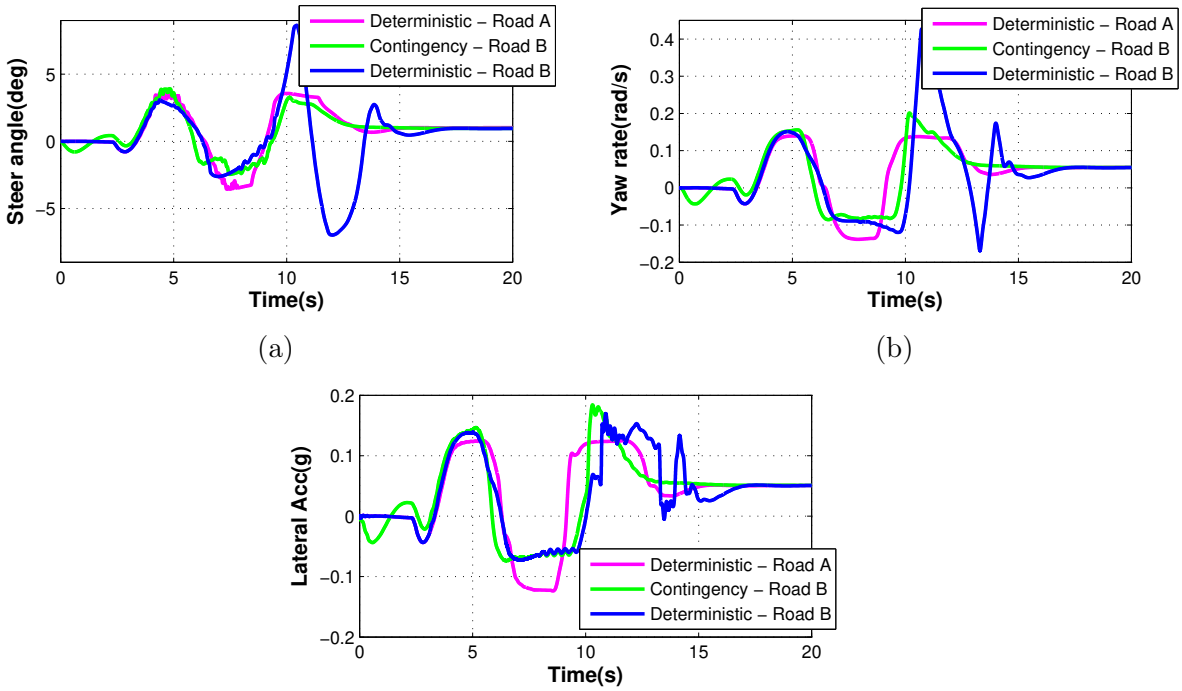

Figure 5.24: (a) The steer angle, (b) yaw rate, and (c) lateral acceleration for the deterministic and contingency path planners on Road A and Road B in the third contingency scenario.

improving lateral agility using conservative differential braking was evaluated in two driving scenarios. The simulations were iterated two times, with (1) differential braking OFF (Controller A) and (2) differential braking ON (Controller B), and comparisons show the advantages of the integrated controller. The presented scenarios are the typical challenges of autonomous vehicles. These scenarios are designed to push the vehicle to its limits of handling and to necessitate a quick response in yaw rate to avoid collisions. In harsher scenarios with shorter distances, where the collision is unavoidable, the violation of the collision avoidance constraint for Controller B will still be less than Controller A's.

The contingency controller's performance was assessed in three contingency scenarios, and the results confirmed the controller's ability to ensure collision avoidance. The contingency controller anticipates the friction loss and reacts earlier by planning a conservative

path, while the deterministic controller reacts very late and fails to prevent a collision.

Chapter 6

Conclusions and Future Work

6.1 Conclusions

In this thesis, a prioritization model predictive controller was designed for multi-actuation multi-objective vehicle control problems. The designed controller was employed for three case studies with three actuations: front/rear torque shifting, ELSD, and differential braking. The controller performance was evaluated using software simulations as well as experimental tests. A model predictive control design was also designed for the integrated collision avoidance and stabilization of autonomous vehicles, and its effectiveness was assessed numerically in several harsh maneuvers. The major findings and contributions of this thesis are listed below.

A prioritization control structure was designed that restricted the engagement of low priority actuators to high priority control objectives. The proposed MPC controller was employed for two actuation sets 1) front/rear torque shifting and differential braking, 2) ELSD and differential braking. It was discussed that using a costly actuator for improving vehicle handling is not a good idea when the other available actuators can provide the same control effort with less cost. For this reason, differential braking was considered as the low priority actuation to reduce unwanted speed dop and energy waste.

A coupled force vehicle prediction model was designed to enable the MPC controller to optimize front/rear torque distribution. The prediction model was designed by linearizing the nonlinear lateral tire force model with respect to variations of slip angle and torque to

capture the effect of longitudinal forces on lateral forces. It was shown that the sensitivity of the lateral force to the changes in the applied torque increases by increasing the axle torque. It was shown schematically that the corrective yaw moment capacity, generated by front/rear torque shifting, increases when the drive torque increases up to an optimum point and then starts decreasing.

Vehicle lateral stability and roll stability were integrated to ensure vehicle stability in any road friction and road angle conditions. To ensure the controller's effectiveness on non-flat roads, the effects of road angles on vehicle dynamics and vehicle stability limits were considered in the control design. It was shown that the road bank and grade affect the rollover index and shift the yaw rate safety limits downward, which must be included in the controller.

A dynamic model was designed for an ELSD clutch to provide an appropriate estimation of the clutch torque. It was discussed that the existing research on ELSD control mostly assumes an algebraic equation for ELSD clutch torque based on wheel speed differences, which can cause chattering or unwanted oversteering yaw moments. This challenge was resolved by designing a dynamic ELSD model based on the spring-damper model by assuming torsional spring and damper elements between ELSD clutch plates. Including a forgetting factor in the model allowed accumulated errors to fade away. Using this ELSD model enabled the controller to correctly activate and deactivate the ELSD clutch by simultaneously predicting the clutch torque.

The performance of the proposed controller was evaluated using co-simulations of MATLAB/Simulink and CarSim. A high-fidelity model of an electric Chevrolet Equinox and an E-Class SUV vehicle in CarSim were used in these simulations. Integrated axle torque distribution and differential braking were used in two case studies with multiple control objectives. The vehicle performance was assessed in several accelerating driving scenarios such as acceleration in turn, acceleration in slalom, and acceleration in flick under different road frictions on flat and non-flat roads. The simulation results showed the controller's ability in improving handling and stability and enhancing the vehicle's performance in longitudinal motion by decreasing the engagement of differential braking. The controller was able to prevent rollover in high friction roads and avoid skidding or spinning on low friction surfaces.

The proposed prioritization control scheme was implemented in real-time on dSpace Autobox and tested on an electric Chevrolet Equinox and a Cadillac CTS. The real-time

performance of the controller was evaluated in different driving maneuvers. The controlled vehicle's responses were compared with the uncontrolled vehicle's responses. The controller was able to activate the control actuations with the defined priorities to improve vehicle response and stability in all the driving maneuvers. In addition, the performance of the ELSD model was evaluated in different open-loop and closed-loop driving maneuvers. The estimated ELSD clutch torque was compared with the measured value by wheel force sensors, and the results confirmed the performance of the ELSD model in properly estimating clutch torque distribution. The results of on-throttle maneuvers also confirmed the ELSD controller's ability in preventing unwanted oversteering yaw moments.

The designed vehicle stability controller was extended to incorporate integrated collision avoidance and stabilization of autonomous vehicles. Combining differential braking with front steering enabled the controller to improve the vehicle's lateral agility in emergency collision avoidance scenarios. The controller used differential braking conservatively by adjusting the constraints on differential braking and its distribution between the front and rear axles based on vehicle response to maintain vehicle stability while improving lateral responsiveness.

A contingency path planning/tracking controller was designed to maintain vehicle safety and avoidance in uncertain road conditions. Combining a nominal prediction horizon and a contingency prediction horizon that have equal action at their first step enabled the controller to plan a conservative and safe path that avoids collisions. This control strategy provided robustness to potential friction losses in contingency scenarios.

The performance of the controller designed for emergency collision avoidance was evaluated in several emergency maneuvers. Each maneuver was performed with and without differential braking, and comparisons showed the integrated controller's capability of improving lateral agility to avoid collisions. The results also showed the capability of the controller in prioritizing the control objectives when it temporarily violates the stability criteria to ensure the collision avoidance objective. In addition, the contingency controller's performance was assessed and compared with the deterministic controller's performance in three contingency maneuvers with road friction and road bank uncertainties. The results confirmed the CMPC controller's ability to prevent collision by acting conservatively and preparing for the potential losses of the lateral acceleration capacity.

6.2 Future Work

A few suggestions are made in this section to continue the work done in this thesis to improve the performance of the developed models and controllers. These suggestions aim to extend the contributions of this thesis to multi-actuated vehicle control and autonomous vehicle control.

- Extending the prioritization control structure based on vehicle states: In this thesis, a prioritization control design was developed for multi-actuated vehicles with multiple control objectives. This design can be extended to consider the vehicle states in objective prioritization. In addition, the actuation prioritization can be updated in real-time based on vehicle states and the capabilities of actuations.

- Considering the roll stability in local path planning/tracking control designs: In emergency collision avoidance scenarios on surfaces with a high friction coefficient, the vehicle roll rate and roll angle are considerable, resulting in significant lateral load transfer. Therefore, to prevent vehicle rollover, the vehicle's roll dynamics and roll stability limits need to be included in path planning/tracking control designs.

- Integrating longitudinal path planning with lateral path planning: The local lateral path planning designed in this thesis assumes that the desired vehicle longitudinal velocity is given by a high-level module. This separation of the longitudinal velocity planning and lateral path planning makes the controller unable to plan the maximum optimal speed in the maneuver. The integration of longitudinal and lateral path planning would improve the performance of path planning/tracking controllers in emergency collision avoidance scenarios.

- Extending the contingency MPC controller for use in other contingency events: In this thesis, a contingency path planning/tracking controller was designed to handle uncertain road conditions. This design can be extended to address other contingency events in vehicle motion planning problems such as uncertain behavior of other road vehicles or pedestrians crossing the road. To ensure safety, the contingency controller can be extended to plan contingency horizons for both longitudinal and lateral motions.

References

[1] Feng Zhao, Shuzhi Sam Ge, Fangwen Tu, Yechen Qin, and Mingming Dong. Adaptive neural network control for active suspension system with actuator saturation. *IET control theory & applications*, 10(14):1696–1705, 2016.

[2] Seongjin Yim, Kwangki Jeon, and Kyongsu Yi. An investigation into vehicle rollover prevention by coordinated control of active anti-roll bar and electronic stability program. *International Journal of Control, Automation and Systems*, 10(2):275–287, 2012.

[3] Hojjat Kaveh, Hassan Salarieh, and Reza Hajiloo. On the control of unknown continuous time chaotic systems by applying takens embedding theory. *Chaos, Solitons & Fractals*, 109:53–57, 2018.

[4] Amin Habibnejad Korayem, Saeed Rafee Nekoo, and Moharam Habibnejad Korayem. Optimal sliding mode control design based on the state-dependent riccati equation for cooperative manipulators to increase dynamic load carrying capacity. *Robotica*, 37(2):321, 2019.

[5] Yongduan Song, Xiucai Huang, and Changyun Wen. Robust adaptive fault-tolerant pid control of mimo nonlinear systems with unknown control direction. *IEEE Transactions on Industrial Electronics*, 64(6):4876–4884, 2017.

[6] Bahram Yaghooti and Hassan Salarieh. Robust adaptive fractional order proportional integral derivative controller design for uncertain fractional order nonlinear systems using sliding mode control. *Proceedings of the Institution of Mechanical Engineers, Part I: Journal of Systems and Control Engineering*, 232(5):550–557, 2018.

[7] Yuecheng Li, Hongwen He, Jiankun Peng, and Hong Wang. Deep reinforcement learning-based energy management for a series hybrid electric vehicle enabled by history cumulative trip information. *IEEE Transactions on Vehicular Technology*, 68(8):7416–7430, 2019.

[8] R Hajiloo, H Salarieh, and A Alasty. Chaos control in delayed phase space constructed by the takens embedding theory. *Communications in Nonlinear Science and Numerical Simulation*, 54:453–465, 2018.

[9] A Habibnejad Korayem, Saeed Rafee Nekoo, and MH Korayem. Sliding mode control design based on the state-dependent riccati equation: theoretical and experimental implementation. *International Journal of Control*, 92(9):2136–2149, 2019.

[10] R Hajiloo, M Shahrokhi, and H Salarieh. Adaptive delayed feedback chaos control of a class of uncertain chaotic systems subject to external disturbance. *Iranian Journal of Science and Technology, Transactions of Mechanical Engineering*, 43(1):517–525, 2019.

[11] Bahram Yaghooti, Ali Siahi Shadbad, Kaveh Safavi, and Hassan Salarieh. Adaptive synchronization of uncertain fractional-order chaotic systems using sliding mode control techniques. *Proceedings of the Institution of Mechanical Engineers, Part I: Journal of Systems and Control Engineering*, 234(1):3–9, 2020.

[12] Dian Sheng, Yiheng Wei, Songsong Cheng, and Jianmei Shuai. Adaptive backstepping control for fractional order systems with input saturation. *Journal of the Franklin Institute*, 354(5):2245–2268, 2017.

[13] MH Korayem, H Tourajizadeh, A Zehfroosh, and AH Korayem. Optimal path planning of a cable-suspended robot with moving boundary using optimal feedback linearization approach. *Nonlinear Dynamics*, 78(2):1515–1543, 2014.

[14] MH Korayem, Hami Tourajizadeh, A Zehfroosh, and AH Korayem. Optimal regulation of a cable robot in presence of obstacle using optimal adaptive feedback linearization approach. *Robotica*, 33(4):933, 2015.

[15] Yanjun Huang, Hong Wang, Amir Khajepour, Hongwen He, and Jie Ji. Model predictive control power management strategies for hevs: A review. *Journal of Power Sources*, 341:91–106, 2017.

[16] Matteo Corno, Mara Tanelli, Ivo Boniolo, and Sergio M Savaresi. Advanced yaw control of four-wheeled vehicles via rear active differential braking. In *Proceedings of the 48h IEEE Conference on Decision and Control (CDC) held jointly with 2009 28th Chinese Control Conference*, pages 5176–5181. IEEE, 2009.

[17] Chenming Zhao, Weidong Xiang, and Paul Richardson. Vehicle lateral control and yaw stability control through differential braking. In *2006 IEEE international symposium on industrial electronics*, volume 1, pages 384–389. IEEE, 2006.

[18] Mehdi Abroshan, Reza Hajiloo, Ehsan Hashemi, and Amir Khajepour. Model predictive-based tractor-trailer stabilisation using differential braking with experimental verification. *Vehicle System Dynamics*, pages 1–24, 2020.

[19] Seyedeh Asal Nahidi. Reconfigurable integrated vehicle stability control using optimal control techniques. 2017.

[20] Dhanaraja Kasinathan, Alireza Kasaiezadeh, Andy Wong, Amir Khajepour, Shih-Ken Chen, and Bakhtiar Litkouhi. An optimal torque vectoring control for vehicle applications via real-time constraints. *IEEE Transactions on Vehicular Technology*, 65(6):4368–4378, 2015.

[21] Asal Nahidi, Alireza Kasaiezadeh, Saeid Khosravani, Amir Khajepour, Shih-Ken Chen, and Bakhtiar Litkouhi. Modular integrated longitudinal and lateral vehicle stability control for electric vehicles. *Mechatronics*, 44:60–70, 2017.

[22] Milad Jalali, Ehsan Hashemi, Amir Khajepour, Shih-ken Chen, and Bakhtiar Litkouhi. Integrated model predictive control and velocity estimation of electric vehicles. *Mechatronics*, 46:84–100, 2017.

[23] Lin Zhang, Haitao Ding, Jianpeng Shi, Yanjun Huang, Hong Chen, Konghui Guo, and Qin Li. An adaptive backstepping sliding mode controller to improve vehicle maneuverability and stability via torque vectoring control. *IEEE Transactions on Vehicular Technology*, 69(3):2598–2612, 2020.

[24] Efstathios Siampis, Efstathios Velenis, Salvatore Gariuolo, and Stefano Longo. A real-time nonlinear model predictive control strategy for stabilization of an electric vehicle at the limits of handling. *IEEE Transactions on Control Systems Technology*, 26(6):1982–1994, 2017.

[25] Craig S Ross, Clinton E Carey, Todd Schanz, Edmund F Gaffney, and Michael Catalano. Development of an electronically-controlled, limited-slip differential (elsd) for fwd applications. Technical report, SAE Technical Paper, 2007.

[26] Marco Gadola and Daniel Chindamo. The mechanical limited-slip differential revisited: high-performance and racing car applications. *Int J Appl Eng Res*, 13:1478–1495, 2018.

[27] Leonardo De Novellis, Aldo Sorniotti, and Patrick Gruber. Wheel torque distribution criteria for electric vehicles with torque-vectoring differentials. *IEEE Transactions on Vehicular Technology*, 63(4):1593–1602, 2013.

[28] K Sawase and K Inoue. Maximum acceptable differential speed ratio of lateral torque-vectoring differentials for vehicles. *Proceedings of the Institution of Mechanical Engineers, Part D: Journal of Automobile Engineering*, 223(8):967–978, 2009.

[29] Damrongrit Piyabongkarn, Jae Lew, John Grogg, and Robert Kyle. Stability-enhanced traction and yaw control using electronic limited slip differential. *SAE Transactions*, pages 931–941, 2006.

[30] Damrongrit Piyabongkarn, Jae Y Lew, Rajesh Rajamani, John A Grogg, and Qinghui Yuan. On the use of torque-biasing systems for electronic stability control: Limitations and possibilities. *IEEE Transactions on Control Systems Technology*, 15(3):581–589, 2007.

[31] Daniel Rubin and Shai A Arogeti. Vehicle yaw stability control using active limited-slip differential via model predictive control methods. *Vehicle System Dynamics*, 53(9):1315–1330, 2015.

[32] Philip Koehn and Michael Eckrich. Active steering-the bmw approach towards modern steering technology. Technical report, SAE technical paper, 2004.

[33] Baozhen Zhang, Amir Khajepour, and Avesta Goodarzi. Vehicle yaw stability control using active rear steering: Development and experimental validation. *Proceedings of the Institution of Mechanical Engineers, Part K: Journal of Multi-body Dynamics*, 231(2):333–345, 2017.

[34] Said Mammar and Damien Koenig. Vehicle handling improvement by active steering. *Vehicle system dynamics*, 38(3):211–242, 2002.

[35] Craig Earl Beal and J Christian Gerdes. Model predictive control for vehicle stabilization at the limits of handling. *IEEE Transactions on Control Systems Technology*, 21(4):1258–1269, 2012.

[36] Johannes Tjonnas and Tor A Johansen. Stabilization of automotive vehicles using active steering and adaptive brake control allocation. *IEEE Transactions on Control Systems Technology*, 18(3):545–558, 2009.

[37] Matthijs Klomp. On drive force distribution and road vehicle handling-a study of understeer and lateral grip. 2007.

[38] Basilio Lenzo, Francesco Bucchi, Aldo Sorniotti, and Francesco Frendo. On the handling performance of a vehicle with different front-to-rear wheel torque distributions. *Vehicle System Dynamics*, 2018.

[39] Francesco Bucchi, Basilio Lenzo, Francesco Frendo, Wouter De Nijs, and A Sorniotti. The effect of the front-to-rear wheel torque distribution on vehicle handling: an experimental assessment. In *Dynamics of Vehicles on Roads and Tracks Vol 1: Proceedings of the 25th International Symposium on Dynamics of Vehicles on Roads and Tracks (IAVSD 2017), 14-18 August 2017, Rockhampton, Queensland, Australia*, page 31. CRC Press, 2017.

[40] David Ruiz Diez, Efstathios Velenis, Davide Tavernini, Edward N Smith, Efstathios Siampis, and Amir Soltani. Front/rear axle torque vectoring control for electric vehicles. *Journal of Dynamic Systems, Measurement, and Control*, 141(6), 2019.

[41] Zhengyi He, Yang Ou, and Jingming Yuan. Research on the torque dynamic distribution algorithm of in-wheel-motor electric vehicle. In *Proceedings of the FISITA 2012 World Automotive Congress*, pages 257–266. Springer, 2013.

[42] Aibin Wu, Chao Li, Yongqiang Zhao, and Jinlong Cui. Axle torque distribution to improve vehicle handling and stability. Technical report, SAE Technical Paper, 2019.

[43] Russell P Osborn and Taehyun Shim. Independent control of all-wheel-drive torque distribution. *Vehicle system dynamics*, 44(7):529–546, 2006.

[44] Jonathan C Wheals, Hanna Baker, Keith Ramsey, and Will Turner. Torque vectoring awd driveline: design, simulation, capabilities and control. *SAE transactions*, pages 557–576, 2004.

[45] Jonathan C Wheals. Torque vectoring driveline: Suv-based demonstrator and practical actuation technologies. *SAE transactions*, pages 631–648, 2005.

[46] Milad Jalali, Saeid Khosravani, Amir Khajepour, Shih-ken Chen, and Bakhtiar Litkouhi. Model predictive control of vehicle stability using coordinated active steering and differential brakes. *Mechatronics*, 48:30–41, 2017.

[47] G Burgio and P Zegelaar. Integrated vehicle control using steering and brakes. *International Journal of Control*, 79(05):534–541, 2006.

[48] Junjie He, David A Crolla, MC Levesley, and WJ Manning. Coordination of active steering, driveline, and braking for integrated vehicle dynamics control. *Proceedings of the Institution of Mechanical Engineers, Part D: Journal of Automobile Engineering*, 220(10):1401–1420, 2006.

[49] Byeongcho Lee, Amir Khajepour, and Kamran Behdinan. Vehicle stability through integrated active steering and differential braking. *SAE Transactions*, pages 948–965, 2006.

[50] Moustapha Doumiati, Olivier Sename, Luc Dugard, John-Jairo Martinez-Molina, Peter Gaspar, and Zoltan Szabo. Integrated vehicle dynamics control via coordination of active front steering and rear braking. *European Journal of Control*, 19(2):121–143, 2013.

[51] Hussein Termous, Hassan Shraim, Reine Talj, Clovis Francis, and Ali Charara. Coordinated control strategies for active steering, differential braking and active suspension for vehicle stability, handling and safety improvement. *Vehicle System Dynamics*, 57(10):1494–1529, 2019.

[52] Junmin Wang and Raul G Longoria. Coordinated vehicle dynamics control with control distribution. In *2006 American control conference*, pages 6–pp. IEEE, 2006.

[53] Amin Tahouni, Mehdi Mirzaei, and Behrouz Najjari. Novel constrained nonlinear control of vehicle dynamics using integrated active torque vectoring and electronic

stability control. *IEEE Transactions on Vehicular Technology*, 68(10):9564–9572, 2019.

[54] Domenico Bianchi, Alessandro Borri, Maria Domenica Di Benedetto, Stefano Di Gennaro, and Gilberto Burgio. Adaptive integrated vehicle control using active front steering and rear torque vectoring. *International Journal of Vehicle Autonomous Systems*, 8(2-4):85–105, 2010.

[55] EM Elbeheiry, YF Zeyada, and ME Elaraby. Handling capabilities of vehicles in emergencies using coordinated afs and armc systems. *Vehicle System Dynamics*, 35(3):195–215, 2001.

[56] Stefano Di Cairano, Hongtei Eric Tseng, Daniele Bernardini, and Alberto Bemporad. Vehicle yaw stability control by coordinated active front steering and differential braking in the tire sideslip angles domain. *IEEE Transactions on Control Systems Technology*, 21(4):1236–1248, 2012.

[57] Barys Shyrokau, Danwei Wang, Dzmitry Savitski, Kristian Hoepping, and Valentin Ivanov. Vehicle motion control with subsystem prioritization. *Mechatronics*, 30:297–315, 2015.

[58] Jangyeol Yoon and Kyongsu Yi. A rollover mitigation control scheme based on rollover index. In *2006 American control conference*, pages 6–pp. IEEE, 2006.

[59] Mansour Ataei, Amir Khajepour, and Soo Jeon. A general rollover index for tripped and un-tripped rollovers on flat and sloped roads. *Proceedings of the Institution of Mechanical Engineers, Part D: Journal of automobile engineering*, 233(2):304–316, 2019.

[60] Jangyeol Yoon, Wanki Cho, Juyong Kang, Bongyeong Koo, and Kyongsu Yi. Design and evaluation of a unified chassis control system for rollover prevention and vehicle stability improvement on a virtual test track. *Control Engineering Practice*, 18(6):585–597, 2010.

[61] SeongJin Yim, Yongjin Park, and K Yi. Design of active suspension and electronic stability program for rollover prevention. *International journal of automotive technology*, 11(2):147–153, 2010.

[62] YI Ryu, DO Kang, SJ Heo, and JH In. Rollover mitigation for a heavy commercial vehicle. *International journal of automotive technology*, 11(2):283–287, 2010.

[63] Thomas J Wielenga and Milton A Chace. A study in rollover prevention using anti-rollover braking. Technical report, SAE Technical Paper, 2000.

[64] Brad Schofield and Tore Hagglund. Optimal control allocation in vehicle dynamics control for rollover mitigation. In *2008 American Control Conference*, pages 3231–3236. IEEE, 2008.

[65] PJ Liu, Subhash Rakheja, and AKW Ahmed. Dynamic rollover threshold of articulated freight vehicles. *International Journal of Heavy Vehicle Systems*, 5(3-4):300–322, 1998.

[66] Mansour Ataei, Amir Khajepour, and Soo Jeon. Reconfigurable integrated stability control for four-and three-wheeled urban vehicles with flexible combinations of actuation systems. *IEEE/ASME Transactions on Mechatronics*, 23(5):2031–2041, 2018.

[67] Mansour Ataei, Amir Khajepour, and Soo Jeon. Model predictive rollover prevention for steer-by-wire vehicles with a new rollover index. *International Journal of Control*, 93(1):140–155, 2020.

[68] Chen Tang, Mansour Ataei, and Amir Khajepour. A reconfigurable integrated control for narrow tilting vehicles. *IEEE Transactions on Vehicular Technology*, 68(1):234–244, 2018.

[69] Mansour Ataei, Amir Khajepour, and Soo Jeon. Model predictive control for integrated lateral stability, traction/braking control, and rollover prevention of electric vehicles. *Vehicle system dynamics*, 58(1):49–73, 2020.

[70] Milad Jalali, Ehsan Hashemi, Amir Khajepour, Shih-ken Chen, and Bakhtiar Litkouhi. Model predictive control of vehicle roll-over with experimental verification. *Control Engineering Practice*, 77:95–108, 2018.

[71] Zhilin Jin, Lei Zhang, Jiale Zhang, and Amir Khajepour. Stability and optimised H-infinite control of tripped and untripped vehicle rollover. *Vehicle System Dynamics*, 54(10):1405–1427, 2016.

[72] Chuan Hu, Zhenfeng Wang, Yechen Qin, Yanjun Huang, Jinxiang Wang, and Rongrong Wang. Lane keeping control of autonomous vehicles with prescribed performance considering the rollover prevention and input saturation. *IEEE Transactions on Intelligent Transportation Systems*, 2019.

[73] Liang Li, Yishi Lu, Rongrong Wang, and Jie Chen. A three-dimensional dynamics control framework of vehicle lateral stability and rollover prevention via active braking with mpc. *IEEE Transactions on Industrial Electronics*, 64(4):3389–3401, 2016.

[74] Yrvann Emzivat, Javier Ibañez-Guzmán, Hervé Illy, Philippe Martinet, and Olivier H Roux. A formal approach for the design of a dependable perception system for autonomous vehicles. In *2018 21st International Conference on Intelligent Transportation Systems (ITSC)*, pages 2452–2459. IEEE, 2018.

[75] Ehsan Mohammadbagher, Neel P Bhatt, Ehsan Hashemi, Baris Fidan, and Amir Khajepour. Real-time pedestrian localization and state estimation using moving horizon estimation. In *2020 IEEE 23rd International Conference on Intelligent Transportation Systems (ITSC)*, pages 1–7. IEEE, 2020.

[76] Nan Xu, Hassan Askari, Yanjun Huang, Jianfeng Zhou, and Amir Khajepour. Tire force estimation in intelligent tires using machine learning. *IEEE Transactions on Intelligent Transportation Systems*, 2020.

[77] Bruno Henrique Groenner Barbosa, Nan Xu, Hassan Askari, and Amir Khajepour. Lateral force prediction using gaussian process regression for intelligent tire systems. *arXiv preprint arXiv:2009.12463*, 2020.

[78] Nan Xu, Yanjun Huang, Hassan Askari, and Zepeng Tang. Tire slip angle estimation based on the intelligent tire technology. *arXiv preprint arXiv:2010.06803*, 2020.

[79] Amin Habibnejad Korayem, Amir Khajepour, and Baris Fidan. Vehicle-trailer lateral velocity estimation using constrained unscented transformation. *Vehicle System Dynamics*, pages 1–28, 2020.

[80] Patrick Lin. Why ethics matters for autonomous cars. In *Autonomous driving*, pages 69–85. Springer, Berlin, Heidelberg, 2016.

[81] Yoshiaki Kuwata, Justin Teo, Gaston Fiore, Sertac Karaman, Emilio Frazzoli, and Jonathan P How. Real-time motion planning with applications to autonomous urban driving. *IEEE Transactions on control systems technology*, 17(5):1105–1118, 2009.

[82] Jens Rieken, Richard Matthaei, and Markus Maurer. Toward perception-driven urban environment modeling for automated road vehicles. In *2015 IEEE 18th International Conference on Intelligent Transportation Systems*, pages 731–738. IEEE, 2015.

[83] Michael Montemerlo, Jan Becker, Suhrid Bhat, Hendrik Dahlkamp, Dmitri Dolgov, Scott Ettinger, Dirk Haehnel, Tim Hilden, Gabe Hoffmann, Burkhard Huhnke, et al. Junior: The stanford entry in the urban challenge. *Journal of field Robotics*, 25(9):569–597, 2008.

[84] Sébastien Glaser, Benoit Vanholme, Saïd Mammar, Dominique Gruyer, and Lydie Nouveliere. Maneuver-based trajectory planning for highly autonomous vehicles on real road with traffic and driver interaction. *IEEE Transactions on intelligent transportation systems*, 11(3):589–606, 2010.

[85] Gowtham Garimella, Joseph Funke, Chuang Wang, and Marin Kobilarov. Neural network modeling for steering control of an autonomous vehicle. In *2017 IEEE/RSJ International Conference on Intelligent Robots and Systems (IROS)*, pages 2609–2615. IEEE, 2017.

[86] David Fernández Llorca, Vicente Milanés, Ignacio Parra Alonso, Miguel Gavilán, Iván García Daza, Joshué Pérez, and Miguel Ángel Sotelo. Autonomous pedestrian collision avoidance using a fuzzy steering controller. *IEEE Transactions on Intelligent Transportation Systems*, 12(2):390–401, 2011.

[87] Yadollah Rasekhipour, Amir Khajepour, Shih-Ken Chen, and Bakhtiar Litkouhi. A potential field-based model predictive path-planning controller for autonomous road vehicles. *IEEE Transactions on Intelligent Transportation Systems*, 18(5):1255–1267, 2016.

[88] Hong Wang, Yanjun Huang, Amir Khajepour, Yubiao Zhang, Yadollah Rasekhipour, and Dongpu Cao. Crash mitigation in motion planning for autonomous vehicles. *IEEE Transactions on Intelligent Transportation Systems*, 20(9):3313–3323, 2019.

[89] Georg Schildbach and Francesco Borrelli. Scenario model predictive control for lane change assistance on highways. In *2015 IEEE Intelligent Vehicles Symposium (IV)*, pages 611–616. IEEE, 2015.

[90] Andreas Homann, Markus Buss, Martin Keller, Karl-Heinz Glander, and Torsten Bertram. Multi stage model predictive trajectory set approach for collision avoidance. In *2018 21st International Conference on Intelligent Transportation Systems (ITSC)*, pages 945–950. IEEE, 2018.

[91] Tomas Berglund, Andrej Brodnik, Håkan Jonsson, Mats Staffanson, and Inge Soderkvist. Planning smooth and obstacle-avoiding b-spline paths for autonomous mining vehicles. *IEEE Transactions on Automation Science and Engineering*, 7(1):167–172, 2009.

[92] Ji-wung Choi, Renwick E Curry, and Gabriel Hugh Elkaim. Continuous curvature path generation based on bézier curves for autonomous vehicles. *International Journal of Applied Mathematics*, 40(2), 2010.

[93] Jhonghyun An, Baehoon Choi, Taehun Hwang, and Euntai Kim. A novel rear-end collision warning system using neural network ensemble. In *2016 IEEE Intelligent Vehicles Symposium (IV)*, pages 1265–1270. IEEE, 2016.

[94] Vicente Milanés, Joshué Pérez, Jorge Godoy, and Enrique Onieva. A fuzzy aid rear-end collision warning/avoidance system. *Expert Systems with Applications*, 39(10):9097–9107, 2012.

[95] Jose E Naranjo, Carlos Gonzalez, Ricardo Garcia, and Teresa De Pedro. Lane-change fuzzy control in autonomous vehicles for the overtaking maneuver. *IEEE Transactions on Intelligent Transportation Systems*, 9(3):438–450, 2008.

[96] Xuewu Ji, Xiangkun He, Chen Lv, Yahui Liu, and Jian Wu. Adaptive-neural-network-based robust lateral motion control for autonomous vehicle at driving limits. *Control Engineering Practice*, 76:41–53, 2018.

[97] Long Chen, Xuemin Hu, Wei Tian, Hong Wang, Dongpu Cao, and Fei-Yue Wang. Parallel planning: a new motion planning framework for autonomous driving. *IEEE/CAA Journal of Automatica Sinica*, 6(1):236–246, 2018.

[98] Michael T Wolf and Joel W Burdick. Artificial potential functions for highway driving with collision avoidance. In *2008 IEEE International Conference on Robotics and Automation*, pages 3731–3736. IEEE, 2008.

[99] Muhammad Awais Abbas, Ruth Milman, and J Mikael Eklund. Obstacle avoidance in real time with nonlinear model predictive control of autonomous vehicles. *Canadian journal of electrical and computer engineering*, 40(1):12–22, 2017.

[100] Yongsoon Yoon, Jongho Shin, H Jin Kim, Yongwoon Park, and Shankar Sastry. Model-predictive active steering and obstacle avoidance for autonomous ground vehicles. *Control Engineering Practice*, 17(7):741–750, 2009.

[101] Yadollah Rasekhipour, Iman Fadakar, and Amir Khajepour. Autonomous driving motion planning with obstacles prioritization using lexicographic optimization. *Control Engineering Practice*, 77:235–246, 2018.

[102] Hong Wang, Yanjun Huang, Amir Khajepour, Dongpu Cao, and Chen Lv. Ethical decision-making platform in autonomous vehicles with lexicographic optimization based model predictive controller. *IEEE Transactions on Vehicular Technology*, 2020.

[103] Jiechao Liu, Paramsothy Jayakumar, Jeffrey L Stein, and Tulga Ersal. A nonlinear model predictive control formulation for obstacle avoidance in high-speed autonomous ground vehicles in unstructured environments. *Vehicle System Dynamics*, 56(6):853–882, 2018.

[104] Christian Gotte, Martin Keller, Carsten Hass, Karl-Heinz Glander, Alois Seewald, and Torsten Bertram. A model predictive combined planning and control approach for guidance of automated vehicles. In *2015 IEEE International Conference on Vehicular Electronics and Safety (ICVES)*, pages 69–74. IEEE, 2015.

[105] Yiqi Gao, Andrew Gray, H Eric Tseng, and Francesco Borrelli. A tube-based robust nonlinear predictive control approach to semiautonomous ground vehicles. *Vehicle System Dynamics*, 52(6):802–823, 2014.

[106] Yanjun Huang, Haitao Ding, Yubiao Zhang, Hong Wang, Dongpu Cao, Nan Xu, and Chuan Hu. A motion planning and tracking framework for autonomous vehicles based on artificial potential field elaborated resistance network approach. *IEEE Transactions on Industrial Electronics*, 67(2):1376–1386, 2019.

[107] Yanjun Huang, Hong Wang, Amir Khajepour, Haitao Ding, Kang Yuan, and Yechen Qin. A novel local motion planning framework for autonomous vehicles based on resistance network and model predictive control. *IEEE Transactions on Vehicular Technology*, 69(1):55–66, 2019.

[108] Jesse Levinson, Jake Askeland, Jan Becker, Jennifer Dolson, David Held, Soeren Kammel, J Zico Kolter, Dirk Langer, Oliver Pink, Vaughan Pratt, et al. Towards fully autonomous driving: Systems and algorithms. In *2011 IEEE Intelligent Vehicles Symposium (IV)*, pages 163–168. IEEE, 2011.

[109] Junqing Wei, Jarrod M Snider, Junsung Kim, John M Dolan, Raj Rajkumar, and Bakhtiar Litkouhi. Towards a viable autonomous driving research platform. In *2013 IEEE Intelligent Vehicles Symposium (IV)*, pages 763–770. IEEE, 2013.

[110] Joseph Funke, Matthew Brown, Stephen M Erlien, and J Christian Gerdes. Prioritizing collision avoidance and vehicle stabilization for autonomous vehicles. In *2015 IEEE Intelligent Vehicles Symposium (IV)*, pages 1134–1139. IEEE, 2015.

[111] Matthew Brown, Joseph Funke, Stephen Erlien, and J Christian Gerdes. Safe driving envelopes for path tracking in autonomous vehicles. *Control Engineering Practice*, 61:307–316, 2017.

[112] Joseph Funke, Matthew Brown, Stephen M Erlien, and J Christian Gerdes. Collision avoidance and stabilization for autonomous vehicles in emergency scenarios. *IEEE Transactions on Control Systems Technology*, 25(4):1204–1216, 2016.

[113] Nitin R Kapania and J Christian Gerdes. Design of a feedback-feedforward steering controller for accurate path tracking and stability at the limits of handling. *Vehicle System Dynamics*, 53(12):1687–1704, 2015.

[114] Stephen M Erlien, Susumu Fujita, and Joseph Christian Gerdes. Shared steering control using safe envelopes for obstacle avoidance and vehicle stability. *IEEE Transactions on Intelligent Transportation Systems*, 17(2):441–451, 2015.

[115] Avinash Balachandran, Matthew Brown, Stephen M Erlien, and J Christian Gerdes. Predictive haptic feedback for obstacle avoidance based on model predictive control. *IEEE Transactions on Automation Science and Engineering*, 13(1):26–31, 2015.

[116] Stephen M Erlien, Joseph Funke, and J Christian Gerdes. Incorporating non-linear tire dynamics into a convex approach to shared steering control. In *2014 American Control Conference*, pages 3468–3473. IEEE, 2014.

[117] Vincent A Laurense, Jonathan Y Goh, and J Christian Gerdes. Path-tracking for autonomous vehicles at the limit of friction. In *2017 American Control Conference (ACC)*, pages 5586–5591. IEEE, 2017.

[118] Hyungchai Park and J Christian Gerdes. Optimal tire force allocation for trajectory tracking with an over-actuated vehicle. In *2015 IEEE Intelligent Vehicles Symposium (IV)*, pages 1032–1037. IEEE, 2015.

[119] Qingjia Cui, Rongjun Ding, Xiaojian Wu, and Bing Zhou. A new strategy for rear-end collision avoidance via autonomous steering and differential braking in highway driving. *Vehicle system dynamics*, 2019.

[120] Paolo Falcone, Francesco Borrelli, Jahan Asgari, H Eric Tseng, and Davor Hrovat. A model predictive control approach for combined braking and steering in autonomous vehicles. In *2007 Mediterranean Conference on Control & Automation*, pages 1–6. IEEE, 2007.

[121] Paolo Falcone, Manuela Tufo, Francesco Borrelli, Jahan Asgari, and H Eric Tseng. A linear time varying model predictive control approach to the integrated vehicle dynamics control problem in autonomous systems. In *2007 46th IEEE Conference on Decision and Control*, pages 2980–2985. IEEE, 2007.

[122] Ashwin Carvalho, Yiqi Gao, Andrew Gray, H Eric Tseng, and Francesco Borrelli. Predictive control of an autonomous ground vehicle using an iterative linearization approach. In *16th International IEEE Conference on Intelligent Transportation Systems (ITSC 2013)*, pages 2335–2340. IEEE, 2013.

[123] Yiqi Gao, Theresa Lin, Francesco Borrelli, Eric Tseng, and Davor Hrovat. Predictive control of autonomous ground vehicles with obstacle avoidance on slippery roads. In *Dynamic systems and control conference*, volume 44175, pages 265–272, 2010.

[124] Reza Hajiloo, Amir Khajepour, Halit Zengin, Alireza Kasaiezadeh, and Shih-Ken Chen. A coupled force predictive control of vehicle stability using front/rear torque allocation with experimental verification. *Submitted*.

[125] Milad Jalali, Ehsan Hashemi, Amir Khajepour, Shih-ken Chen, and Bakhtiar Litkouhi. A combined-slip predictive control of vehicle stability with experimental verification. *Vehicle system dynamics*, 56(2):319–340, 2018.

[126] Ehsan Hashemi, Mohammad Pirani, Amir Khajepour, and Alireza Kasaiezadeh. A comprehensive study on the stability analysis of vehicle dynamics with pure/combined-slip tyre models. *Vehicle system dynamics*, 54(12):1736–1761, 2016.

[127] Hans Pacejka. *Tire and vehicle dynamics*. Elsevier, 2005.

[128] Keqin Gu, Jie Chen, and Vladimir L Kharitonov. *Stability of time-delay systems*. Springer Science & Business Media, 2003.

[129] Asal Nahidi, Amir Khajepour, Alireza Kasaeizadeh, Shih-Ken Chen, and Bakhtiar Litkouhi. A study on actuator delay compensation using predictive control technique with experimental verification. *Mechatronics*, 57:140–149, 2019.

[130] Matthew Fox and John Grogg. Development of front-wheel-drive elsd for efficient performance and safety. Technical report, SAE Technical Paper, 2012.

[131] Mohammed Abd Elhafiz and Hassan Metered. Design and experimental evaluation of magnetorheologically automotive limited slip differential. *American Journal of Mechanical Engineering and Automation*, 5(4):110, 2018.

[132] H Metered et al. Performance evaluation of magnetorheological limited slip differential for automotive applications. Technical report, SAE Technical Paper, 2018.

[133] Damrongrit Piyabongkarn, Rajesh Rajamani, Jae Y Lew, and Hai Yu. On the use of torque-biasing devices for vehicle stability control. In *2006 American Control Conference*, pages 6–pp. IEEE, 2006.

[134] Riccardo Russo, Salvatore Strano, and Mario Terzo. Enhancement of vehicle dynamics via an innovative magnetorheological fluid limited slip differential. *Mechanical Systems and Signal Processing*, 70:1193–1208, 2016.

[135] Reza Hajiloo, Amir Khajepour, Alireza Kasaiezadeh, Shih-Ken Chen, and Bakhtiar Litkouhi. An intelligent control of electronic limited slip differential for improving vehicle yaw stability with experimental verification. *Submitted*.

[136] Reza Hajiloo, Amir Khajepour, Alireza Kasaiezadeh, Shih-Ken Chen, and Bakhtiar Litkouhi. A prioritization predictive control of active limited slip differential and differential braking for improving vehicle yaw stability with experimental verification. *Submitted*.

[137] Reza Hajiloo, Amir Khajepour, Alireza Kasaiezadeh, Shih-Ken Chen, and Bakhtiar Litkouhi. Integrated lateral and roll stability control of multi-actuated vehicles using prioritization model predictive control. *Submitted*.

[138] Reza Hajiloo, Amir Khajepour, Alireza Kasaiezadeh, Shih-Ken Chen, and Bakhtiar Litkouhi. A prioritization model predictive control for multi-actuated vehicle stability with experimental verification. *Submitted*.

[139] Sairam Valluri and Vikram Kapila. Stability analysis for linear/nonlinear model predictive control of constrained processes. In *Proceedings of the 1998 American Control Conference. ACC (IEEE Cat. No. 98CH36207)*, volume 3, pages 1679–1683. IEEE, 1998.

[140] Wen-Hua Chen. Stability analysis of classic finite horizon model predictive control. *International Journal of Control, Automation and Systems*, 8(2):187–197, 2010.

[141] David Q Mayne, James B Rawlings, Christopher V Rao, and Pierre OM Scokaert. Constrained model predictive control: Stability and optimality. *Automatica*, 36(6):789–814, 2000.

[142] Hans Joachim Ferreau, Christian Kirches, Andreas Potschka, Hans Georg Bock, and Moritz Diehl. qpoases: A parametric active-set algorithm for quadratic programming. *Mathematical Programming Computation*, 6(4):327–363, 2014.

[143] Reza Hajiloo, Mehdi Abroshan, Amir Khajepour, Alireza Kasaiezadeh, and Shih-Ken Chen. Integrated steering and differential braking for emergency collision avoidance in autonomous vehicles. *IEEE Transactions on Intelligent Transportation Systems*, 2020.

[144] Chuan Hu, Hui Jing, Rongrong Wang, Fengjun Yan, and Mohammed Chadli. Robust H-infinite output-feedback control for path following of autonomous ground vehicles. *Mechanical Systems and Signal Processing*, 70:414–427, 2016.

[145] H Zengin, Nursefa Zengin, Baris Fidan, and Amir Khajepour. Blending based multiple-model adaptive control for multivariable systems and application to lateral vehicle dynamics. In *2019 18th European Control Conference (ECC)*, pages 2957–2962. IEEE, 2019.

[146] Lars Svensson, Monimoy Bujarbaruah, Arpit Karsolia, Christian Berger, and Martin Törngren. Traction adaptive motion planning at the limits of handling. *arXiv preprint arXiv:2009.04180*, 2020.

[147] James Dallas, John Wurts, Jeffrey L Stein, and Tulga Ersal. Contingent nonlinear model predictive control for collision imminent steering in uncertain environments. *Arbor*, 1001:48109, 2020.

[148] John P Alsterda, Matthew Brown, and J Christian Gerdes. Contingency model predictive control for automated vehicles. In *2019 American Control Conference (ACC)*, pages 717–722. IEEE, 2019.

[149] Reza Hajiloo, Amir Khajepour, Alireza Kasaiezadeh, Shih-Ken Chen, and Bakhtiar Litkouhi. Emergency collision avoidance in autonomous vehicles using contingency path planning/tracking control design. *Submitted*.